This is to certify that the

thesis entitled

THEORETICAL AND EXPERIMENTAL STUDY OF THE PROXIMITY EFFECTS OF THIN-WIRE ANTENNA IN PRESENCE OF BIOLOGICAL BODIES

presented by

Khalid Karimullah

has been accepted towards fulfillment of the requirements for

Ph.D degree in ELECTRICAL ENGG.

Major professor

Date July 26, 1979.

THEORETICAL AND EXPERIMENTAL STUDY OF THE PROXIMITY EFFECTS OF THIN-WIRE ANTENNA IN PRESENCE OF BIOLOGICAL BODIES

By

Khalid Karimullah

A DISSERTATION

Submitted to
Michigan State University
in partial fulfillment of the requirements
for the degree of

DOCTOR OF PHILOSOPHY

Department of Electrical Engineering

ABSTRACT

THEORETICAL AND EXPERIMENTAL STUDY OF THE PROXIMITY EFFECTS OF THIN-WIRE ANTENNA IN PRESENCE OF BIOLOGICAL BODIES.

by

Khalid Karimullah

This research has been conducted to achieve an in-depth knowledge of the electromagnetic coupling caused by placing a biological body in the vicinity of a radiating antenna. The thesis presents a numerical solution to the above mentioned problem and quantifies the current distribution on the antenna and the induced electric fields inside the biological body. This study is necessitated due to the widespread use of high power transmitters, CB radios, etc., where the operator of such a device is exposed to a possible radiation hazard.

A detailed analysis investigating the problem of electromagnetic coupling between an antenna and a biological body in the near zone of the antenna has been carried out in the introductory chapters. A basic theoretical approach assuming a thin-wire, center-fed linear dipole antenna as the radiating source has been adopted which leads to the coupled integral equations. Using the method of moments, these equations are transformed into a system of consistent simultaneous equations which are then solved on a computer. In addition, elaborate instructions for using the computer program are also provided.

Experiments have been conducted using a plexiglass container of suitable dimensions filled with saline solution to represent the biological body. Perturbation of input impedance from its free-space value is plotted as a function of distance of separation between antenna and the body and is found to be in good agreement with theoretical values. Also current distribution along the length of the antenna and the electric fields induced inside the biological body are in good agreement.

Comparison of fields induced inside a body from a radiating antenna with those from a plane wave with intensity of 10 mW/cm^2 shows that use of high powered transmitters could prove hazardous.

ACKNOWLEDGEMENTS

I offer my most grateful thanks to many persons who helped me in this project. Special thanks are extended to Dr. Kun-Mu Chen for his sincere guidance and counsel , under whose supervision this research was conducted. I am equally thankful to Dr. D. P. Nyquist for his invaluable suggestions and guidance. I thank Dr. D.K. Reinhard and J.H. Shapiro, the other members of my guidance committee, for their cooperation.

Thanks are extended to the Division of Engineering Research and the Department of Electrical Engineering and System Science at Michigan State University for the financial assistance rendered during the Doctoral program.

I must sincerely thank Ms. Joanna Gruber of the Diary Science Department at Michigan State University for her prompt typing services. I am also thankful to Enid Maitland and Mary Bentley who were extremely cooperative in providing me with the typing facility at the office. Last but not the least, I am indebted to my wife Cynthia for helping me in the preparation of the rough draft of my dissertation and I appreciate her patience, understanding and encouragement during the graduate program.

TABLE OF CONTENTS

LIST OF TABLES

LIST OF FIGURES

CHAPTER 1

INTRODUCTION

In recent years the interaction between high frequency electromagnetic fields and biological bodies has been extensively investigated. These studies were motivated by the potential biological hazards associated with such electromagnetic radiations, (1,2). Chen et.al., (3,4) have determined the internal electromagnetic fields induced in biological bodies of arbitrary shapes excited by a plane electromagnetic wave. Also extending this technique to any known impressed electric field was a simple matter. The results of their work provided the information necessary for a realistic assessment of potential radiation hazards.

As an immediate consequence of this study scientists were alerted to another related situation which could prove a potential danger. Modern technological developments in the field of high frequency transmission/reception of electromagnetic waves have led to CB radios, back pack transmitters, portable transmitters, etc., which have given new dimensions to wireless communications. However, these devices have also exposed their operators to a situation which could be dangerous to health if high power transmitters are used for long range communications.

This problem attracted considerable attention and the main objective was to determine the induced electromagnetic field inside the body of an operator who is using such a device. An approach to this problem was adopted by Nyquist et.al. (5) who obtained the impressed fields that excite the biological body, by a "known" current distribution on the antenna. It is worthwhile to mention that the presence of a biological body in the vicinity of an antenna will perturb the current distribution from its "free-space" distribution and hence by this approach, substantial inaccuracies are imminent.

Broadly speaking the fundamental aspect of this thesis is to develop a method by virtue of which, unknown currents on the antenna can be determined numerically by computer aided analysis. Once the induced electric fields are obtained, a comparison with those obtained when the body is illuminated by a plane wave, with electric field intensity equal to the maximum intensity allowed by the federal radiation safety standard, can be made. Theory for solving this problem has been developed for arbitrary shaped,thin-wire antennas, however, the research is concentrated at center-fed linear dipole antennas (or base-fed monopole antennas over infinitely extending ground plane).

Since a biological body is usually a heterogeneous finite body with an irregular shape, the determination of the internal electromagnetic fields becomes a formidable task. For mathematical simplicity, a body with simple geometry will be considered (even though the computer program can successfully deal with the problem of spatially dependent electrical parameters of the body, uniform conductivity and permittivity have been used in all experiments and theoretical models).

The theoretical development for calculating the fields induced in the body and the currents on the antenna is given in Chapter II. This chapter also gives a short description of Hallen's integral equation in "free-space", which helps in determining the free-space impedance and current distribution of the antenna; and also radiation-zone fields generated by the antenna-body system are determined.

In Chapter III, method of moments, which is a transformation that converts the system of integral equations into a set of simultaneous linear equations, is discussed. Elements of the matrix of coefficients representing the system are explained in detail and the corresponding subroutines that evaluate these coefficients are identified. A numerical test of accuracies of the integration process carried out in the subroutines is also explained.

In Chapter IV a basic derivation is given for determining a linearly scaled version of the biological bodies whose true dimensions are large and impractical for laboratory experiments. Properties of saline solution along with the graphs used to obtain a desired effective conductivity are reproduced.

Chapter V is devoted to the theoretical and experimental results on the induced electric fields inside the body and the currents maintained on the antenna. It includes explanation of the experimental techniques used to measure impedance, current distribution on the antenna and the electric fields inside the biological body. A short account on possible sources of errors, that may have been encountered during the experiment, is also given.

Chapter VI discusses the practical importance and the outcome of this research. A realistic model (uniform biological body resembling a human body placed in the vicinity of an antenna) is investigated and commented. A brief account on solving a problem where arbitrary shaped, thin-wire antennas are involved is given.

Chapter VII provides a complete description of the computer program. Definition of input variables, construction of data files and the instructions for its use are given in detail. In addition, an illustrative example is worked out to give the user a better understanding of the computer program. Suggested modifications which a user may want to make are also mentioned. A listing of the computer program which gives the free-space impedance and current distribution is also given in this chapter.

CHAPTER II

THE STUDY OF FIELDS IN A BIOLOGICAL BODY EXPOSED TO NEAR-ZONE FIELDS OF ANTENNA

2.1 Introduction.

In the beginning of the first chapter it was mentioned that potential radiation hazards may be encountered when working with high-power CB radios, back-pack antennas etc. Simulation of the exact situation created by such antennas is difficult and solution for fields/currents is a complicated task especially when the current on the antenna is not known. It is for this reason the study was restricted to a situation as shown in Fig. 2.1. Consideration of arbitrarily shaped, thin-wire antennas was an appropriate choice for most practical purposes. At a later stage it was necessary to specialize this situation to a linear dipole antenna to achieve greater mathematical simplicity and system as depicted in Fig. 2.2 was adopted. This approach could also successfully represent the case of a base-fed monopole antenna over a ground plane of infinite extent using the image technique. The following major topics are to be covered.

(a) The quantification of current distribution and input impedance of the antenna in proximity of a biological body.

(b) Determination of free-space current distribution and input impedance of the antenna.

(c) Quantification of electromagnetic (EM) fields induced inside the biological body when it is in the vicinity of the antenna.

(d) The total power deposition inside the biological body under the exposure of EM radiation from antenna.

(e) The EM fields generated in the far-zone by the antenna-body coupled system.

2.2 Theoretical Development.

When a biological body, such as a human body, is illuminated by an EM radiation, EM fields are induced inside the body and an EM wave is scattered by the body into space. Obviously these EM fields are dependent on the physiological parameter and geometry, frequency and polarization of the exciting EM radiation. The total field in the space containing the body and antenna is therefore different from the field that would be present in the absence of the body. Field, current etc. associated with the antenna in the absence of the body are termed as free-space quantities .

Since currents and charges on the surface of the antenna are always maintained in such a way as to satisfy the boundary conditions there; the current and charge distributions on this surface are expected to be perturbed from their free-space values in the presence of a biological body in its vicinity. The perturbation however, is dependent upon the distance of separation between the two "sources" namely, the primary source antenna and the secondary source, excited biological body. The phenomenon underlying the cause of these perturbations is called "coupling". Coupling may be strong or weak depending upon the separation distance between the two sources.

It is apparent in the forementioned discussion that EM fields induced inside the body and the current on the antenna are both unknown quantities, and as such, it is necessary to determine them simultaneously. This paragraph gives a brief description of the theoretical analysis of the problem at hand. Firstly a tensor integral equation for fields inside the body is derived. The derivation is quite general in that, an arbitrarily-shaped, thin-wire antenna is used as an exciting source as shown in Fig. 2.1. Secondly, Hallen's integral equation is derived for a special case of centerfed linear dipole antenna as shown in Fig. 2.2. Our analysis is therefore aimed at solving the system excited by a thin-wire linear dipole antenna. These two equations together are referred to as coupled-integral-equations (CIEs) throughout this analysis and in the following chapters. Next, method of moments (using pulse functions) is utilized to transform the CIEs into a system of simultaneous equations. These equations yield a matrix of coefficients which is square with non-zero diagonal entries. Gauss's elimination process is used to solve this system once the matrix elements have been computed. The solution yields the current on antenna, input impedance of antenna, EM fields inside the body and the power deposition in the body. Lastly, radiation-zone fields of the antenna-body system are computed.

2.3 Coupled-Integral-Equations.

In this section we aim to derive the coupled-integral-equations that were mentioned briefly in the previous section. It is emphasized that time-harmonic analysis is being adopted and a time dependency of the form $\exp(j\omega t)$ is being assumed. We will first derive a tensor integral equation for a general case.

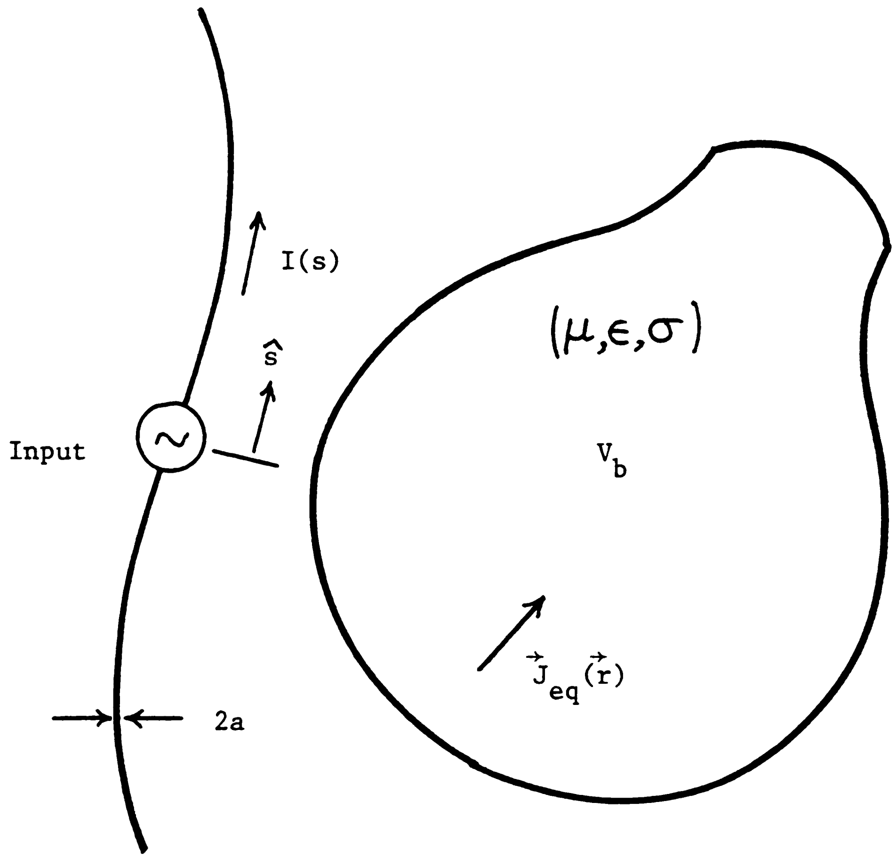

Fig. 2.1 A thin-wire antenna coupled to a biological body of volume V_b. This situation is also defined as antenna-body system.

(a) Tensor integral equation:

We consider a localized current source with current density $\vec{J}(\vec{r})$ existing in free-space and occupying a volume V. Maxwell's (curl) equations can be written for such a system in the following form

$$\nabla \times \vec{E}(\vec{r}) = -j\omega\mu_o \vec{H}(\vec{r}) \tag{2.1}$$

$$\nabla \times \vec{H}(\vec{r}) = \vec{J}(\vec{r}) + j\omega\varepsilon_o \vec{E}(\vec{r}). \tag{2.2}$$

Using the continuity equation $\nabla\cdot\vec{J}(\vec{r}) + j\omega\rho(\vec{r}) = 0$, which gives the relationship between the current density $\vec{J}(\vec{r})$ and the free charge density $\rho(\vec{r})$ we get

$$\nabla \cdot \vec{E}(\vec{r}) = \frac{j}{\omega\varepsilon_o} \nabla\cdot\vec{J}(\vec{r}). \tag{2.3}$$

For a system of equations as given above, a solution for the electric field is obtained by using tensor Green's function. Derivation of this equation, which enables one to write the electric field in terms of a tensor integral expression has been carried out elsewhere (6), (16). Electric field is given as

$$\vec{E}(\vec{r}) = \text{P.V.} \int_V \vec{J}(\vec{r}\,') \cdot \overleftrightarrow{G}(\vec{r},\vec{r}\,')\, dv' - \frac{\vec{J}(\vec{r})\cdot\overleftrightarrow{I}}{3j\omega\varepsilon_o} \tag{2.4}$$

for all points $\vec{r}$ interior to volume V. The symbol P.V. denotes the principal value of the integral meaning that the integral is carried out by excluding a small volume surrounding the field point first and then letting this small volume approach zero (7). <u>For points exterior to V, the field is represented by the tensor integral only</u>. In above

$\overleftrightarrow{I}$ is the identity tensor

$\overleftrightarrow{G}$ is the tensor Green's function

$$\overleftrightarrow{G}(\vec{r},\vec{r}') = \frac{-j\omega\mu_o}{4\pi}\left[\overleftrightarrow{I} + \frac{\nabla\nabla}{k_o^2}\right]\frac{1}{|\vec{r}-\vec{r}'|}\exp(-jk_o|\vec{r}-\vec{r}'|) \qquad (2.5)$$

where $k_o = \omega\sqrt{\mu_o\varepsilon_o}$, $\vec{r}$ and $\vec{r}'$ are field point and source point radius vectors respectively.

We now examine the system depicted in Fig. 2.1. In this system, EM field is originated by a current density $\vec{J}^a(\vec{r})$ in the antenna of volume V_a. It is termed as "incident-field". This field excites conduction and polarization currents inside the biological body of volume V_b which in turn produces an EM field of its own. The field produced exclusively by these secondary sources is termed as "scattered-field". The problem would have been relatively simple had it been possible to assume $\vec{J}^a(\vec{r})$ as an independent known quantity. But due to the coupling this simplified assumption can not be used; and therefore both the primary and secondary sources are unknown.

Total EM field $\{\vec{E}(\vec{r}), \vec{H}(\vec{r})\}$ is the sum of the incident and the scattered field at all points in space. For this field to be a valid solution to Maxwell's equations it must satisfy the following

$$\nabla \times \vec{E}(\vec{r}) = -j\omega\mu_o \vec{H}(\vec{r}) \tag{2.6}$$

$$\nabla \times \vec{H}(\vec{r}) = \vec{J}^a(\vec{r}) + \sigma(\vec{r})\, \vec{E}(\vec{r}) + j\omega\varepsilon(\vec{r})\vec{E}(\vec{r}) \tag{2.7}$$

where $\sigma(\vec{r})$ and $\varepsilon(\vec{r})$ are varying and discontinuous functions of space. This situation will therefore be a very complicated one if an attempt is made to solve for the $\vec{E}(\vec{r})$ field using tensor-Green's-function approach. Also $\nabla\cdot\vec{E}(\vec{r})$ is not a simple expression when related to the free charge density. The method of superposition gives a convienient way out of this situation. We introduce two EM fields as follows.

$\begin{bmatrix} \vec{E}^a(\vec{r}) \\ \vec{H}^a(\vec{r}) \end{bmatrix}$ Impressed EM fields from the ANTENNA.

$\begin{bmatrix} \vec{E}^b(\vec{r}) \\ \vec{H}^b(\vec{r}) \end{bmatrix}$ Scattered EM fields from the BIOLOGICAL BODY.

By superposition

$$\vec{E}(\vec{r}) = \vec{E}^a(\vec{r}) + \vec{E}^b(\vec{r}) \tag{2.8}$$

$$\vec{H}(\vec{r}) = \vec{H}^a(\vec{r}) + \vec{H}^b(\vec{r}). \tag{2.9}$$

Electric field $\vec{E}^a(\vec{r})$ is assumed to be produced exclusively by the current density $\vec{J}^a(\vec{r})$ in antenna. Therefore the following expressions are true.

$$\nabla \times \vec{E}^a(\vec{r}) = -j\omega\mu_o\vec{H}^a(\vec{r}) \tag{2.10}$$

$$\nabla \times \vec{H}^a(\vec{r}) = \vec{J}^a(\vec{r}) + j\omega\varepsilon_o\vec{E}^a(\vec{r}) \tag{2.11}$$

$$\nabla \cdot \vec{E}^a(\vec{r}) = \frac{j}{\omega\varepsilon_o} \nabla\cdot\vec{J}^a(\vec{r}). \tag{2.12}$$

Similarly, we can write a set of equations for $\{\vec{E}^b(\vec{r}), \vec{H}^b(\vec{r})\}$ with a condition that equations (2.6) and (2.7) are satisfied identically.

$$\nabla \times \vec{E}^b(\vec{r}) = -j\omega\mu_o\vec{H}^b(\vec{r}) \tag{2.13}$$

$$\nabla \times \vec{H}^b(\vec{r}) = \vec{J}_{eq}(\vec{r}) + j\omega\varepsilon_o\vec{E}^b(\vec{r}) \tag{2.14}$$

$$\nabla \cdot \vec{E}^b(\vec{r}) = \frac{j}{\omega\varepsilon_o} \nabla\cdot\vec{J}_{eq}(\vec{r}). \tag{2.15}$$

Adding (2.10) and (2.13); and using (2.8) and (2.9); the expression for curl of total electric field in (2.6) is satisfied trivially.

Next, using (2.11) and (2.14); and again using (2.8) and (2.9); the expression for curl of total magnetic field in (2.7) is satisfied with $\vec{J}_{eq}(\vec{r}) = \tau(\vec{r})\ \vec{E}(\vec{r})$ where $\tau(\vec{r}) \triangleq \sigma(\vec{r}) + j\omega[\varepsilon(\vec{r})-\varepsilon_o]$ is called

the complex conductivity, a parameter which completely determines the conduction and polarization currents induced in the biological body.

A comparison of the set of equations (2.10), (2.11) and (2.12), and (2.13), (2.14), and (2.15) with the set (2.1), (2.2), and (2.3), will enable us to write down the expressions for $\vec{E}^a(\vec{r})$ and $\vec{E}^b(\vec{r})$ directly. Since we are assuming the antenna a perfect conductor, points inside the antenna will not be included in the following analysis, therefore the expression (2.16) below is valid for all points outside the antenna. Therefore

$$\vec{E}^a(\vec{r}) = \int_{V_a} \vec{J}^a(\vec{r}\,') \cdot \overleftrightarrow{G}(\vec{r},\vec{r}\,')dv'. \tag{2.16}$$

Also,

$$\vec{E}^b(\vec{r}) = \text{P.V.} \int_{V_b} \vec{J}_{eq}(\vec{r}\,') \cdot \vec{G}(\vec{r},\vec{r}\,')dv' - \frac{\vec{J}_{eq}(\vec{r}) \cdot \overleftrightarrow{I}}{3j\omega\varepsilon_o} \tag{2.17}$$

for all points $\vec{r}$ inside the body's volume V_b. Total electric field will be given by the following expression (in which thin-wire approximation has been used) using equation (2.8)

$$\vec{E}(\vec{r}) = \int_{ant} I(s')\, \hat{s}' \cdot \overleftrightarrow{G}(\vec{r},\vec{s}\,')ds' + \text{P.V.} \int_{V_b} \vec{J}_{eq}(\vec{r}\,') \cdot \overleftrightarrow{G}(\vec{r},\vec{r}\,')dv'$$

$$\frac{-\vec{J}_{eq}(\vec{r}) \cdot \overleftrightarrow{I}}{j3\omega\varepsilon_o} \tag{2.18}$$

for all points $\vec{r}$ in V_b. Other quantities are as before and I(s) is the current on the antenna.

(b) Hallen's Integral Equation:

Before we attempt to derive the Hallen's integral equation it will be necessary to specialize the general situation of Fig. 2.1, therefore we now analyze the system shown in Fig. 2.2. Furthermore the antenna conductor is assumed to be perfect so that the electric field interior to the antenna is zero.

Using the boundary condition for the tangential component of electric fields along the entire length of the antenna we get, for $-h \leq x \leq h$

$$E_x^a(x) + E_x^b(x) = -V_o \delta(x) \tag{2.19}$$

where V_o is the impressed voltage (input of the antenna is situated at the origin).

Subscript "x" signifies the tangential component and it is the same as $\vec{x}$ - component of electric field.

The electric field produced exclusively by the antenna satisfies the relation (on the surface of antenna)

$$\vec{E}^a(x) = -\nabla\phi_a(x) - j\omega\vec{A}_a(x)$$

$$\phi_a(x) = \text{scalar potential}$$

for all points $\vec{r}$ in V_b. Other quantities are as before and I(s) is the current on the antenna.

(b) Hallen's Integral Equation:

Before we attempt to derive the Hallen's integral equation it will be necessary to specialize the general situation of Fig. 2.1, therefore we now analyze the system shown in Fig. 2.2. Furthermore the antenna conductor is assumed to be perfect so that the electric field interior to the antenna is zero.

Using the boundary condition for the tangential component of electric fields along the entire length of the antenna we get, for $-h \leq x \leq h$

$$E_x^a(x) + E_x^b(x) = -V_o \delta(x) \tag{2.19}$$

where V_o is the impressed voltage (input of the antenna is situated at the origin).

Subscript "x" signifies the tangential component and it is the same as $\vec{x}$ - component of electric field.

The electric field produced exclusively by the antenna satisfies the relation (on the surface of antenna)

$$\vec{E}^a(x) = -\nabla\phi_a(x) - j\omega\vec{A}_a(x)$$

$$\Phi_a(x) = \text{scalar potential}$$

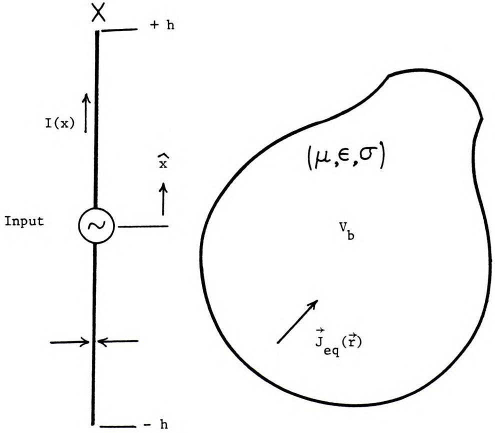

Fig. 2.2 A thin-wire linear centerfed dipole antenna coupled to a biological body of volume V_b.

$$\vec{A}_a(x) = \text{vector potential}$$

therefore,

$$E_x^a(x) = -\frac{\partial\phi_a(x)}{\partial x} - j\omega A_{ax}(x). \tag{2.20}$$

For points on the surface or outside the antenna a good approximation is to assume the current flowing along the antenna axis.

Then

$$A_{ax}(x) = \frac{\mu_o}{4\pi}\int_{-h}^{h} I(x')K_a(x,x')dx' \tag{2.21}$$

$$K_a(x,x') = \frac{1}{R}\exp(-jk_oR), \quad R = [(x-x')^2+a^2]^{1/2}$$

where "a" is the radius of the antenna conductor. This is a valid approximation only for the cases where EM field outside the antenna is required. Starting from the basic expression for $\Phi_a(x)$ in integral form, using continuity and boundary condition $I(h) = I(-h) = 0$, it is easy to arrive at the following expression for

$$\Phi_a(x) = \frac{j}{4\pi\varepsilon_o\omega}\frac{\partial}{\partial x}\int_{-h}^{h} I(x')K_a(x,x')dx' \tag{2.22}$$

using (2.21), (2.22) in equation (2.20) and substituting these in equation (2.19) and after some algebra we can arrive at the following differential equation.

$$\frac{\partial^2 F(x)}{\partial x^2} + k_o{}^2 F(x) = \frac{-j4\pi k_o}{\eta_o}[V_o\delta(x)+E_x^b(x)] \qquad (2.23)$$

where

$$F(x) = \int_{-h}^{h} I(x')\,K_a(x,x')dx' \text{ and } \eta_o = \sqrt{\mu_o/\varepsilon_o}\,.$$

At this point we state without proof that for a differential equation of the form

$$\frac{\partial^2 y}{\partial x^2} + \lambda^2 y = g(x)\,,$$

a solution, using the Lagrange variational method, can be obtained as,

$$y = C_1 \sin \lambda x + C_2 \cos \lambda x + \frac{1}{\lambda}\int_o^x g(u) \sin \lambda(x-u)du.$$

By inspection of equation (2.23) we arrive at the desired Hallen's integral formulation for the current distribution on antenna in the presence of a biological body. The equation is,

$$\int_{-h}^{h} I(x')K_a(x,x')dx' + A \cos k_o x + B \sin k_o x$$

$$+ j\frac{4\pi}{\eta_o}\int_o^x E_x^b(u) \sin k_o(x-u)du = -j\frac{2\pi}{\eta_o} V_o \sin k_o|x|. \qquad (2.24)$$

<u>The free-space Hallen's integral equation</u> is exactly like the one in (2.24) above except the contributing term due to body effects is zero, that is $E_x^b(u) = 0$ in (2.24) above.

Also reproducing equations (2.18) with the length vetor $\vec{s}$ replaced by $\vec{x}$ as shown in Fig. 2.2, and some rearranging, we have for $\vec{r}$ in V_b

$$[1 + \frac{\tau(\vec{r})}{3j\omega\varepsilon_o}]\ \vec{E}(\vec{r})\ -\text{P.V.}\int_{V_b} \tau(\vec{r}\,')\ \vec{E}(\vec{r}\,') \cdot \overleftrightarrow{G}(\vec{r},\vec{r}\,')dv'$$

$$= \int_{-h}^{h} I(x')\ \hat{x}\cdot\overleftrightarrow{G}(\vec{r},\vec{r}\,')dx'. \qquad (2.25)$$

Equations (2.24) and (2.25) together are referred to as coupled-integral-equations (CIEs) and these will be solved numerically on a computer. In Chapter III a detailed analysis of the numerical methods used for the computer solution is given.

2.4 Radiation field maintained by antenna-body system.

In this section we aim at obtaining the radiation pattern of the EM system which is formed by the antenna and the irradiated body. The far-zone field pattern is greatly dependent on the separating distance between the body and the antenna. The situation is similar to an antenna with a parasitic element.

For the system under consideration, we have two sources, namely

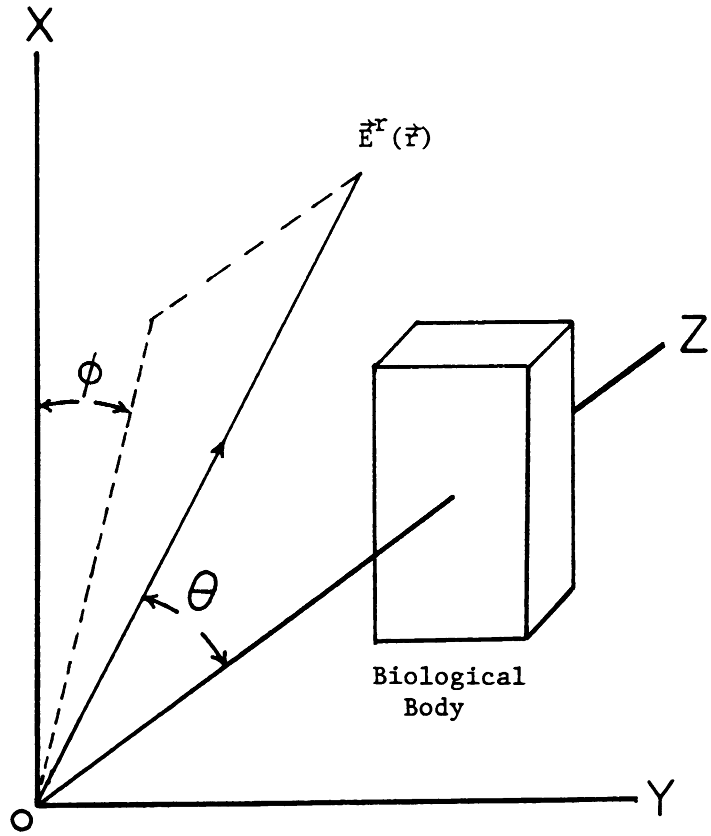

Fig. 2.3 Coordinate system chosen to define the far-zone radiation field pattern.

the current I(x) on the antenna and current density $\vec{J}_{eq}(\vec{r}) = \tau(\vec{r})\,\vec{E}(\vec{r})$ where $\tau(\vec{r})$ is the complex conductivity as defined previously and $\vec{E}(\vec{r})$ is the total electric field inside the body. The coordinate system is chosen as given in Fig. 2.3.

The electric field expression is given as

$$\vec{E}(\vec{r}) = -j\,\eta_o k_o \int_V \vec{J}(\vec{r}) \cdot [\overleftrightarrow{I} + \frac{\nabla\nabla}{k_o^2}]\, G_o(\vec{r},\vec{r}\,')dv' \tag{2.26}$$

$$G_o(\vec{r},\vec{r}\,') = \frac{\exp(-jk_oR)}{4\pi R}, \quad R = |\vec{r}-\vec{r}\,'|, \quad \eta_o = \sqrt{\mu_o/\varepsilon_o}.$$

One approach will be to solve for the above integral numerically since the current on the antenna and the induced fields inside the body are obtained (at least at a sufficient number of points) once the CIEs are numerically solved. A much simpler formula can however be derived (5) using radiation-zone field approximation. This approximation requires that $k_oR \gg 1$ and $\vec{r} \gg \vec{r}\,'$, where $\vec{r}$ is the field point and $\vec{r}\,'$ is the source point. An outline of the derivation of this formula follows.

$$\nabla G_o(\vec{r},\vec{r}\,') \doteq -j\frac{k_o}{4\pi R}\exp(-jk_oR)\hat{r} \tag{2.27}$$

also

$$J(\vec{r}\,') \cdot \nabla = J_x(\vec{r}\,')\frac{\partial}{\partial x} + J_y(\vec{r}\,')\frac{\partial}{\partial y} + J_z(\vec{r}\,')\frac{\partial}{\partial z} \tag{2.28}$$

Next,

$$\frac{\partial}{\partial x} \nabla G_o(\vec{r},\vec{r}') \doteq \frac{-k_o^2}{4\pi R} \exp(-jk_oR) \left(\frac{\partial R}{\partial x}\right)\hat{r} \,. \tag{2.29}$$

Using (2.27), (2.28) and (2.29) above one can easily arrive at the following expression;

$$[\vec{J}(\vec{r})\cdot\nabla\nabla]\; G(\vec{r},\vec{r}') = \frac{-\hat{r}k_o^2}{4\pi R} \exp\,(-jk_oR)\;(\hat{r}\cdot\vec{J}(\vec{r}')),$$

and consequently using (2.26) and defining

$$\vec{J}(\vec{r}') = \hat{r}J_r(\vec{r}') + \hat{\theta}J_\theta(\vec{r}') + \hat{\phi}J_\phi(\vec{r}')$$

we get

$$\vec{E} \doteq -j\,\eta_o k_o \int_V [\hat{\theta}J_\theta(\vec{r}') + \hat{\phi}J_\phi(\vec{r}')]\,\frac{\exp(-jk_oR)}{4\pi R}\,dv'. \tag{2.30}$$

Invoking the far zone approximation and using binomial expansion to approximate R we get,

$$R \doteq r - \hat{r}\cdot\vec{r}' \qquad\qquad \text{since } \vec{r} >> \vec{r}'.$$

Next transferring J_θ and J_ϕ into linear combinations of J_x , J_y and J_z

$$\vec{E}^r = \frac{-j\eta_o k_o}{4\pi r} \exp(-jk_o r) \int_V [\hat{\theta}\{J_x(\vec{r}\,') \cos\theta \cos\phi$$

$$+ J_y(\vec{r}\,') \cos\theta \sin\phi - J_z(\vec{r}\,') \sin\theta\} + \hat{\phi}\{-J_x(\vec{r}\,') \sin\phi$$

$$+ J_y(\vec{r}\,') \cos\phi\}] \exp\{-jk_o\,(x' \sin\theta \cos\phi + y' \sin\theta \sin\phi$$

$$+ z' \cos\theta)\}dv' . \qquad (2.31)$$

Equation (2.31) gives the radiation-zone electric field. Volume Integration is carried out over all sources thus, for antenna $\vec{J}(\vec{r}\,')dv'$ will reduce to $I(x')\vec{d}x'$ and for body $\vec{J}(\vec{r}\,') = \vec{J}_{eq}(\vec{r}\,')$ where $\vec{r}\,'$ is inside V_b.

CHAPTER III

NUMERICAL ANALYSIS

3.1 Introduction.

The integrals obtained for the electric field $\vec{E}(\vec{r})$ at any point inside the biological body and the current distribution on the antenna are, in general, very difficult to evaluate. A simple way to obtain an approximate solution is to require that equation (2.24) and (2.25) be satisfied at certain discrete points in the region of interest. This procedure is called point matching. In the moment method, the total volume of the biological body is partitioned into N_B subvolumes or "cells"; and the antenna length into N_A partitions or "segments". We must have N_A an odd integer because we are interested in knowing the current at the central segment, which will be frequently referred to as the input segment. It is worthwhile to mention that method of moments is a generalized technique and the method outlined above is a special case which utilizes "pulse-function-expansion" to approximate the unknown fields/currents . The cells in the body are assumed to be regular cubes, electrically small and in each cell electrical parameters and unknown fields are assumed to be constant. Similarly the current in each segment of the antenna is assumed to be constant. Also recalling from past experience, it has been found that the cell edge should be smaller than one tenth of the wavelength of radiation inside the biological body. This requirement can however, be relaxed in some cases. An upper limit on the size of the antenna segment is $\lambda_o/40$ where λ_o is the free-space wavelength. Information supporting this choice is also experimental. Finally, point matching is done at the central coordinate of each cell and segment.

3.2 Pulse Function Expansion and Point Matching.

At this point we introduce a new notation to replace the conventional rectangular coordinate system variables x,y,z.

$$x_1 = x$$
$$y_1 = y$$
$$z_1 = z$$

The pulse function approximation for current distribution on the antenna is

$$I(x_1) = \sum_{\ell=1}^{N_A} I_\ell p_\ell(x_1), \quad p_\ell(x_1) = \begin{cases} 1, x_1 \text{ in } (\Delta x_1)_\ell \\ 0 \text{ otherwise .} \end{cases} \tag{3.1}$$

The pulse function expansion for the electric field inside the body is

$$\vec{E}(\vec{r}) = \sum_{n=1}^{N_B} \vec{E}^n p_n(\vec{r}), \quad p_n(\vec{r}) = \begin{cases} 1, \vec{r} \text{ in } (\Delta V)_n \\ 0 \text{ otherwise .} \end{cases} \tag{3.2}$$

In equations (3.1) and (3.2) above,

I_ℓ is the current in the ℓ^{th} segment of the antenna,

$(\Delta x_1)_\ell$ represents the span of ℓ^{th} segment of the antenna,

$(\Delta V)_n$ represents the volume enclosed by n^{th} cell of the body,

and $\vec{E}^n$ is the total electric field in the n^{th} cell of the body.

The matrix representation of tensor Green's function $\overleftrightarrow{G}(\vec{r},\vec{r}')$ can be conventiently written in terms of the new notation for coordinates. For simplicity, arguments are not specified in the matrix expression.

$$\overleftrightarrow{G} = \begin{pmatrix} G_{x_1x_1} & G_{x_1x_2} & G_{x_1x_3} \\ G_{x_2x_1} & G_{x_2x_2} & G_{x_2x_3} \\ G_{x_3x_1} & G_{x_3x_2} & G_{x_3x_3} \end{pmatrix} \qquad (3.3)$$

where the matrix elements have been evaluated by Livesay and Chen (8).

$$G_{x_px_q} = \frac{-j\omega\mu_o}{4\pi\alpha^3} k_o \exp(-j\alpha) \{(\alpha^2-1-j\alpha)\,\delta_{pq} + (x_p-x'_p)\,(x_q-x'_q)(3-\alpha^2+3j\alpha)\,\frac{1}{R^2}\}$$

$$\alpha \triangleq k_oR \quad \text{and } R = |\vec{r}-\vec{r}'| \qquad (3.4)$$

$\delta_{pq} = 1$, if $p = q$, otherwise zero.

The pulse function expansion for the current is then used in the L.H.S. term of equation (2.24) to yield a sum of integrals over each segment. This gives

$$\int_{-h}^{h} I(x'_1)\, K_a(x_1,x'_1)dx_1 = \sum_{\ell=1}^{N_A} I_\ell \int_{a_-^\ell}^{a_+^\ell} K_a(x_1,x'_1)dx'_1$$

where

$-h \le x_1 \le h$ and x'_1 in $(\Delta x_1)\ell$.

Also

$$a_-^{\ell} \triangleq x_1^{\ell} - \frac{1}{2}(\Delta x_1)\ell$$

$$a_+^{\ell} \triangleq x_1^{\ell} + \frac{1}{2}(\Delta x_1)\ell$$

where x_1^{ℓ} is the central location of ℓ^{th} segment.

Next the pulse function expansion for the electric field will give us the following expression for field at $\vec{r}$ outside the body produced by the currents and charges induced inside the body

$$\vec{E}^b(\vec{r}) = \sum_{n=1}^{N_B} \tau_n \vec{E}^n \cdot \int_{(\Delta v)_n} \overleftrightarrow{G}(\vec{r},\vec{r}')dv', \vec{r}' \text{ in } (\Delta v)_n .$$

This can be used to determine the tangential component of $\vec{E}^b$ at the surface of the antenna where $\vec{r} = \vec{x}_1$ and $-h \le x_1 \le h$. This can be assumed for the surface of the antenna when thin-wire approximation is made or when the diameter of the antenna conductor is very small compared to the wavelength. To a first order approximation, this component is written as,

$$E^b_{x_1}(x_1) = \sum_{n=1}^{N_B} \sum_{p=1}^{3} \tau_n (\Delta v)_n E^n_{x_p} G_{x_p x_1}(\vec{x}_1, \vec{r}^n) , \text{ where}$$

$\vec{r}^n$ is the central coordinate of n^{th} cell inside the body. The integrand of the 4^{th} term in the L.H.S. of (2.25) can be written at some vector location $\vec{u}$ on the antenna as

$$\text{Integrand} = \left(\sum_{n=1}^{N_B} \sum_{p=1}^{3} \tau_n(\Delta v)_n \, E^n_{x_p} \, G_{x_p x_1}(\vec{u},\vec{r}^n)\right)\sin k_o(x_1-u)$$

where $\vec{u} = u\hat{x}_1$ and represents the dummy variable introduced to perform the integration in the interval $\{0,x_1\}$.

We are now in a position to transform the equation (2.24) into the "sum-of-integral" form of Hallen's equation. It is

$$A \operatorname{Cos} k_o x_1 + B \operatorname{Sin} k_o x_1 + \sum_{\ell=2}^{N_A-1} I_\ell \int_{a_-^\ell}^{a_+^\ell} K_a(x_1,x'_1)dx_1$$

$$+j\frac{4\pi}{\eta_o} \sum_{n=1}^{N_B} \sum_{p=1}^{3} \tau_n(\Delta v)_n \, E^n_{x_p} \int_o^{x_1} G_{x_p x_1}(\vec{u},\vec{r}^n) \operatorname{Sin} k_o(x_1-u)du$$

$$= -j\frac{2\pi}{\eta_o} V_o \operatorname{Sin} k_o |x_1| \tag{3.5}$$

where currents in the outermost segments of the antenna have been assumed to be zero. Similarly the right hand side of equation (2.25) is transformed as follows by using pulse function expansion for the current on the antenna. It is

$$\int_{-h}^{h} I(x'_1)\hat{x}_1 \cdot \overleftrightarrow{G}(\vec{r},\vec{x}'_1)dx'_1 = \sum_{p=1}^{3} \hat{x}_p \left\{\sum_{\ell=1}^{N_A} I_\ell \int_{a_-^\ell}^{a_+^\ell} G_{x_p x_1}(\vec{r},\vec{x}'_1)dx'_1\right\}$$

where

$\vec{r}$ is the field point inside the body, of the central coordinate of any cell, and

$\hat{x}_p$ represents the unit vectors for p = 1,2,3.

Next, the L.H.S. of equation (2.25) is represented by the following expression (except for polarity) for the field point $\vec{r}$,

$$\text{P.V.}\int_{V_B} \tau(\vec{r}\,')\vec{E}(\vec{r}\,') \cdot \overleftrightarrow{G}(\vec{r},\vec{r}\,')dv' - \{1+\frac{\tau(\vec{r})}{3j\omega\varepsilon_o}\}\,\vec{E}(\vec{r})$$

$$= \sum_{p=1}^{3} \hat{x}_p\{\sum_{n=1}^{N_B}\sum_{q=1}^{3} E^n_{x_q}(\tau_n \text{P.V.}\int_{(\Delta v)_n} G_{x_p x_q}(\vec{r},\vec{r}\,')dv' - \delta_{pq}\delta_{\vec{r}\vec{r}^n}(1+\frac{\tau_n}{j3\omega\varepsilon_o}))\}$$

where

$$\delta_{pq} = \begin{cases} 1 \text{ if } p = q \\ 0 \text{ otherwise}, \end{cases} \qquad \delta_{\vec{r}\vec{r}^n} = \begin{cases} 1 \text{ if } \vec{r} = \vec{r}^n \\ 0 \text{ otherwise}, \end{cases} \quad \text{and}$$

$\vec{r}^n$ is the central coordinate of n^{th} cell. τ_n will be the complex conductivity of the cell in which $\vec{r}^n$ lies.

These two expressions replaced into equation (2.25) will yield the "sum-of-integral" form of tensor integral equation. Subscripted unit vector along with the summation over p = 1,2,3 yield a set of 3 scalar equations for each point.

$$\sum_{p=1}^{3} \hat{x}_p\, [\sum_{\ell=1}^{N_A} I_\ell \int_{a^\ell_-}^{a^\ell_+} G_{x_p x_1}(\vec{r},\vec{x}\,'_1)dx'_1$$

$$+ \sum_{n=1}^{N_B}\sum_{q=1}^{3} E^n_{x_q}\{\tau_n \text{P.V.}\int_{(\Delta v)_n} G_{x_p x_q}(\vec{r},\vec{r}\,')dv'$$

$$- \delta_{pq}\delta_{\vec{r}\vec{r}^n}(1+\frac{\tau_n}{3j\omega\varepsilon_o})\}] = \vec{0} \qquad (3.6)$$

where the component terms and variables have already been defined in previous pages.

Equation (3.5) is point matched at the central location of each segment of the antenna. This is done by substituting $\{x^i_1\}$ in place of field point x_1 in that equation, thereby generating N_A equations. Since currents $I_1 = I_{N_A} = 0$ because of the boundary conditions, there are exactly $[N_A + 3N_B]$ terms in each of the N_A equations. Similarly, equation (3.6) is point matched at the central location of each cell of the body. This will be accomplished by substituting the central co-ordinates $\{\vec{r}^m\}$ of each cell in place of field point $\vec{r}$ of equation (3.6). This will generate $3N_B$ equations (N_B equations for each vector component) and each will contain $(N_A + 3N_B) -2$ terms, two terms less because the boundary condition $I_1 = I_{N_A} = 0$ is imposed.

The two groups of equations thus developed by point matching, form a system of $(3N_B+N_A)$ equations and the same number of unknowns. The matrix of coefficients is therefore square and since each equation has a distinct matching point, we expect the matrix to be full rank with a unique inverse. The matrix is depicted in Fig. 3.1.

Submatrix A_A is $N_A \times N_A$ matrix,
submatrix A_B is $N_A \times 3N_B$ matrix,
submatrix B_A is $3N_B \times N_A$ matrix,
submatrix B_B is $3N_B \times 3N_B$ matrix.

Since $I_1 = I_{N_A} = 0$ are already known the top and bottom current positions in $\bar{x}$ are replaced by A and B, the unknown constants of Hallen's equation.

Vector $\bar{y}_A$ has $y_i = -j\frac{2\pi}{\eta_o} V_o \operatorname{Sin} k_o|x^i_1|$, $i = 1,2,..N_A$

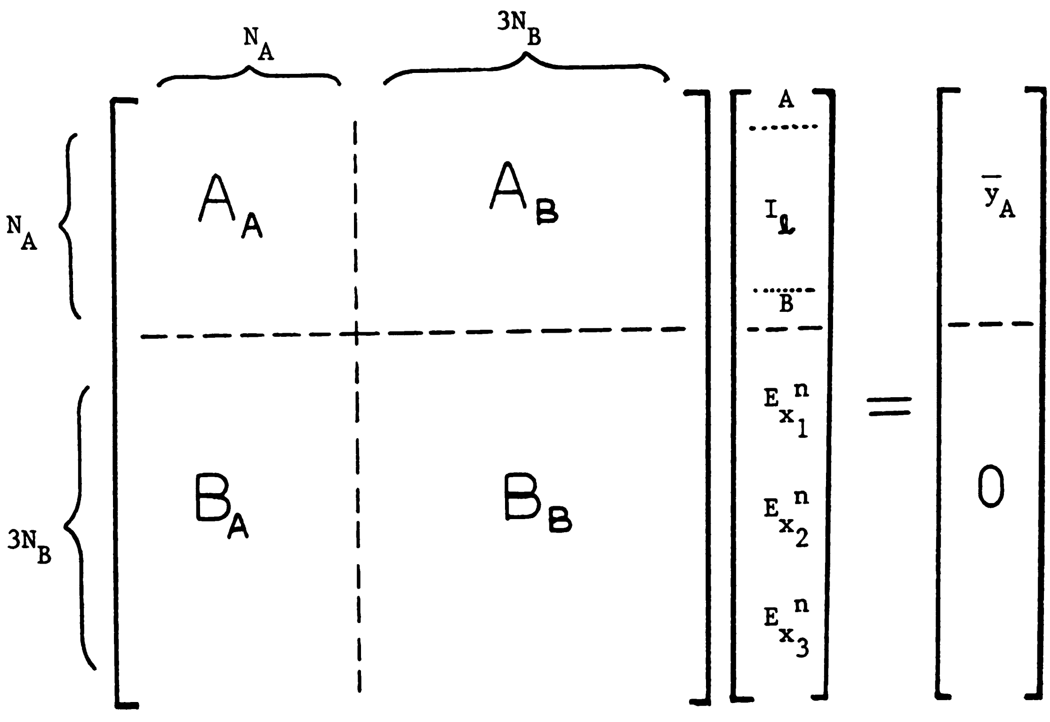

Fig. 3.1 Representation of the system of equations defined by $\bar{A}\bar{x} = \bar{y}$ where $\bar{A}$ is the matrix of coefficients.

3.3 Computer Program.

This section is devoted to the explanation of the major subroutines that are used to evaluate the matrix developed in the preceeding section. Also included is a brief description of computing processes involved in computation of these elements, which will enable the reader to have an overall understanding of the computer program.

In the computer program four subroutines are assigned to compute the elements of the coefficient matrix (one for each submatrix) and are named accordingly: for example, subroutine "MATAB" computes the elements of submatrix A_B of Fig. 3.1. Another subroutine "CMATP" then solves the system of equations by Gauss's elimination process. Finally, subroutine "RAD" is used to determine the normalized far-zone radiation fields using the discrete numerical data obtained from the solution of equations. This section deals only with the four subroutines that are used to evaluate matrix elements. Following is the computational assignment of each subroutine.

SUBROUTINE NAME	SUBMATRIX ELEMENT		COMPUTATION
1. MATAA	$(A_A)_{i\ell}$		$\int_{a_-^\ell}^{a_+^\ell} K_a(x_1^i, x_1')dx_1'$
	$i = 1$ to N_A	or	$\sin k_o x_1^i$
	$\ell = 1$ to N_A		$\cos k_o x_1^i$

SUBROUTINE NAME	SUBMATRIX ELEMENTS	COMPUTATION
2. MATAB	$(A_B)_{ik}$ $i = 1$ to N_A $k = (p-1)N_B+n$ where $n = 1$ to N_B $p = 1,2,3$	$j\frac{4\pi}{\eta_o}\tau_n(\Delta v)_n \int_o^{x_1^i} G_{x_p x_1}(\vec{u},\vec{r}^n)\sin k_o(x_1^i-u)du$
3. MATBA	$(B_A)_{r\ell}$ $\ell = 1$ to N_A $r = (p-1)N_B + m$ where $m = 1$ to N_B $p = 1,2,3$	$\int_{a_-^\ell}^{a_+^\ell} G_{x_p x_1}(\vec{r}^m,\vec{x}_1')dx_1'$
4. MATBB	$(B_B)_{rk}$ $r = (q-1)N_B + m$ $k = (p-1)N_B + n$ where $m,n = 1$ to N_B $p,q = 1,2,3$	$\{\tau_n \mathrm{P.V.}\int_{(\Delta v)_n} G_{x_p x_q}(\vec{r}^m,\vec{r}^n)dv' - \delta_{pq}\delta_{\vec{r}^n\vec{r}^m}(1+\frac{\tau_m}{3j\omega\varepsilon_o})\}$

The diagonal entries of the matrix of the entire system are the diagonal entries of submatrix A_A and B_B of Fig. 3.1. These entries correspond to the situation in which the field point lies in the same cell (segment) of the body (antenna) over which the integration has to be performed.

The diagonal elements of submatrix A_A are obtained by the following approximation.

$$\text{Integrand} = \frac{\exp(-jkR)}{R} \doteq \frac{1}{R}$$

$$\text{where} \quad R = \{(x_1^{\ell}-x_1')^2 + a^2\}^{1/2}.$$

Integrating between the lower limit $x'_1 = a_-^{\ell}$ and the upper limit a_+^{ℓ} of the ℓ^{th} partition, whose central coordinate is x_1^{ℓ}, we get

$$(A_A)_{\ell\ell} = \log_e \frac{(x_1^{\ell}-a_-^{\ell}) + \sqrt{\{(x_1^{\ell}-a_-^{\ell})^2 + a^2\}}}{(x_1^{\ell}-a_+^{\ell}) + \sqrt{\{(x_1^{\ell}-a_+^{\ell})^2 + a^2\}}}$$

"a" being the radius of the antenna conductor.

The diagonal elements of B_B are obtained by an involved process which yields an analytic expression (8). The expression thus obtained is given by

$$(B_B)_{nn} = \frac{-2}{3} j\omega\mu_o\tau_n\{(1+jk_oa_n) \exp(-jk_oa_n)-1\}\frac{1}{k_o^2}$$

$$- \{1 + \frac{\tau_n}{3j\omega\varepsilon_o}\} \qquad (3.8)$$

where

$$a_n \triangleq (\frac{3(\Delta v)_n}{4\pi})^{1/3}.$$

Subroutines MATAA, MATAB and MATBA make use of Simpson's method for numerical integration. Subroutine MATBB processes volume integration over each cell of the body subdividing the cell into sufficiently small subdivisions and summing up the contribution from each subcell. Accuracy and the cost of computations are the factors which govern the choice of the number of subdivisions and has been discussed elsewhere (9).

We shall now discuss the accuracy of the Simpson's integration processes that were used in the above mentioned subroutines. Our objective is to come up with an optimum number of subdivisions of the span of integration so that reasonable accuracy is achieved with minimum computational cost. A separate computer program is written to determine the appropriate number of subdivisions to meet the prescribed accuracy limit. In this program the worst possible situation, meaning, that the case in which integrand's behavior is not smooth, is chosen for integration. An arbitrary number (usually 4) of subdivisions are used as a starting point and the integral evaluated. The number of subdivisions is doubled and the integral is reevaluated. This new value is compared with the previous value. If the percent difference is less than 0.1% the current number of subdivisions are accepted otherwise the process is repeated. This method was tested by evaluating the diagonal element by equation (3.7) and from the above process. The error was found to be less than 0.01%. The separate program for Simpson's integration is used, so that the user can test the accuracy before he actually starts solving the problem. Once the required number of subdivisions are determined the corresponding adjustment can be made in the main program by changing just one card. Due to the simplicity of the test program its details have not been mentioned herein. In Chapter V the computed values of impedance and current distribution etc. have been found to agree reasonably well with the experiment and we are encouraged to assume a satisfactory convergence of the numerical techniques employed in this program.

CHAPTER IV

FREQUENCY SCALING

4.1 Introduction.

This study is devised to understand the EM coupling effects inside a biological body. The practical aspect however, is to study EM interaction between a human body and a radiating antenna. Theoretically there is no limitation on the size of body as long as the cells are sufficiently small compared to the wavelength; and the number of cells remain under the maximum that can be handled by the computer. As we approach the experimental aspect of this research we find that it would be almost impossible in many cases, to work with the actual dimensions. To illustrate this by an example, consider a system with operating frequency of 30 MHz (wavelength = 10m) and a body of height 1.7 meters with appropriate width and depth. Apart from the fact that the body would be large, a ground plane, that might be considered as being infinite in extent, would be practically impossible to realize for laboratory work. It is possible to cope with this problem by, what is called the "frequency scaling" discussed in the next section. The later part of the chapter deals with the conductivity and dielectric constant of salt solution since a plexiglass container filled with salt solution has been used to replicate biological systems.

4.2 Frequency Scaling.

In order to achieve a geometrical configuration suitable for

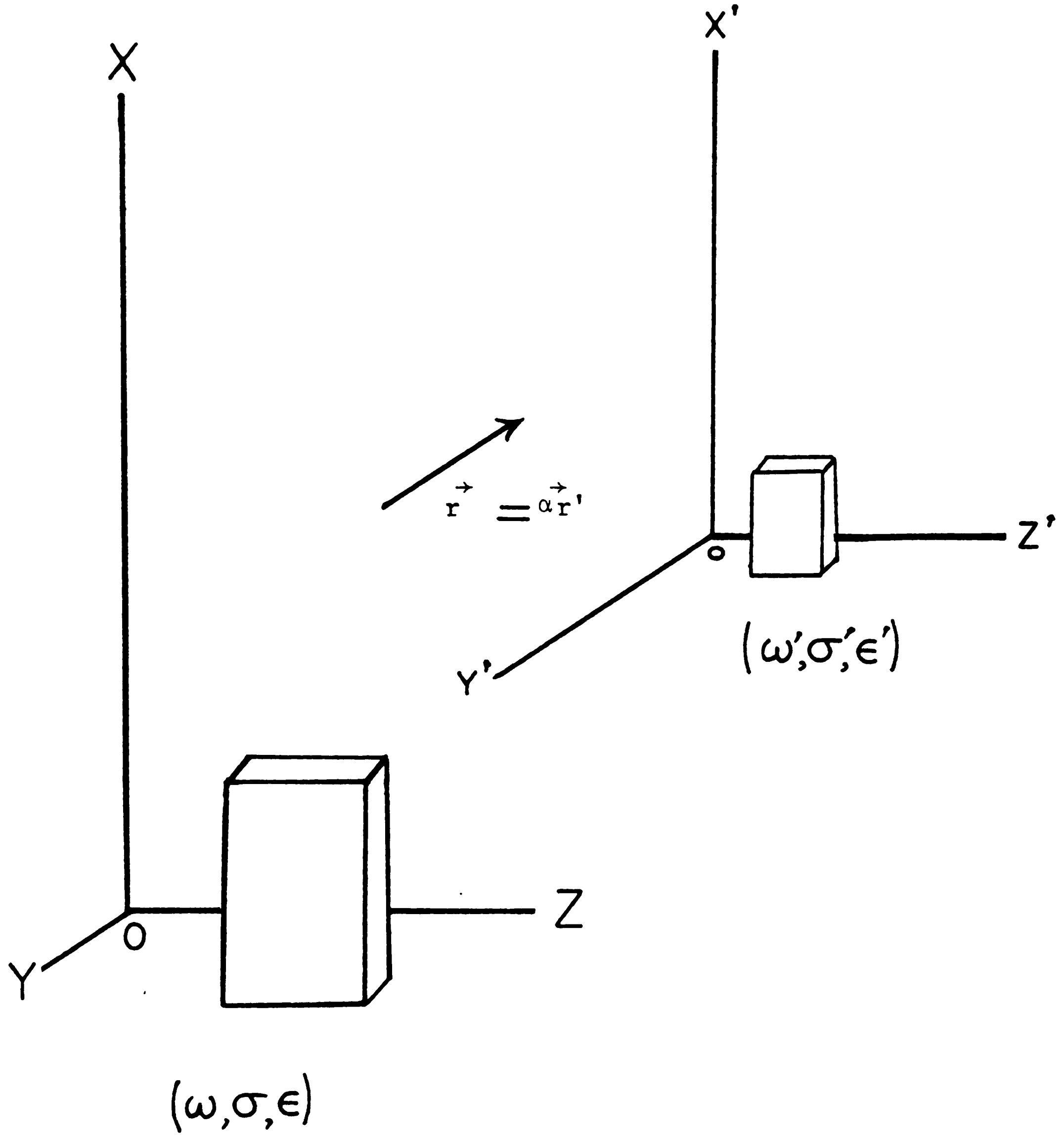

Fig. 4.1. Illustration of frequency scaling.

laboratory purposes and yet retain identical situation as posed by the actual problem, it is necessary to transform the actual coordinate system into a scaled version, such that the field quantities and therefore, the absorbed power remains the same. The following analysis will provide the answer to this problem. It is possible to replicate an EM field configuration in a scaled space by frequency scaling.

Consider the actual system represented by unprimed coordinates and the scaled version by primed coordinates as shown in Fig. 4.1. For a scaling factor α as defined by $\vec{r} = \alpha\vec{r}'$ the operator ∇ in the unprimed system is related to the operator ∇' in the primed system by the relation .

$$\nabla = \frac{1}{\alpha}\nabla'. \tag{4.1}$$

In the actual (unprimed coordinate) system the vector Helmholtz equation for the configuration shown in Fig. 4.1, and for points interior to the body

$$\nabla \times \nabla \times \vec{E}(\vec{r}) - \omega^2\mu_o\overline{\varepsilon}\vec{E}(\vec{r}) = 0 \tag{4.2}$$

where

$$\overline{\varepsilon} = (\varepsilon - j\frac{\sigma}{\omega})$$

is the complex permittivity. The spatial dependence of $\overline{\varepsilon}$ is determined by that of σ and ε of the biological system. Using the relationship of ∇ operators from (4.1) and substituting in equation (4.2) we get

$$\nabla' \times \nabla' \times \vec{E}(\alpha\vec{r}') - \omega^2\alpha^2\mu_o\bar{\varepsilon}\vec{E}(\alpha\vec{r}') = 0 \qquad (4.3)$$

Let

$$\omega' = \alpha\omega, \quad \sigma' = \alpha\sigma \quad \text{and } \varepsilon' = \varepsilon,$$

then

$$\nabla' \times \nabla' \times \vec{E}(\alpha\vec{r}') - \omega'^2\mu_o\bar{\varepsilon}\vec{E}(\alpha\vec{r}') = 0 \qquad (4.4)$$

where $\bar{\varepsilon} = (\varepsilon - j\frac{\sigma'}{\omega'})$.

Now equation (4.4) is exactly the vector Helmholtz equation that would be obtained in the primed coordinate system with ω' and σ' as the angular frequency and conductivity respectively. This means that we can use the scaled version of the true problem with appropriate ω' and σ' for our analysis. Later on the true field quantities may be obtained by using the fact that

$$\vec{E}(\vec{r}) = [\vec{E}(\alpha\vec{r}')]$$

$$\vec{r}' = \vec{r}/\alpha$$

where $\vec{E}(\alpha\vec{r}')$ will be the solution to equation (4.4). In the experiments performed in Chapter V it has been found appropriate to choose a suitable size of the container and work with 600 MHz frequency, since at that stage, we are primarily interested in comparing the theoretical and experimental results.

4.3 Frequency Dependence of Electrical Parameters.

To carry out the experiments with salt solution it is necessary to know its electrical properties which are defined by the conductivity and permittivity. These quantities exhibit strong frequency dependence at frequencies above 1 GHz and hence it is essential to know the values of these parameters at the operating frequency. The details of the molecular theory used to explain the frequency dependence is given in (10), (11), and (12). We have found it sufficient to incorporate the emperical results given by those sources and have used their experimental data to our advantage.

Total or effective conductivity which determines the dissipation of energy in salt solution is composed of two parts, namely, the ionic conductivity and the dipolar or dielectric conductivity. Ionic conductivity is caused by a lateral flow of ions and is the dominant part of the total conductivity at frequencies below 300 MHz. At higher frequencies the dielectric conductivity, which is an apparent conductivity arising from viscous retardation of induced rotation of the modecular water dipole, also becomes a contributing part. In all such cases, total conductivity will be the sum of ionic and the dielectric conductivity. The method for determining the total conductivity and complex permittivity of salt solution is given below.

Let ε_w denote the complex permittivity of distilled water. If this quantity is defined by its real and imaginary parts as $\varepsilon_w = \varepsilon' - j\varepsilon''$ then, $\varepsilon' = \varepsilon_o \varepsilon'_r$ and $\varepsilon'' = \varepsilon_o \varepsilon''_r$ where

$$\varepsilon'_r = \frac{\varepsilon_s - 4\cdot 9}{1+(\omega\tau)^2} + 4.9 \qquad (4.5)$$

$$\varepsilon''_r = \frac{(\varepsilon_s - 4\cdot 9)\omega\tau}{1+(\omega\tau)^2} , \qquad (4.6)$$

ε_s and τ are obtained from the Figs. 4.2 and 4.3. The former is called the static-dielectric-constant and the later is called relaxation time parameter.

When salt is added to distilled water, sodium and chloride ions produce what is called the ionic conductivity. The real permittivity of salt solution remains the same as that of water. The complex permittivity ε of salt solution is therefore

$$\varepsilon = \varepsilon' - j\varepsilon'' - j\frac{\sigma_i}{\omega} , \qquad (4.7)$$

σ_i is the ionic conductivity and is obtained from Fig. 4.4.

We can rewrite ε, to identify the total conductivity explicitly in equation (4.7) as follows

$$\varepsilon = \varepsilon' - \frac{j}{\omega} (\sigma_i + \omega\varepsilon''). \qquad (4.8)$$

Total conductivity σ_t is identified by the expression in parenthesis.

$$\sigma_t = \sigma_i + \omega\varepsilon'' = \sigma_i + \omega\varepsilon_o\varepsilon''_r . \qquad (4.9)$$

The frequency dependence of ε' and σ_t can be determined from equations

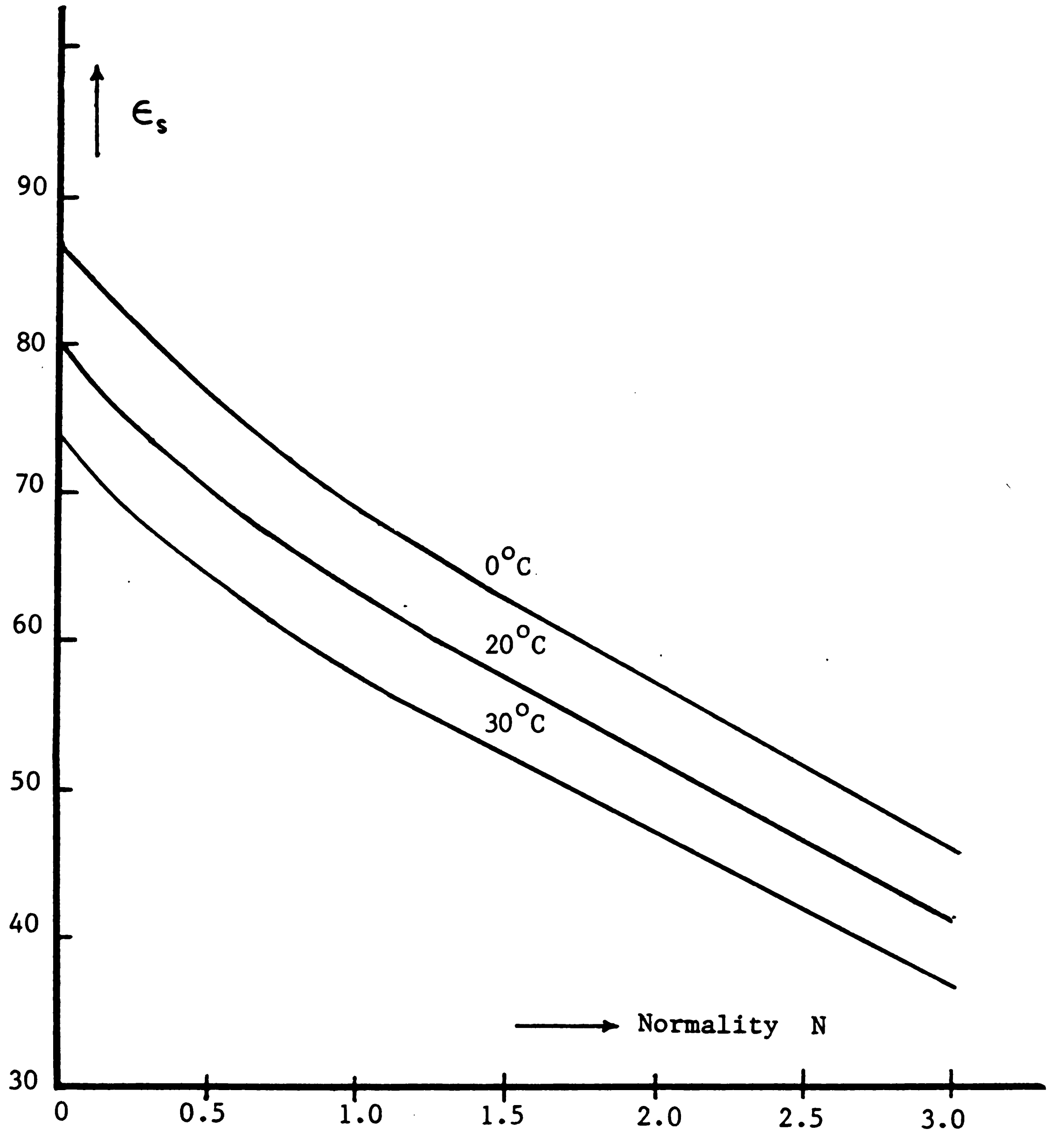

Fig. 4.2. Static-dielectric-constant ϵ_s versus normality of saline solution.

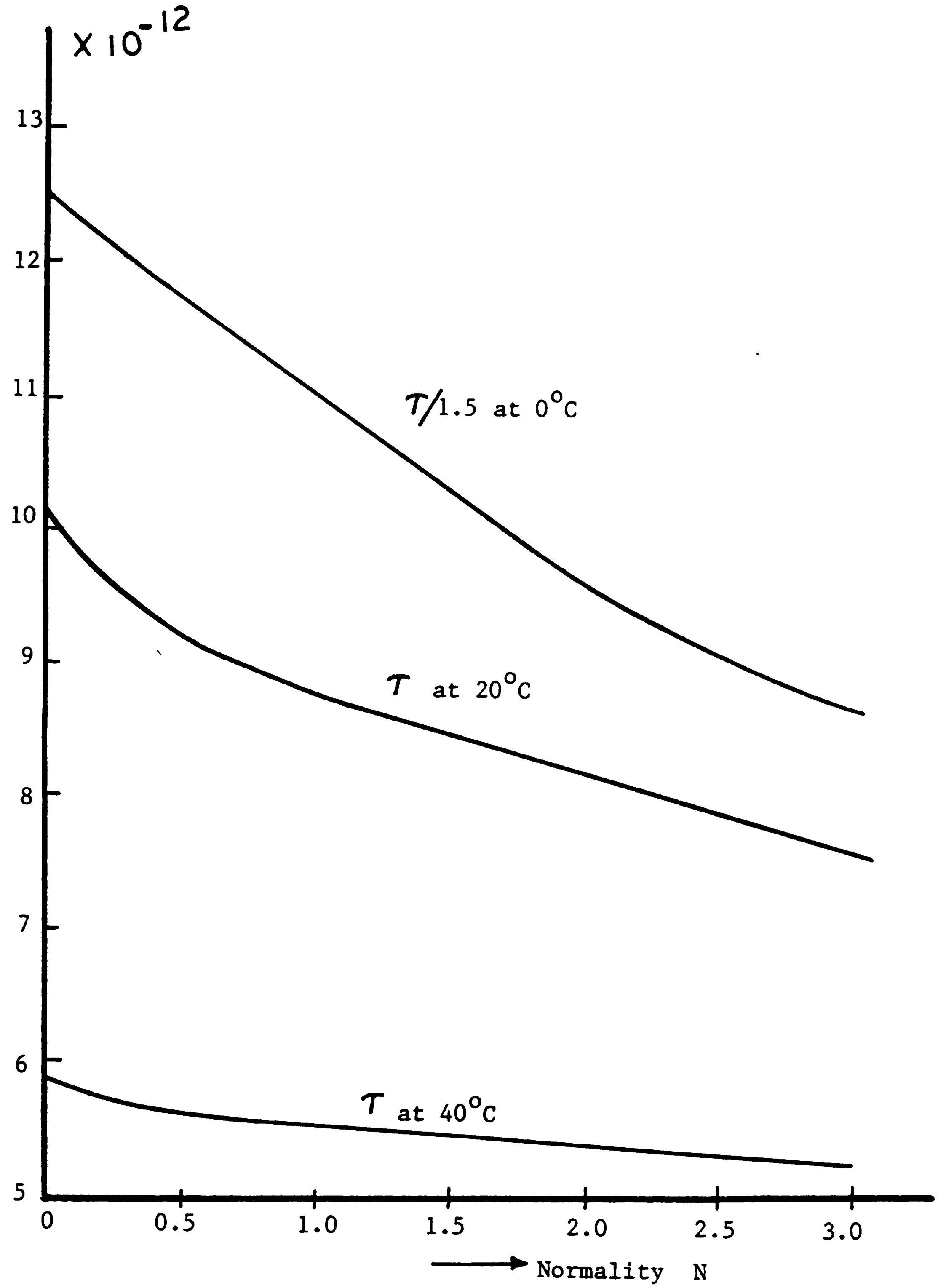

Fig. 4.3. Relaxation time parameter τ (secs) versus normality of saline solution.

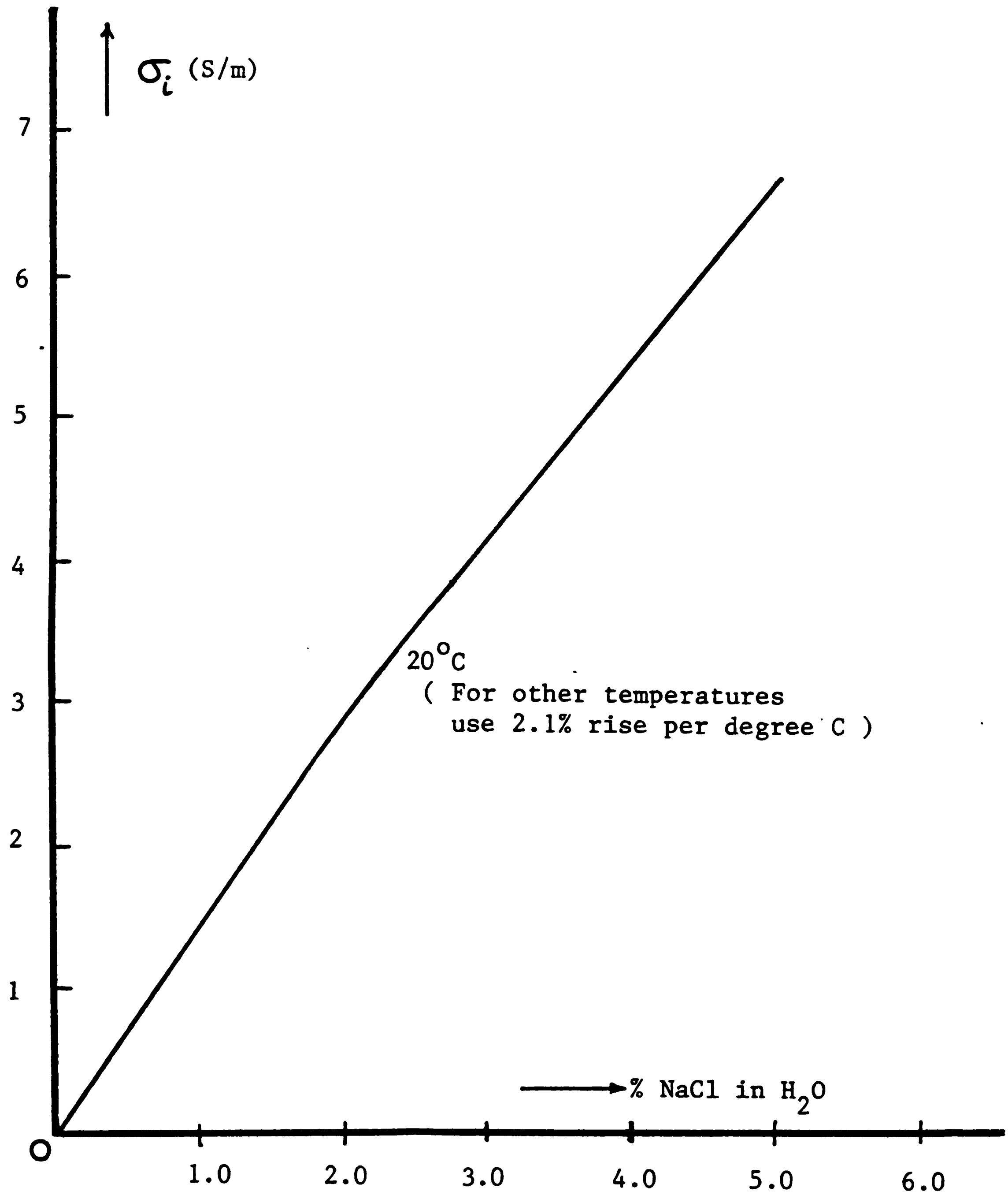

Fig.4.4. Ionic conductivity of the saline solution σ_i vs. percentage of NaCl in distilled water by wt.

(4.5) and (4.9). Whenever conductivity is referred to, it is understood that we are referring to total conductivity σ_t of the medium. Care must be taken to enter proper parameter into the computer program when working with such mediums. As a final remark, graphs shown in Figs. 4.2, 4.3 and 4.4 have been obtained by the experimental data given by Saxton and Lane (12).

CHAPTER V

EXPERIMENTAL VERIFICATION OF THEORETICAL RESULTS

5.1 Introduction.

In this chapter experimental evidence to support the theoretical development given in Chapters II and III is given. The first step in this connection is to choose a suitable laboratory model. A monopole antenna over an infinite conducting ground plane is undoubtedly the best choice since not only the terminal zone effects are reduced but also feeding transmission lines do not interfere with the measuring apparatus. It must be kept in mind that this model when transformed to some actual situation by frequency scaling, must represent a realistic case. The model can not be too small because of practical difficulties encountered, especially when making electric field measurements inside the body. The model is of plexiglass and has a 2.0 - 2.5 mm thick copper plate base so that once filled with salt solution and sealed, it can be moved from point to point on the conducting plane. Use of copper plate however restricts us to the use of lower frequencies since at very high frequencies the plate thickness will become a source of disturbance. On the other hand use of lower frequencies will require a large ground plane which will become impractical for laboratory work. All these factors are to be kept in mind when making a choice of frequency, size of container and the conductivity.

There are essentially three aspects to be verified experimentally. Firstly, we attempt to verify the perturbation in the input impedance of the antenna from the free-space value; secondly, we want to verify the current distribution inside the body; thirdly, we want to verify the induced electric field distribution. In each of the above experiments performance of the apparatus is tested by first doing experiments in free-space and later on with the body. The three aspects above have been discussed in seperate sections however the antenna-body system, unless specified, is the same for all experiments and is discussed next.

5.2 The Antenna-Body System

The antenna-body system chosen for the experimental verification of theoretical analysis is given in Fig. 5.1. The dimensions of the container are to be kept as (12.5 x 6.25 x 1.5625) cms. The operating frequency has been chosen to be 600 MHz giving a free-space wavelength of 50 cms. A 0.5 N sodium cholride solution has been used throughout these experiments. Using the graphs of Chapter IV, the conductivity is obtained as 4.4 S/m and the dielectric constant (real) of 71.00 at a temperature of 20° C. If this model is assumed to be a scaled version of an actual problem, then a scale factor of $\alpha = 10$ gives a situation at least of the same order as that given by a radiating antenna of 60 MHz. The actual height of an operator is usually 1.7 m and conductivity at 60 MHz is approximately 0.7 S/m, assuming it is a homogeneous system. By the above system we get a height of 1.25 m and a conductivity of 0.44 S/m which are of the same order of magnitude.

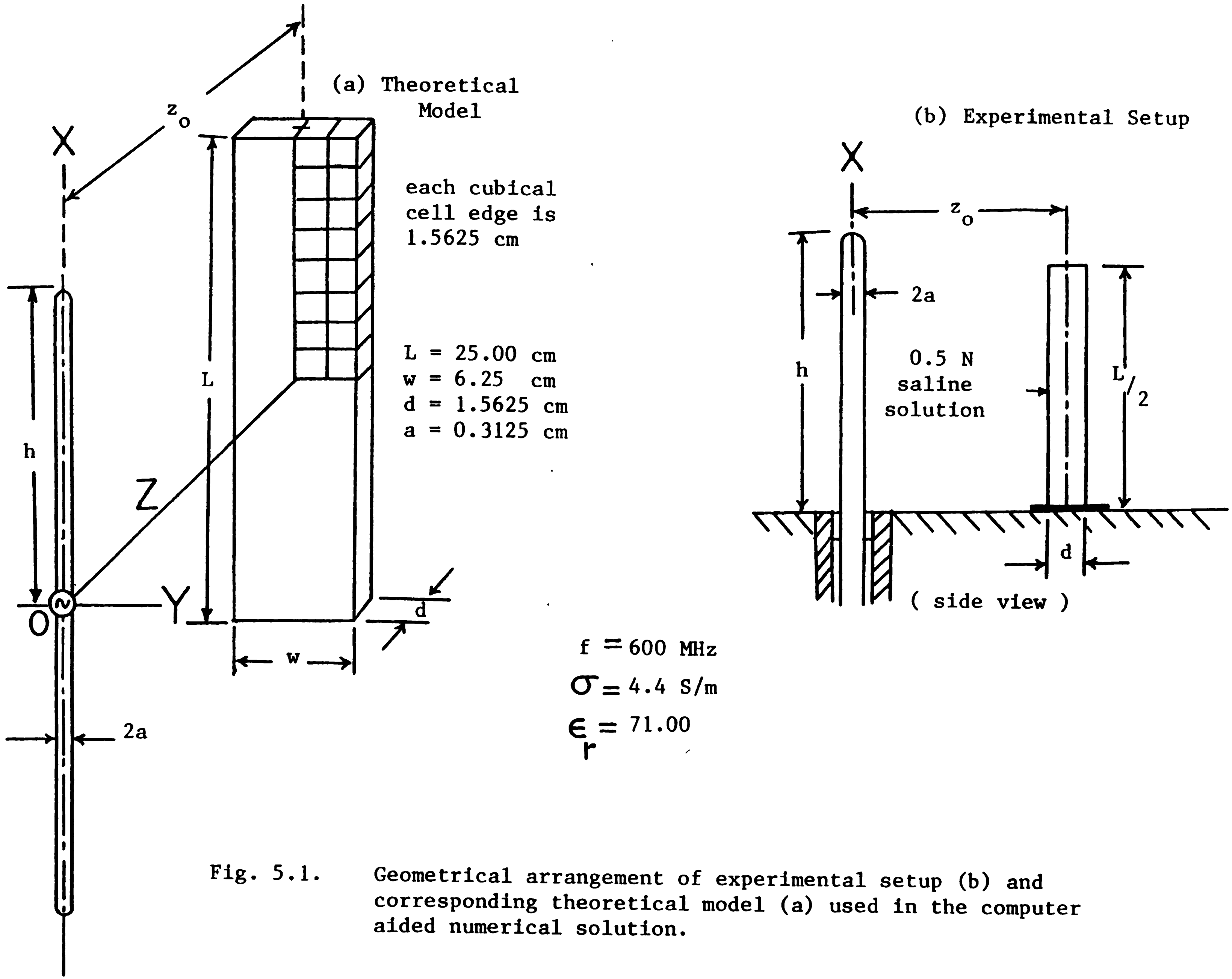

Fig. 5.1. Geometrical arrangement of experimental setup (b) and corresponding theoretical model (a) used in the computer aided numerical solution.

The computer model for this system is obtained by using image theory. The situation is shown in Fig. 5.1 and has a 4-quadrant symmetry. It is necessary to maintain this kind of symmetry while the experiments are being performed. Also the upper right quadrant is divided into 16 cells, each cell being 1.5625 cm. cube. The antenna height "h" is divided into 10 segments plus the input segment, for $h < \lambda_o/4$ and into 20 segments plus the input segment for $h > \lambda_o/4$. Even though a higher number of cells and segments could have been chosen this would have become an uneconomical choice. The results of theory and experiment have shown that these values do provide a satisfactory convergence of the solution. In all experiments, with the exception of final part of section 5.5, the body model described above has been used.

5.3 Input Impedance Measurements.

In this section experimental techniques used for the measurement of input impedance of the antenna are first discussed. Following this, is a brief discussion regarding the free-space impedance measurement, and then the experiment with the body, is explained.

5.3.1 Experimental Setup.

The apparatus comprise of a microwave Oscillator, E-H probe guide, vector voltmeter and anechoic chamber. The roof of the chamber contains sheet aluminum plate while other sides are completely covered by microwave absorbers which prevent back scattering. The antenna is formed by extending the central conductor of the 50 Ω characteristic impedance co-axial waveguide (WG), which terminates at the ground plane

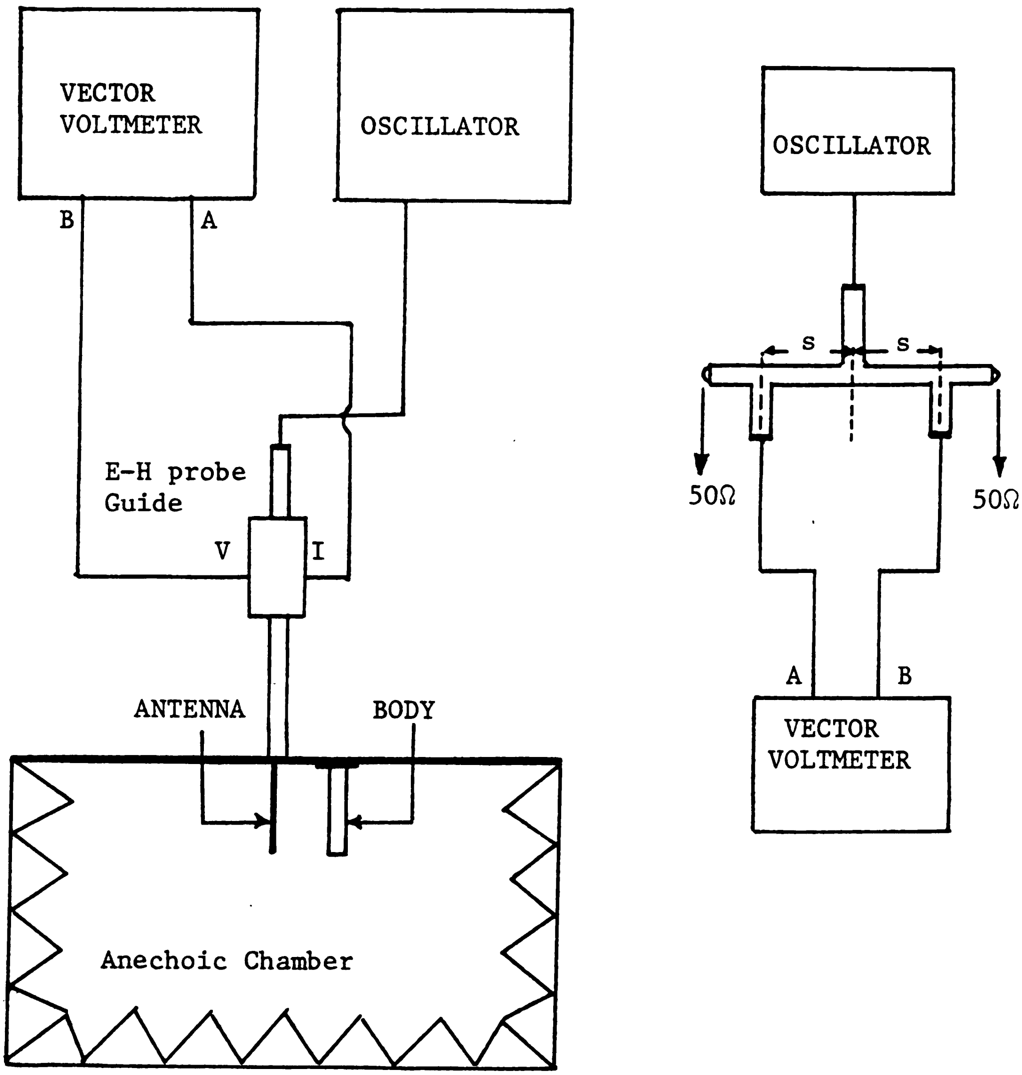

(a) (b)

Fig. 5.2. Experimental setup for measurement of the input impedance of the antenna by using vector voltmeter.

of the chamber. The schematic diagram is depicted in Fig. 5.2 (a). Extension of the central conductor is made by making a threaded hole along the axis of the conductor where a copper rod can be screwed into, to form the linear monopole antenna over ground plane.

The vector voltmeter in conjunction with the E-H probe guide gives an extremely efficient method of impedance measurement. This meter is a very sensitive device which can measure the voltages at two input ports labeled "A" and "B" and simultaneously measures the phase of the signal at B with respect to A. Details of the E-H probe guide are given elsewhere (13). The probe guide is inserted between the WG system feeding the load and becomes a part of the 50 Ω wave guide system. We will call the location along the WG at which the E and H field probes are located as probe-section. Signal proportional to the voltage at probe-section appears at the terminal marked B. Signal proportional to the current appears on the terminal marked A. The ratio of these two signals, their phase and the "calibration factor" of the E-H probe guide will give the impedance at the probe-section. Calibration factor $\overline{K}$ is a complex number. It is a constant at a given frequency and is determined experimentally. Effects of probes' geometries, their sensitivities, etc. are contained implicitly in this constant. The impedance at the probe-section is transformed to the load point by using transmission line theory. A brief description of determining an unknown load impedance is given in the following paragraph.

5.3.2 Method of Measurement of Load Impedance.

1. Impedance at probe-section (Z_p): Assume that the calibration factor $\overline{K}$ is known and the following measurements recorded on the vector

Voltmeter.

V_a = Voltage amplitude recorded at port A (volts)

V_b = Voltage amplitude recorded at port B (volts)

Θ_b = Phase angle of B with respect to A recorded on the phase meter (degrees).

Let $\overline{V}_b = V_b \underline{|\Theta_b}$. V_a is a real number. The impedance at the probe-section is

$$Z_p = (\frac{\overline{V}_b}{V_a})\,\overline{K} \text{ ohms.} \tag{5.1}$$

2. Impedance at load point (Z_L): Assuming that the electrical length from the probe-section to the load is known equal to L cms then

$$Z_L = Z_c(Z_p - jZ_c \tan kL)/(Z_c - jZ_p \tan kL) \quad \text{ohms} \tag{5.2}$$

where

$k = \frac{2\pi}{\lambda}$, λ = wavelength in the guide (cms) and

Z_c = Characteristic Impedance = 50 ohms.

In (5.2) knowledge of tan kL is sufficient and electrical length L need not be computed exclusively.

3. Steps to determine an unknown load impedance:

(i) First we check the amplitude and phase measurement capability of the vector voltmeter. For this see Fig. 5.2(b). By this arrangement the amplitude measured at A and B must be equal and the phase difference should be zero.

(ii) Determination of $\overline{K}$: The end of the E-H probe guide marked LOAD is terminated by a 50 Ω load. E-H probe guide is thus matched. V_a, V_b and Θ_b are recorded. Assuming that a perfect match exists, the impedance Z_p should be 50 Ω. Hence letting Z_p = 50 Ω in (5.1) we get

$$\overline{K} = 50 \left(\frac{V_a}{V_b}\right) \underline{|-\Theta_b} \tag{5.3}$$

(iii) Determination of tan kL: The E-H probe guide is placed in the system and a perfect short is made at the load end. (In case of the antenna as load, a copper plate was screwed at the end of the feeding WG and care was taken to ensure a perfect contact between the inner and outer conductor). V_a, V_b and Θ_b are recorded. Then

$$\tan kL = \frac{Z_p}{jZ_c} \tag{5.4}$$

where Z_p is obtained from (5.1) and must come out as a purely imaginary number in this case.

(iv) Any unknown impedance at the load end can now be determined by recording V_a, V_b and Θ_b, computing Z_p from (5.1) and then finding Z_L from (5.2).

5.3.3 Free-space Impedance Measurement.

Before doing measurements in presence of the body, it was necessary to test the performance of the entire system at the operating frequency of 600 MHz. This was accomplished by comparing the theoretical and

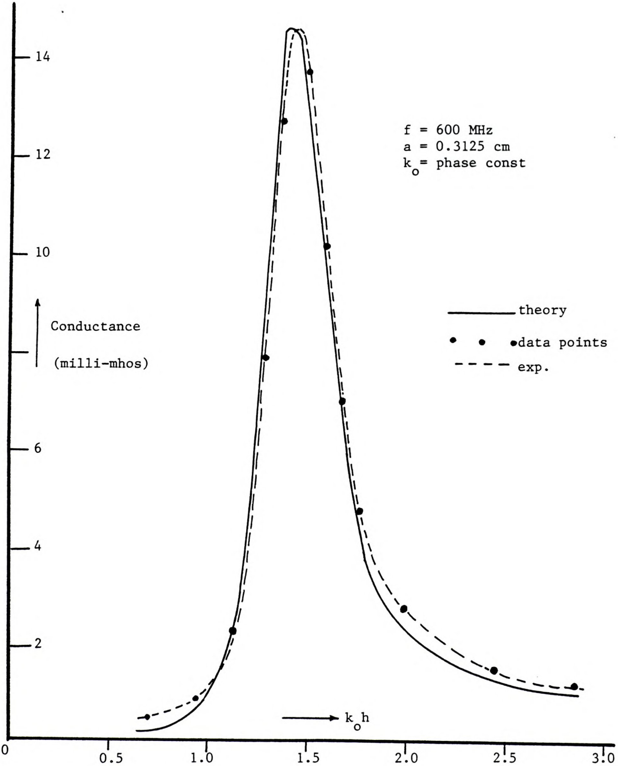

Fig. 5.3. Input conductance of the antenna as a function of $k_o h$, where h is the height of antenna.

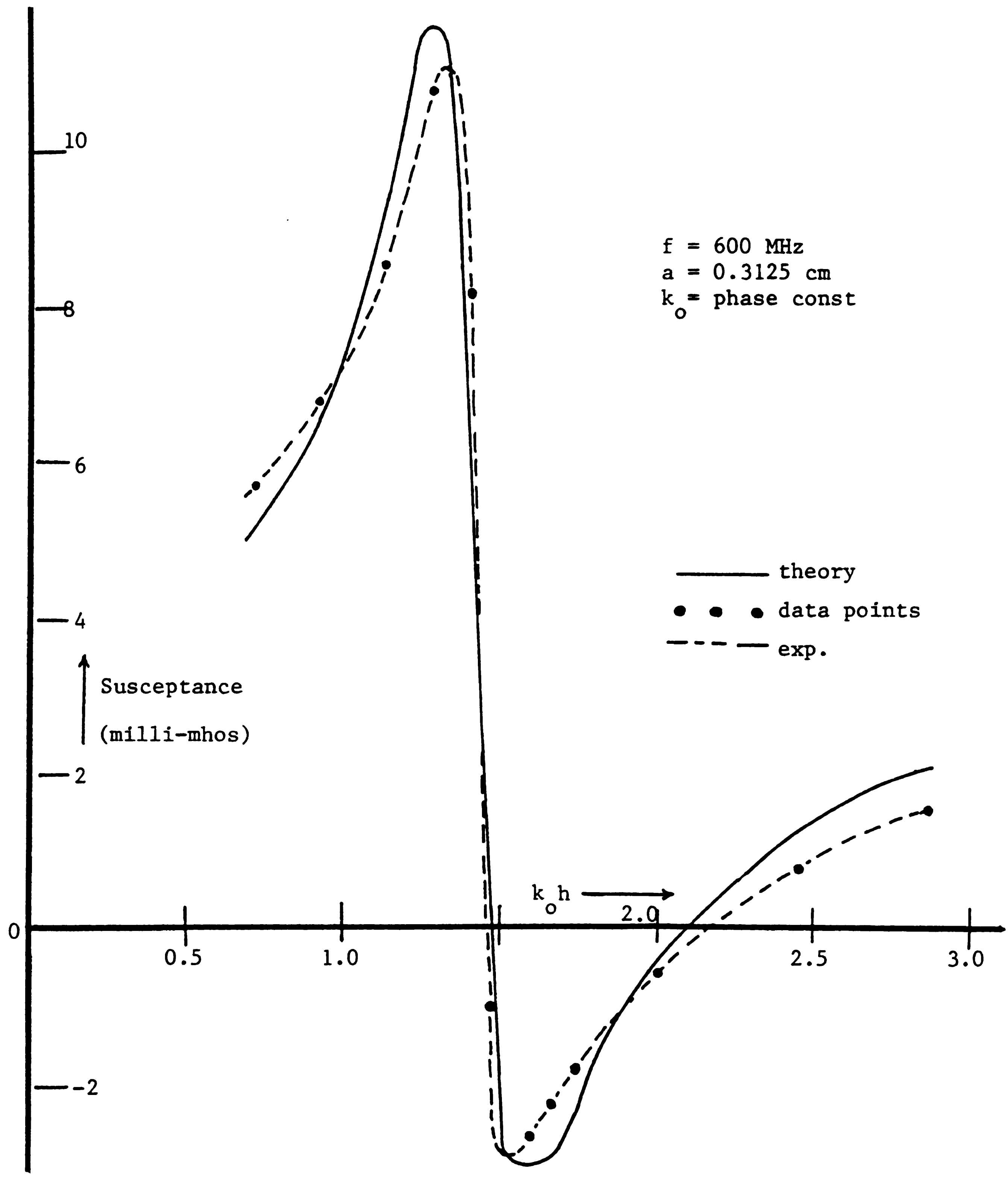

Fig. 5.4. Input susceptance of the antenna as a function of $k_o h$, where h is the height of antenna.

experimental input impedances of the antenna. By virtue of this process the extent of errors, if any occured due to the use of a finite ground plane, could be determined. The program ZFREE discussed in Chapter VII was employed to determine the theoretical input impedances of antennas of various heights. The graphs of Fig. 5.3 and 5.4 were obtained. There was a good agreement between the theory and experiment over a wide range of the heights of the antennas. Our next step was to measure the input impedance in presence of the saline container.

5.3.4 Input Impedance in Presence of the Body.

The container was placed in front of the antenna at various locations and corresponding input impedances of the antenna were determined. Care was taken to ensure that the system under consideration maintains a four quadrant symmetry as required by the computer model. Perturbations in the input impedance are plotted as a function of the spacing between the antenna and the container. The observations were made with four antennas of different heights and the spacing was varied from 3 cms to about 60 cms in each case. The comparison between the theoretical and experimental results is shown in Fig. 5.5 to 5.8.

Fairly good agreement is obtained at spacings beyond 10 cms which is a fifth of the wavelength. In the immediate neighborhood theoretical values may not be very accurate since the field distribution in that region is quite complicated and a rapidly varying function of the spacing. In this region the order of magnitude and the trend in variations are in agreement. A short account on the possible sources of errors is given at the end of this chapter. It is emphasized at

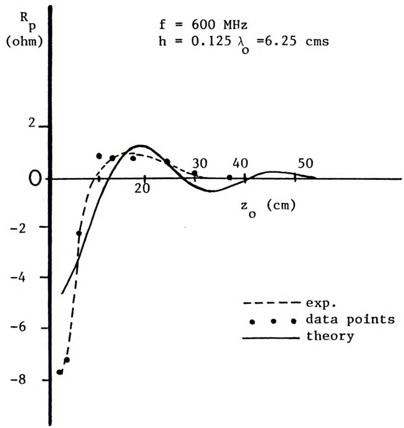

(a) Perturbation R_p to antenna resistance

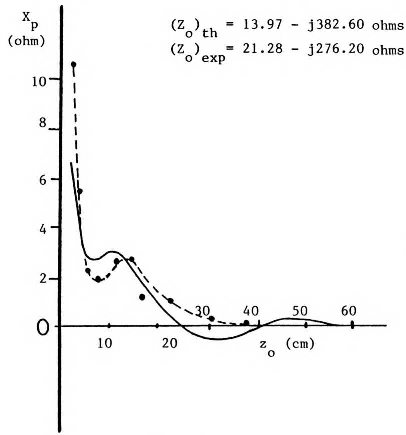

(b) Perturbation X_p to antenna reactance

Fig. 5.5. Perturbation($Z_p = R_p + jX_p$) in input impedance versus the spacing(z_o) between the antenna and the body.

$Z_p = Z_{in} - Z_o$, Z_{in} = input impedance of the antenna due to coupling and Z_o= the free-space impedance

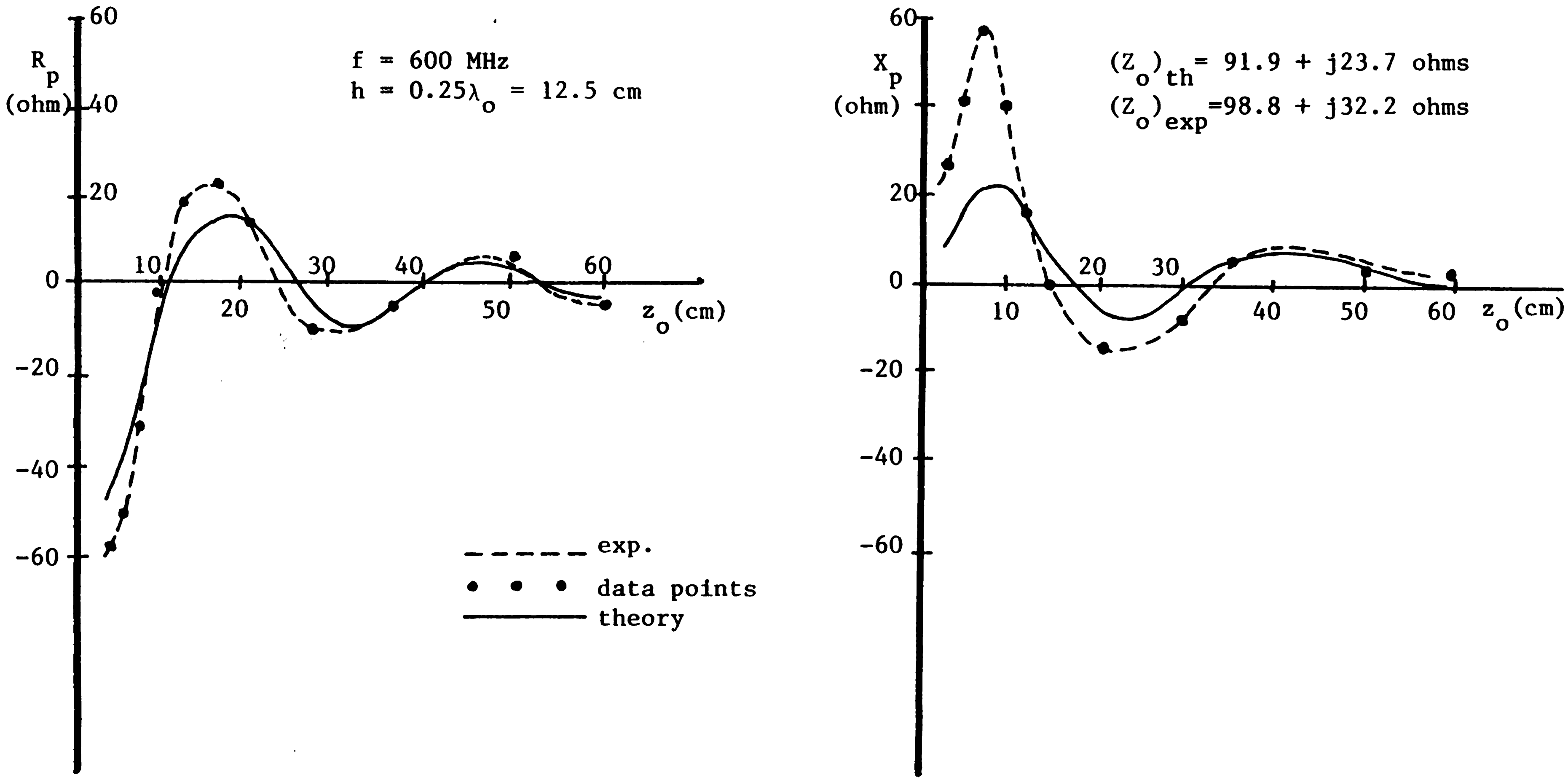

(a) Perturbation R_p to antenna resistance

(b) Perturbation X_p to antenna reactance

Fig. 5.6. Perturbation ($Z_p = R_p + jX_p$) in input impedance versus the spacing(z_o) between the antenna and the body.
$Z_p = Z_{in} - Z_o$, Z_{in}= input impedance of the antenna due to coupling and Z_o is the free-space impedance

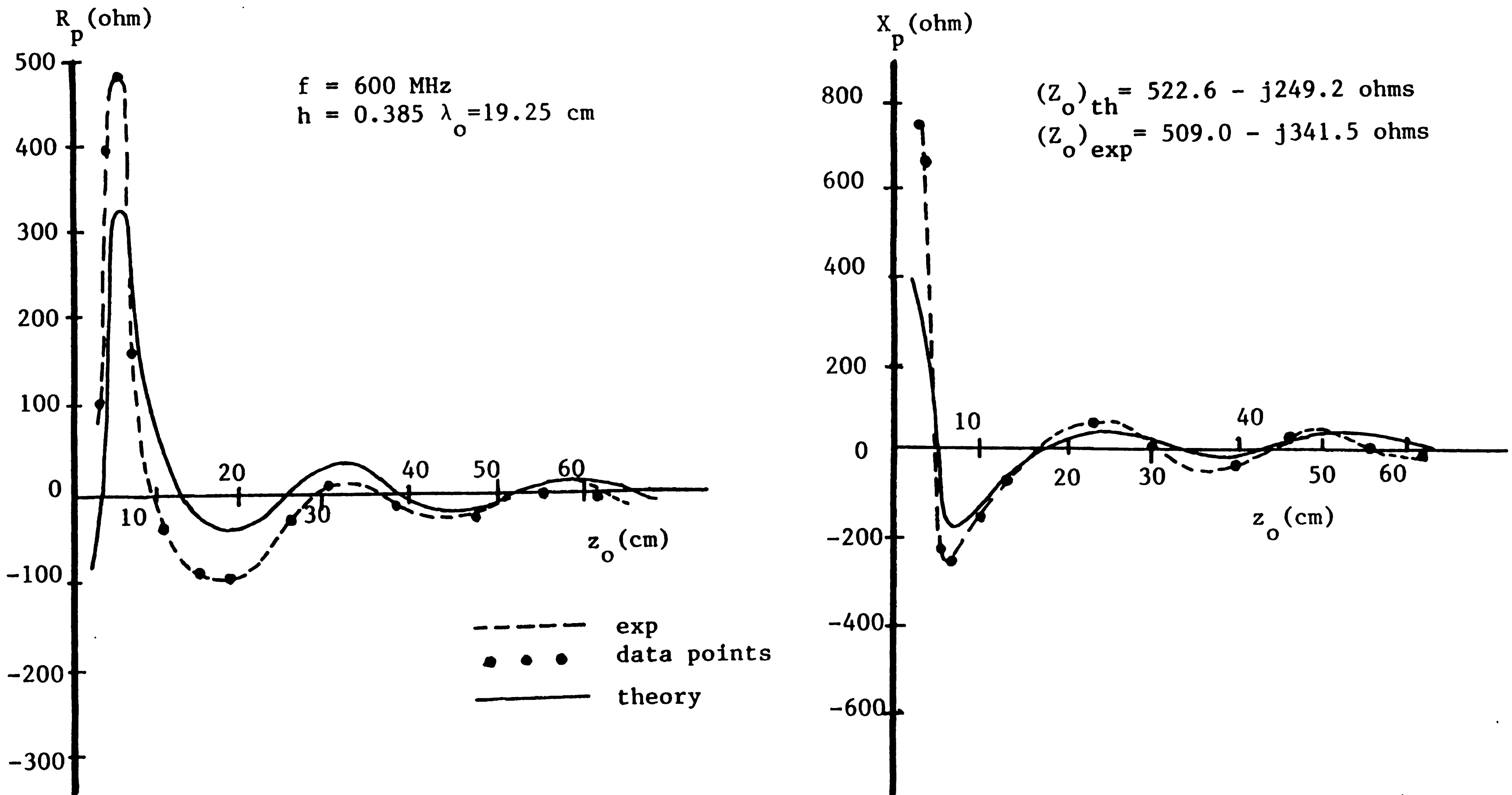

(a) Perturbation R_p to antenna resistance (b) Perturbation X_p to antenna reactance

Fig. 5.7. perturbation ($Z_p = R_p + jX_p$) in input impedance versus the spacing (z_o) between the antenna and the body.
$Z_p = Z_{in} - Z_o$, Z_{in} = the input impedance of the antenna due to the coupling and Z_o is the free-space impedance

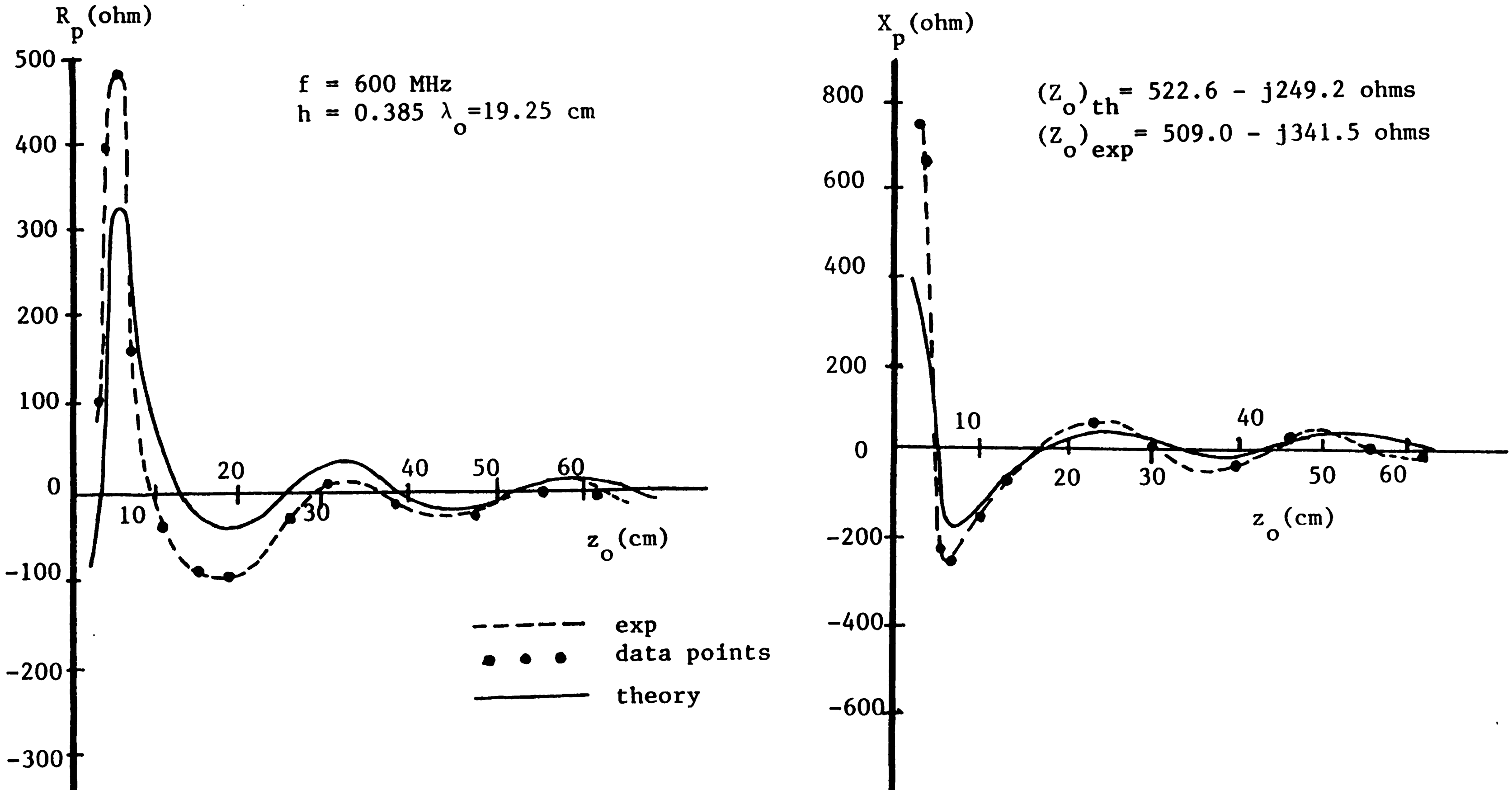

(a) Perturbation R_p to antenna resistance

(b) Perturbation X_p to antenna reactance

Fig. 5.7. perturbation ($Z_p = R_p + jX_p$) in input impedance versus the spacing (z_o) between the antenna and the body.
$Z_p = Z_{in} - Z_o$, Z_{in} = the input impedance of the antenna due to the coupling and Z_o is the free-space impedance

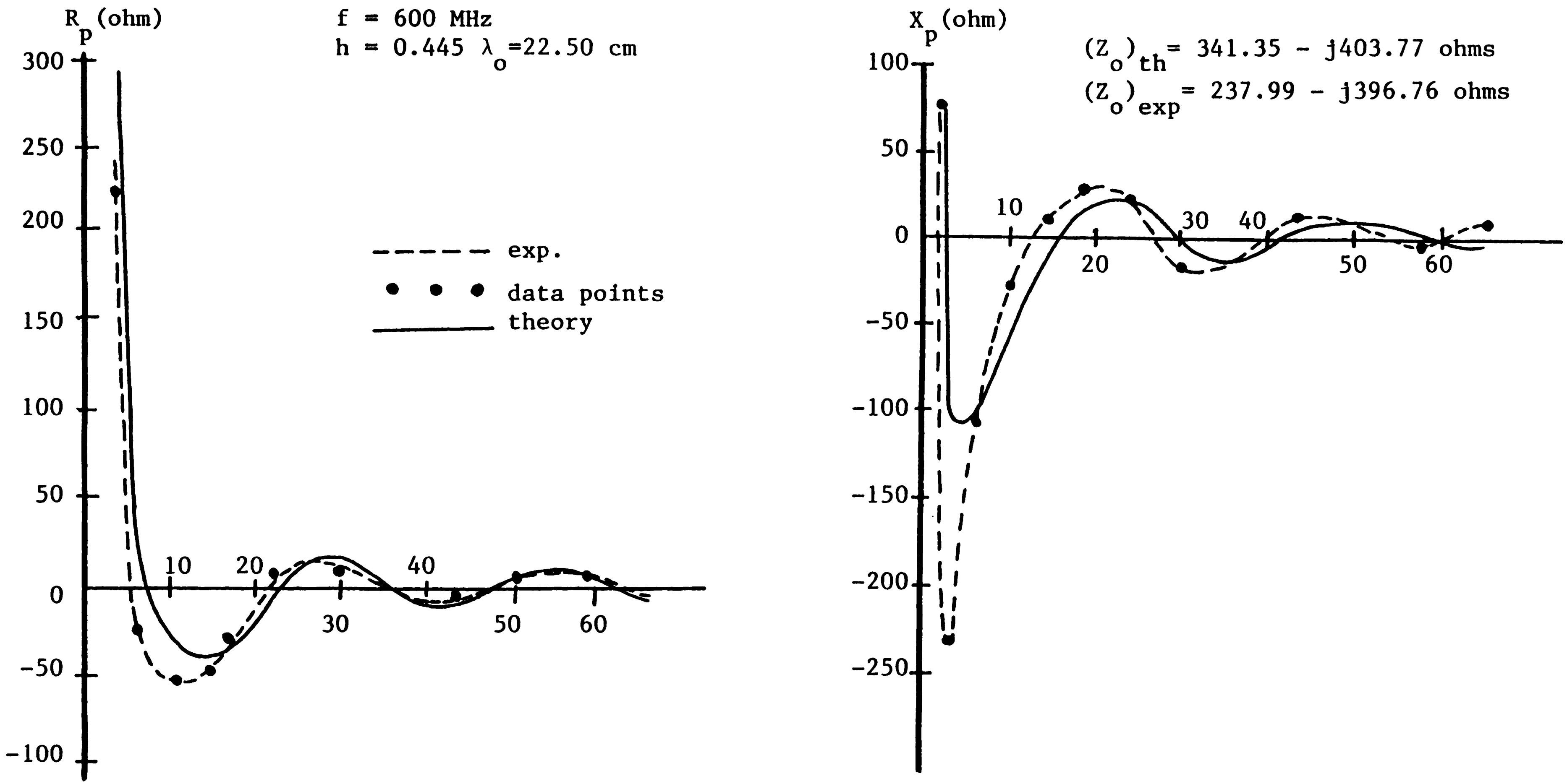

(a) Perturbation R_p to antenna resistance

(b) Perturbation X_p to antenna reactance

Fig. 5.8. perturbation ($Z_p = R_p + jX_p$) in input impedance versus the spacing(z_o) between the antenna the body.
$Z_p = Z_{in} - Z_o$, Z_{in} = the input impedance of the antenna due to coupling and Z_o = the free-space impedance

this point that E-H probe guide in conjunction with vector voltmeter has proven to be the most reliable apparatus for such measurements.

5.4 Measurement of Current Distribution.

In this section we are to determine the theoretical and experimental current distributions on the antenna. Current distribution on the antenna is best determined by using a magnetic field probe (H-probe). The signal sent to the measurement device is proportional to the magnetic field on the surface of the antenna and therefore, to the current at that location.

5.4.1 Experimental Setup

In this experiment the apparatus comprise of the microwave Oscillator, the vector voltmeter and a specially designed antenna which carries the H-probe. The setup is shown in Fig. 5.9 (a) and the waveguide, the antenna and the H-probe are shown in Fig. 5.9 (b). The antenna is made out of a hollow conductor with a slot running along the entire length of its surface. The rod can be moved back and forth to get different antenna heights. The probe moves in the slot and it is kept from touching the antenna conductor by a plastic spacer. This spacer also keeps the probe at a fixed level from the surface of the antenna which is extremely important. An unstable probe will cause errors. The H-probe is a very delicate device and care should be taken when moving it back and forth. The adjustable shorting ring, even though moveable between the inner and outer conductor of the guide, maintains perfect contact with these conductors and insures a perfect short. This ring is used for tuning purposes. The probe signal is

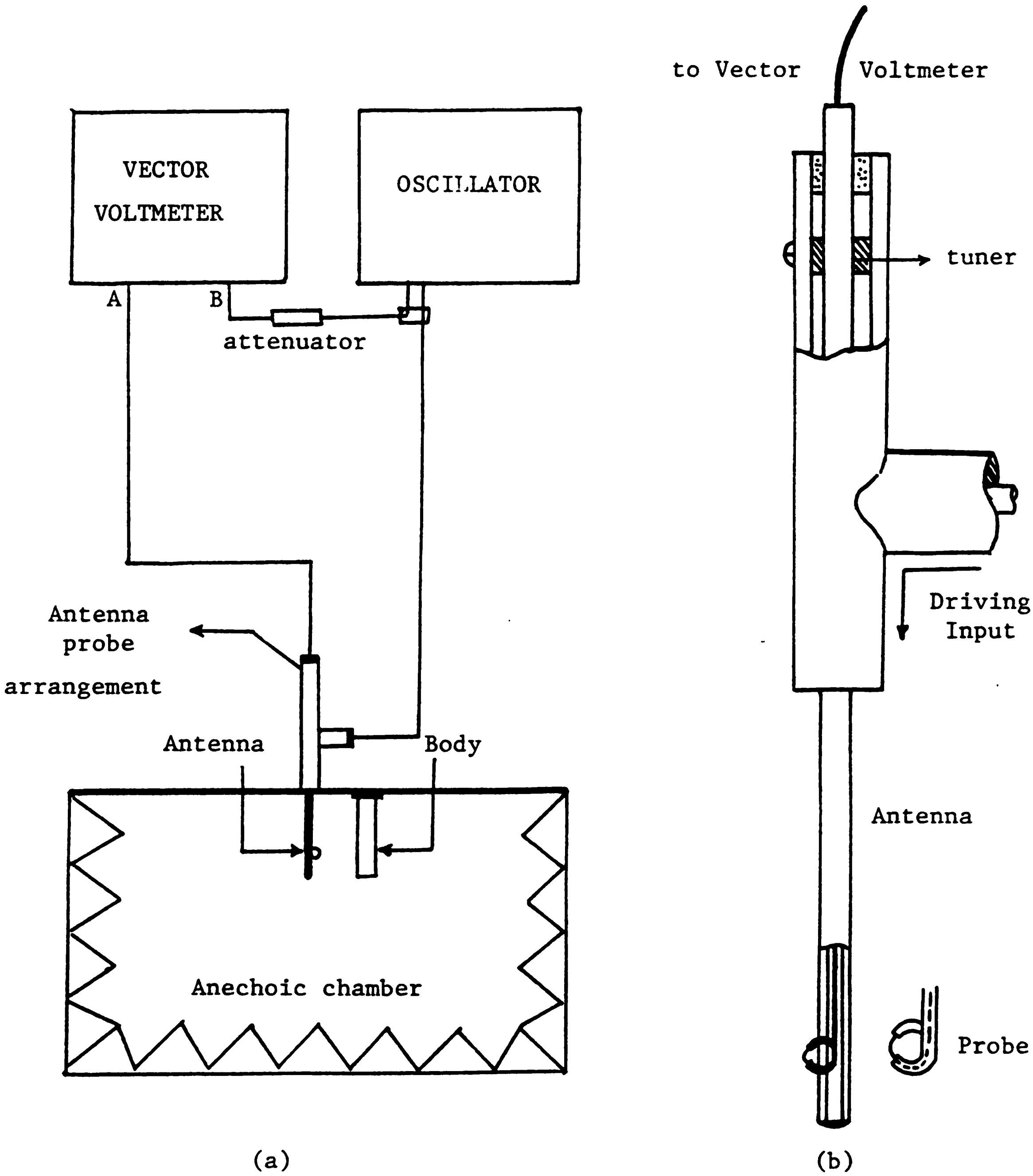

Fig. 5.9. Experimental setup for measurement of the current distribution along the antenna.

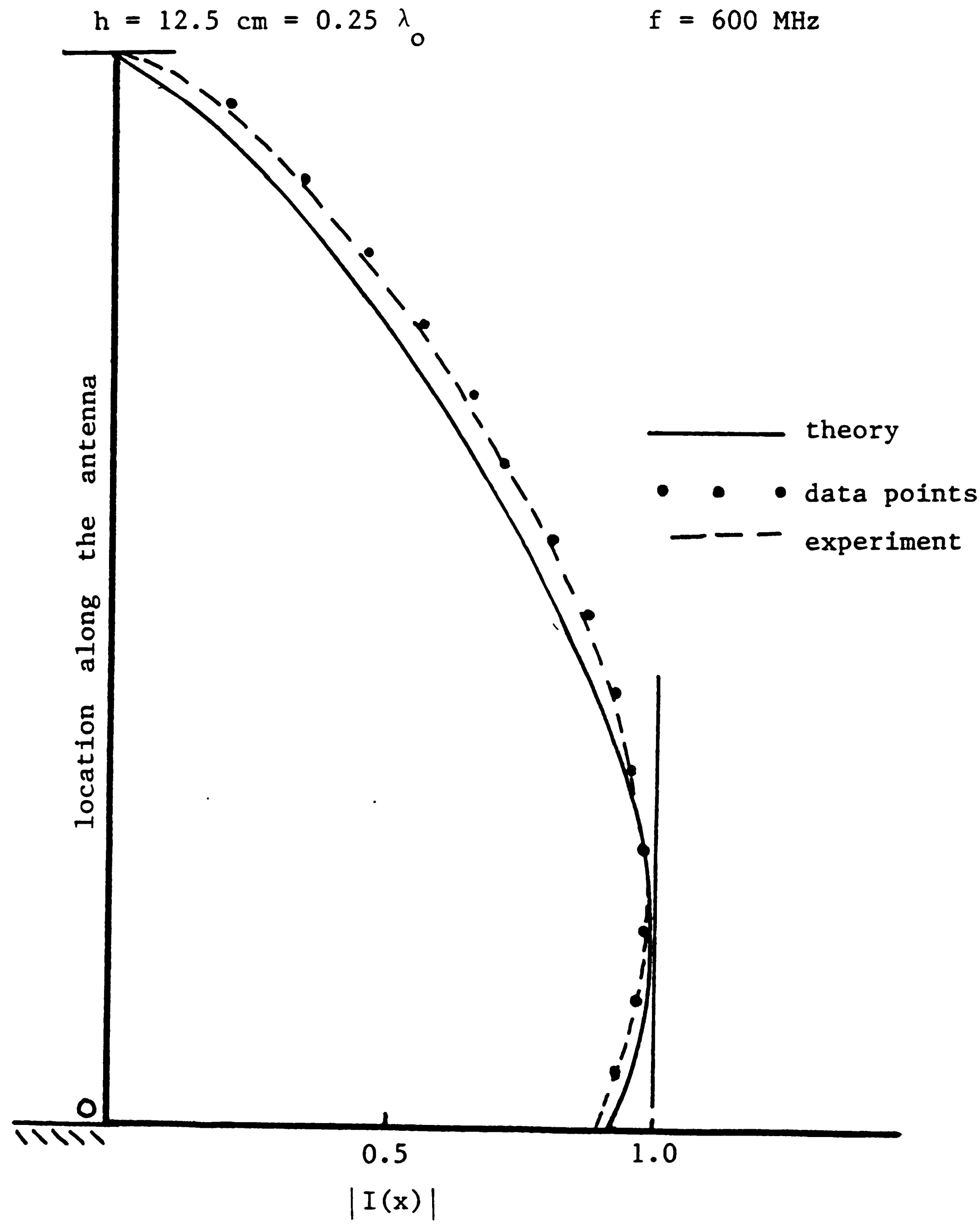

Fig. 5.10. Free-space current distribution on the antenna of height $h = 0.25\ \lambda_o$. Theoretical and experimental values have been normalized by their respective maximum values.

taken to the vector voltmeter at port-B and a reference signal after being attenuated, is applied to port A. The attenuator is a precautionary measure.

5.4.2 Free-space Current Distribution.

As in the previous experiments it was found essential to compare the theory and experiment regarding current distribution on the antenna. These measurements were made with three different lengths of the antenna. The theoretical distributions were determined from ZFREE. The results are shown in Fig. 5.10 to 5.12 and agree quite well. The values given in these figures are normalized values $I(x)/I_{max}$.

5.4.3 Current Distribution in Presence of Body.

Our next step was to determine the current distribution on the antenna when the container is placed in its near-zone. The body was placed at a distance of 4.0 cms and the currents recorded for each of the three cases. The graphs for these are given in Fig. 5.13 to 5.15. The free-space current distribution has been redrawn to show the marked difference in the current distribution on the antenna in free-space and when a volume conductor is placed in its near-zone. The current values have been normalized with the maximum value of the corresponding free-space distribution. In this way even though the role of input impedance perturbation is emphasized, the curves are spread apart and easily discernable. The theoretical and experimental results are in very good agreement. A brief discussion on the sources of errors that may have been encountered is given in the last section of this chapter.

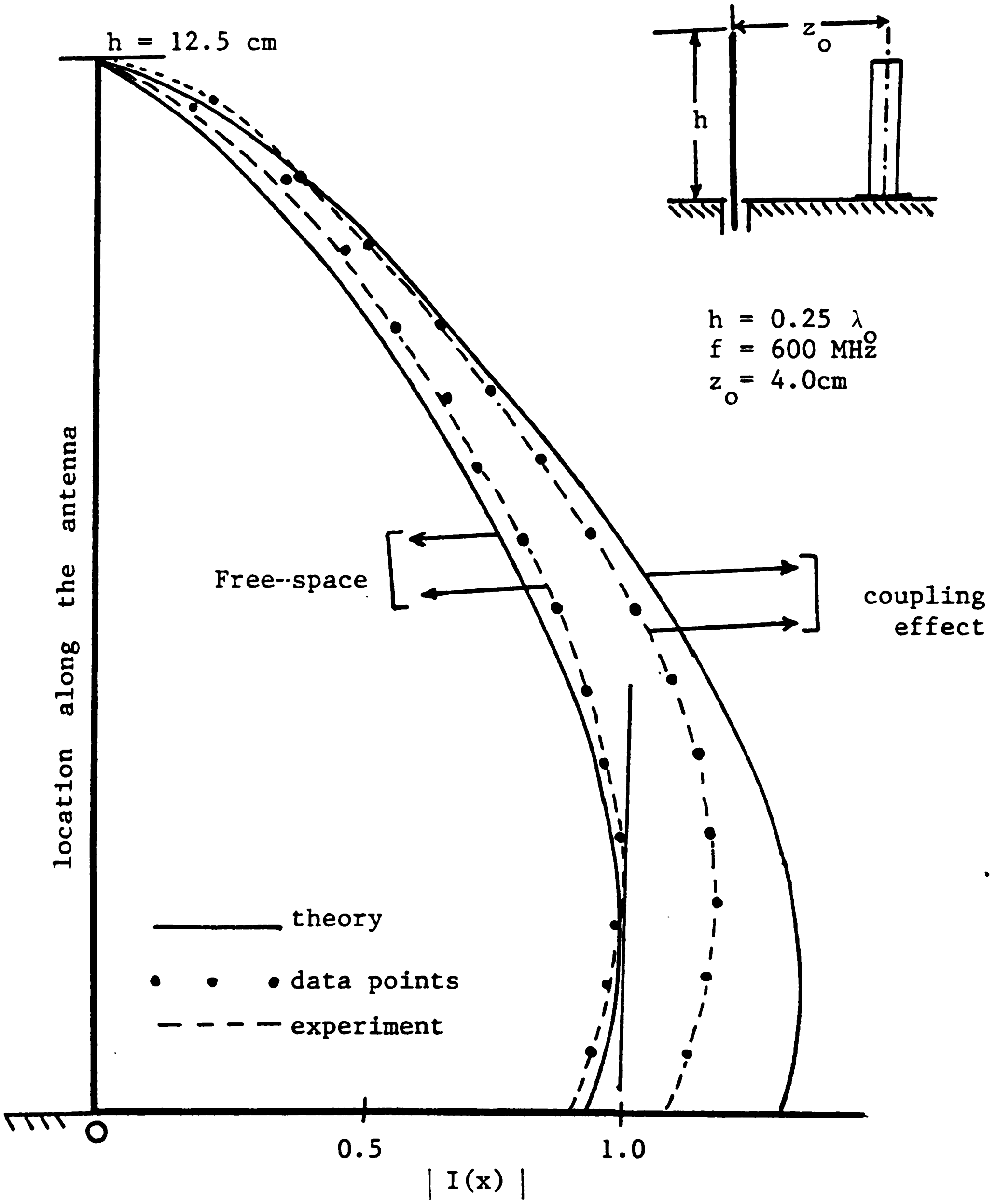

Fig. 5.13. Current distribution on the antenna in presence of a biological body. Theoretical and experimental values have been normalized by their respective free-space maximum values.

5.5 Measurement of Induced Electric Fields Inside the Body.

In this part of the experiment we attempt to verify the induced electric field distribution inside the biological model. A few changes have to be incorporated in the container before it can be used for this experiment. Firstly salt solution is replaced by a synthetic thick jelly like substance called phantom matter. This is prepared by mixing the synthetic powder of a specified proportion into the saline solution. Next, two slots are cut on one face of the container so that the fields at the central location of each cell (Ref. Fig. 5.1) can be probed. Antenna of height $h = \lambda_o/4$ has been used throughout this experiment.

5.5.1 Experimental Setup.

The schematic diagram of the experimental setup is shown in Fig. 5.16(a). Details of the basic construction of the probe has been discussed in (17) and are not included here. The basic requirements for such a probe include: 1. relatively small size; 2. sufficient sensitivity; 3. polarization independence; 4. minimum interference due to the lead lines and; 5. no direct contact with the biological substance. The polarization problem is not of a major concern since the horizontal components (y,z) of the induced electric fields are anticipated to be small as compared to the vertical (x) component. Interference from the lead lines has been minimized as an improvement over the design of (9). This has been accomplished by inserting six resistor symmetrically and in series with the probe. The probe designed in this manner is found to have a high signal to noise ratio, and as evident in the following experiments, its performance at 600 MHz carrier frequency has been extremely satisfactory. The probe is shown in

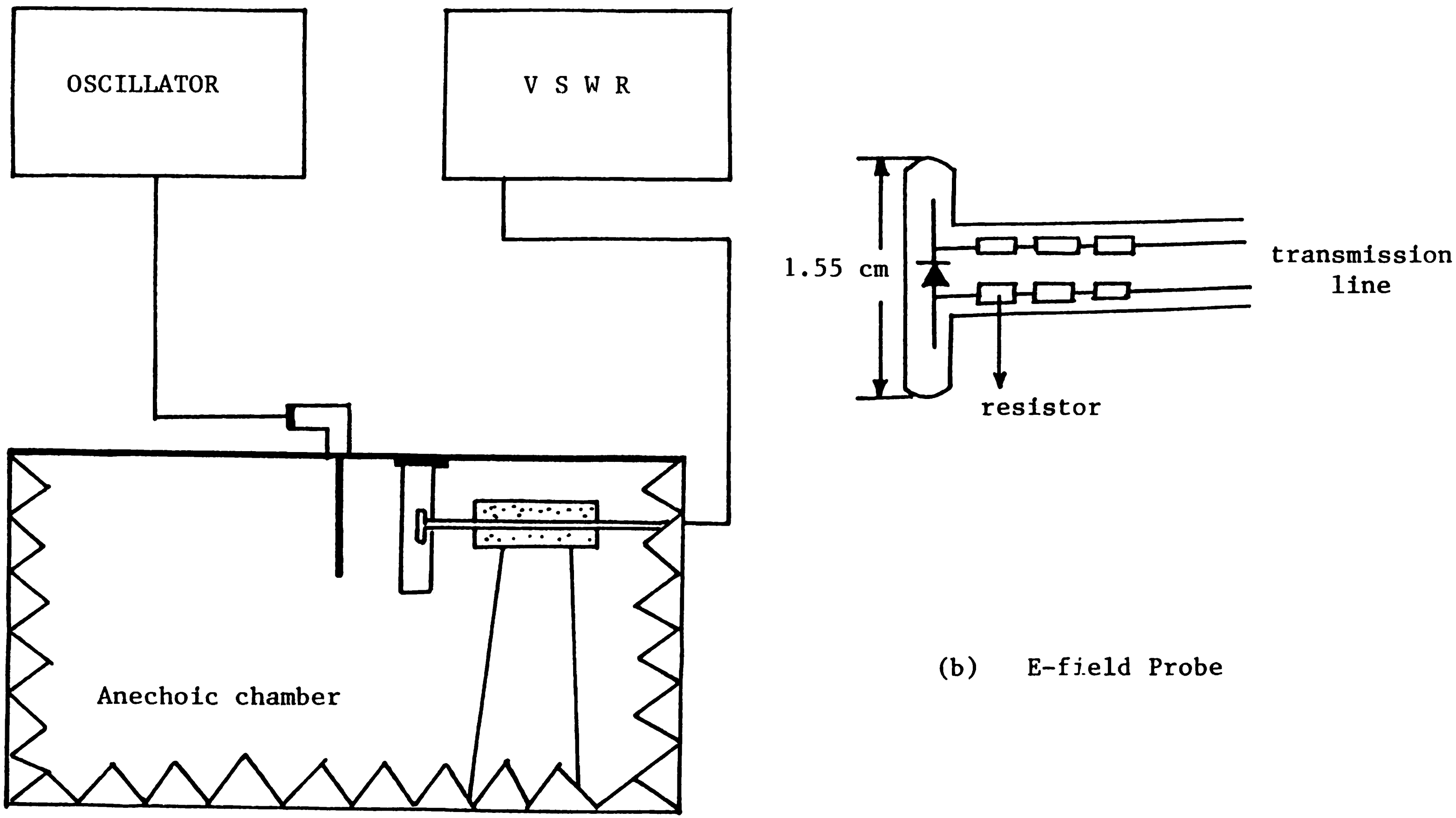

(a)

Fig. 5.16. Experimental setup for the measurement of electric field inside the biological body.

Fig. 5.16 (b).

5.5.2 Free-Space Field Measurement.

As in all previous experiments, free-space measurements were made (before getting involved in the actual problem) using a quarter wavelength antenna. The free-space impedance program ZFREE was used to determine the electric fields at the locations which would be the central coordinates of the cells in the right quadrant of Fig. 5.1. The results of measurement of the components of electric field are given in Fig.5.17/18.There is an excellent agreement between the theoretical and experimental results. Fields were measured in two (imaginary) columns of cells. The inner column exhibits stronger fields than the outer column. This is a trivial point but it must be kept in mind when a similar comparison is made for the above in presence of the body model.

5.5.3 Induced Electric Field Measurements.

The x-components of the induced electric fields inside the body were measured at each cell location. Extreme care was taken to ensure proper alignment and penetration of the probe. Considerable amount of time was spent in this process. The theoretical and experimental results seem to be in fair agreement. The results are shown in Fig. 5.19. As mentioned in the previous paragraph the fields in the outer column are now greater than the fields in the inner column, an important contrast with the free-space case.

Theoretical error due to non-convergence was believed to exist at this stage. A new model was reconstructed with (8x8x1) cm container

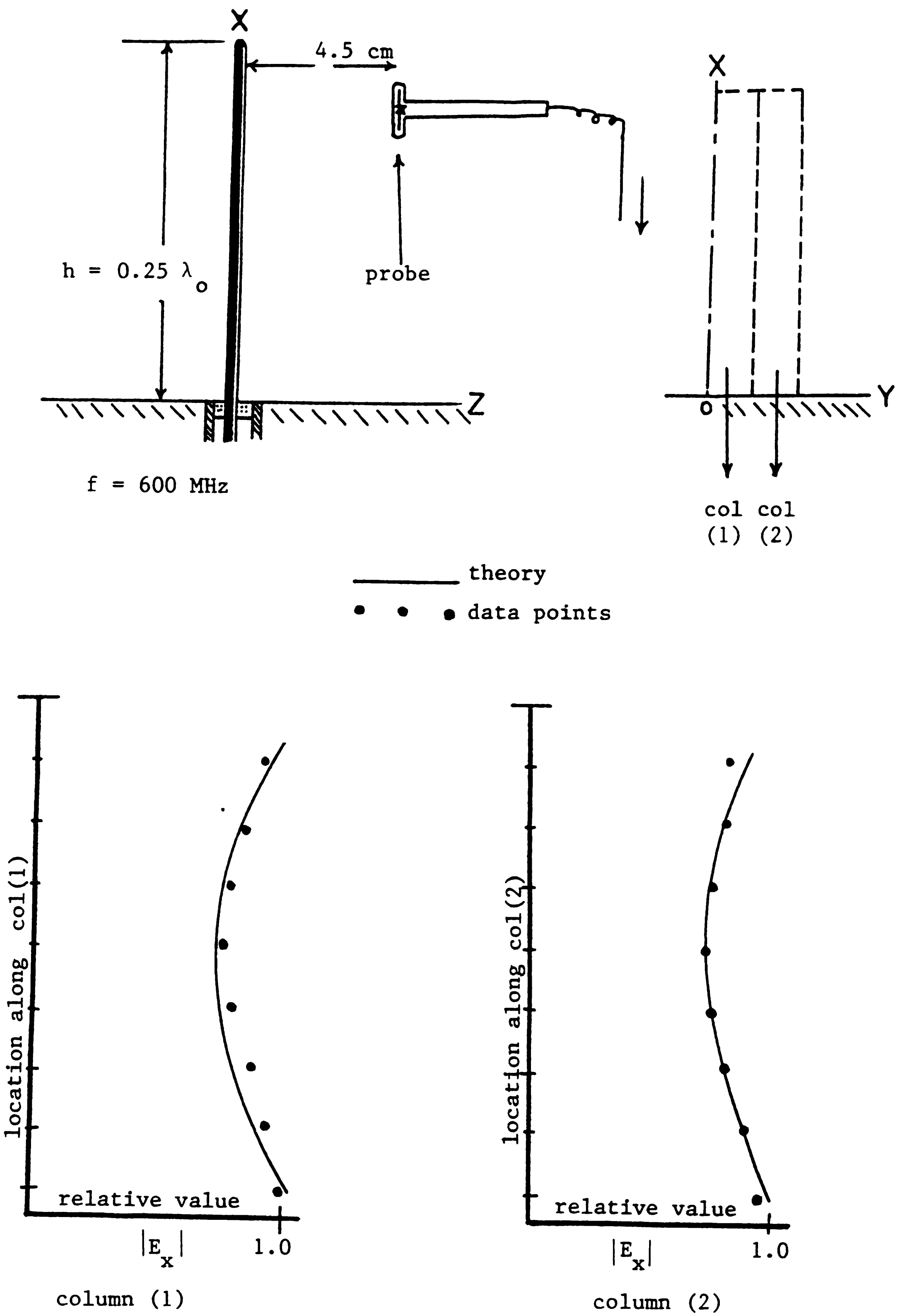

Fig. 5.17. Free-space electric field distribution at points in space corresponding to the central location of body cells.

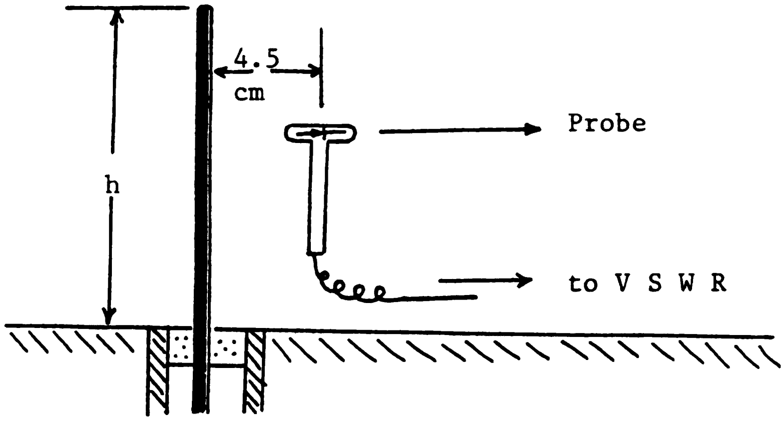

h = 0.25 λ_o

f = 600 MHz

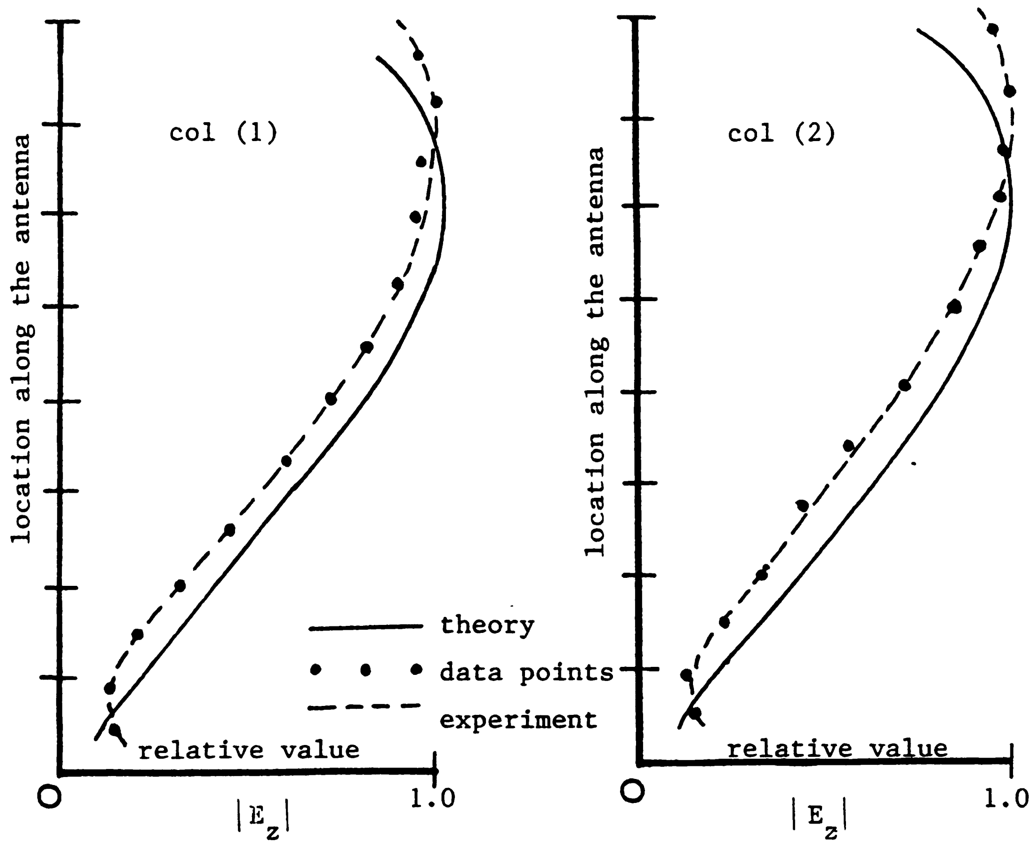

Fig. 5.18. Free-space electric field distribution at the locations specified in the Fig.5.17.

Theory

X	col (1)	col (2)
	0.18	0.12
	0.33	0.38
	0.47	0.53
	0.60	0.68
	0.71	0.80
	0.80	0.90
	0.86	0.97
0	0.88	1.00

Y

Experiment

X	col (1)	col (2)
	0.22	0.27
	0.30	0.37
	0.48	0.65
	o.59	0.84
	0.72	1.00
	0.74	1.14
	0.85	1.21
0	0.97	1.30

Y

σ = 8.8 S/m
ϵ_r = 66.00

——— theory

• • • data points

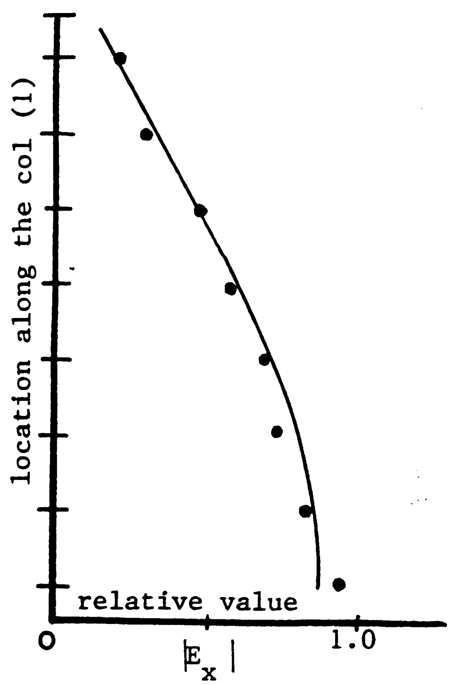

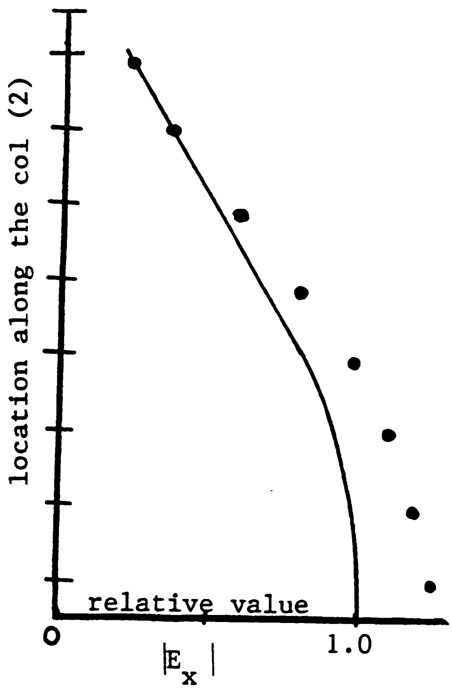

Fig. 5.19. Distribution of induced electric fields inside the biological body of Fig. 5.1 when irradiated by the impressed field from the antenna of height h = 0.25 λ_o at 600 MHz.

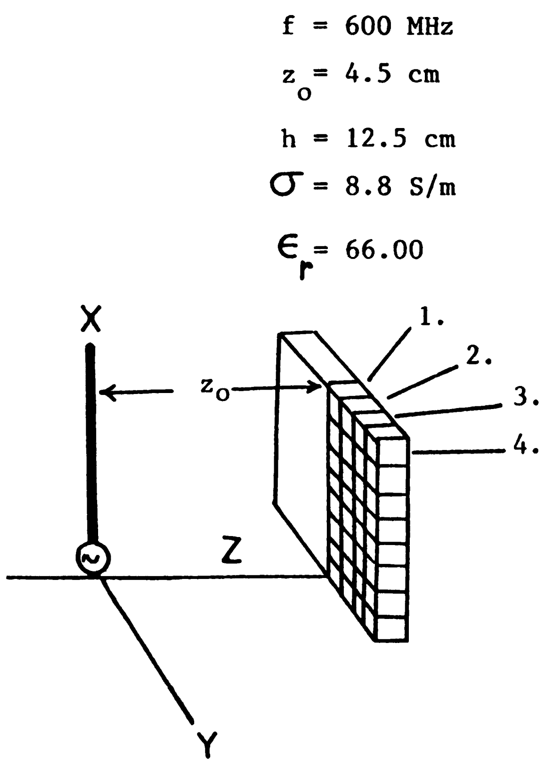

(a)

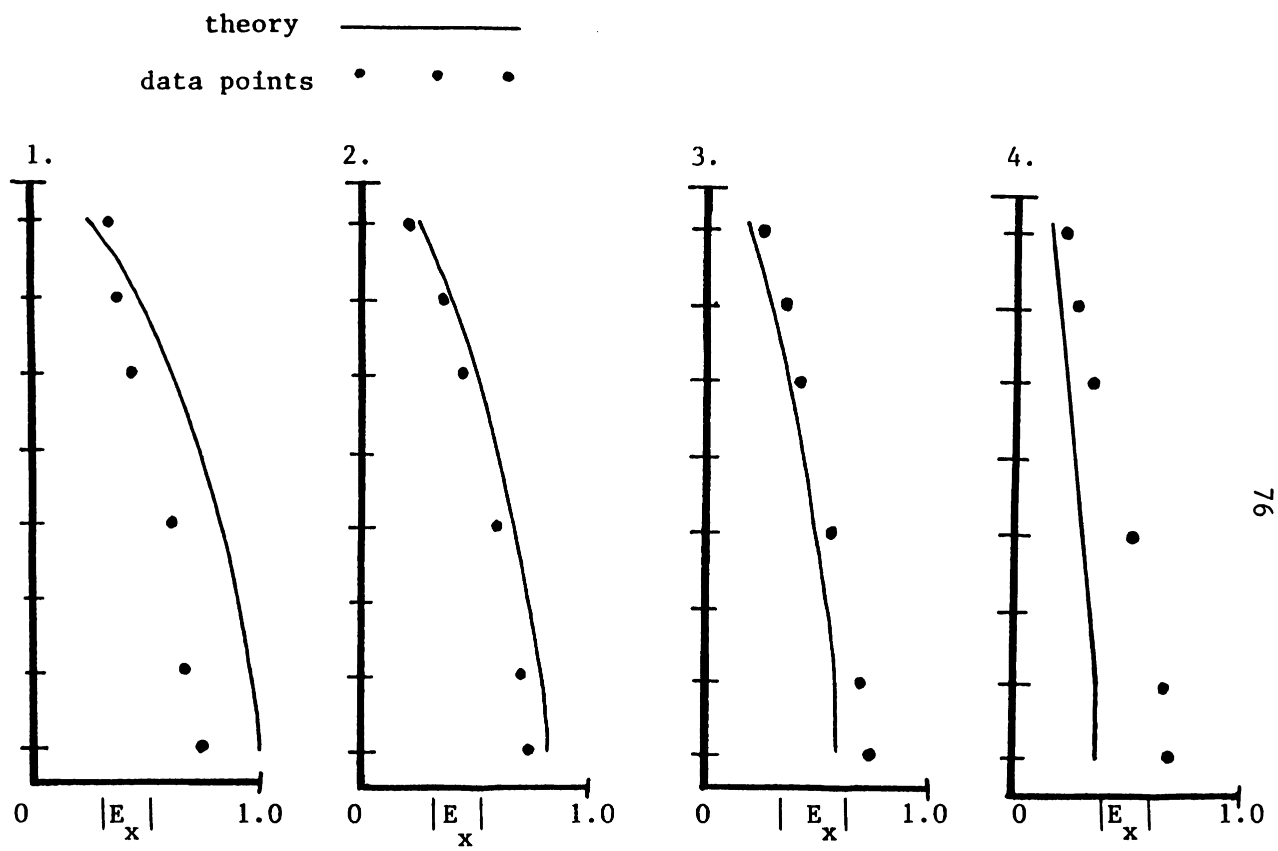

(b)

Fig. 5.20. Distribution of induced electric fields inside the biological body as shown in (a). The antenna is of height $h = 0.25\ \lambda_o$ and the spacing between the antenna and the body is 4.5 cms.

and the computer model of 32 cells in first quadrant was realized. Height of antenna, operating frequency and conductivity of the model were kept the same as before. Results obtained were not in total agreement. The reasons given in the next section, have ascertained that the model chosen in this case was not a reliable experimental choice. The results are given in Fig. 5.20, and are presented merely to emphasize the major drawback in choosing a body of smaller dimensions.

5.6 Sources of errors.

5.6.1 Errors in Impedance Measurements.

As evident from the theoretical and experimental results of Fig. 5.3 and 5.4, experimental errors are practically non-existing. There are three basic errors that may be encountered during such measurements. These are the terminal zone capacitance effect, the effect of dielectric support and the effect due to finite ground plane. From the tables given in (14) for co-axial waveguide and for $b/a = 2.3$, where b is the radius of the outer conductor and a is the radius of the inner conductor, we get terminal zone capacitance of 0.048 pico-farad. The susceptance due to this capacitance will be 0.180 milli-mhos at 600 MHz, which is negligible. Effects of the other two types are minimal.

5.6.2 Errors in Measurement of Current Distribution.

The major source of error is the unstability of the H-probe during its movement inside the antenna rod. A perfect H-probe must extend out equally at all positions along the length of the antenna. This will provide a constant multiplier for the probe due to its gemoetrical shape and thus the induced voltage will be proportional to the current distribution on the antenna and independent of the location along its length. Extreme care was taken to meet this requirement and the results of Section 5.4 show that the H-probe has worked satisfactorily.

5.6.3 Errors in Electric Fields Measurement Inside the Body.

Electric field probe has been designed to meet the requirements as mentioned in the beginning of Section 5.5. However the major source of error is not in the design of the probe but it is dependent upon the location of the probe. A detailed analysis of this problem has been carried out by Smith (15). A summary of the results are given below.

(i) The error in response is decreased if the load admittance is very small compared to the input admittance of the probe.

(ii) An increase in the attenuation constant of the medium surrounding the probe will increase the error when probe is near the surface.

(iii) The error is further reduced by the use of insulated probe such that the permittivity of the medium ϵ_m and that of the insulation ϵ_i satisfy the condition $\epsilon_m/\epsilon_i >> 1$.

(iv) The error is reduced by the use of probe with short receiving conductors.

In the experiment all requirements except the one in (ii) above have been met by the design of Fig. 5.16 (b). In this way the main sources of errors are the noise collected by the transmission line connecting the probe to the measurement apparatus and the nearness of the interface from the probe. The later may have been a dominant error in case of the 32 cell model of Fig. 5.20 where the size of each cell was (1 x 1 x 1) cm. During the experiment the transmission line from the probe was surrounded by microwave absorbers and thus the conductors of the lines were shielded from the electromagnetic fields in the surrounding space.

CHAPTER VI

THEORETICAL STUDY OF VARIOUS MODELS OF ANTENNA-BODY SYSTEM

6.1 Introduction

This chapter is devoted to theoretical studies based on the results obtained from the computer program. In Chapter V, theoretical results have been verified by the experiments and a high degree of confidence in the accuracy of this method has been established. The container model chosen in the previous chapter is merely a model for laboratory work and as such does not resemble a realistic situation. In this chapter we have formulated computer models of situations involving biological bodies of the size of a human adult and studied the various electromagnetic effects due to the coupling phenomena.

The study is broken into three main categories each has a significance of its own. Work has been done with operating frequencies that are being used by various transmitter sets that have their operator in the near-zone of the radiating antenna. Situations given in the following study are not an exact representation of the true ones encountered by the operators, but their practical significance can not be overlooked. The results of this study conclude that radiation from the antenna is a potential radiation hazard especially when high power transmitters are used for communication. Effects of the presence of a biological body in the near-zone of the antenna upon the radiation pattern are given in this chapter. Furthermore, the effects on field

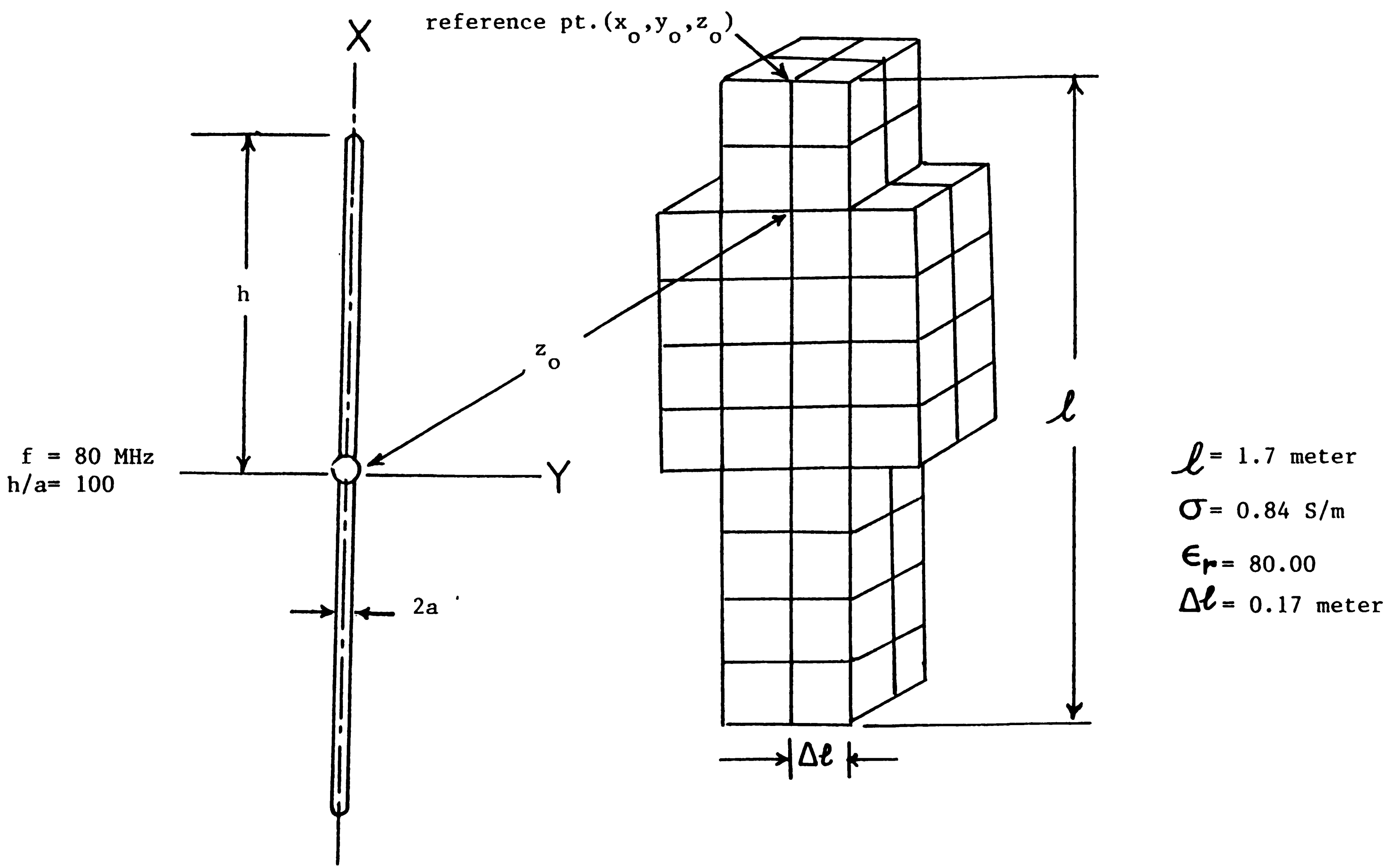

Fig. 6.1 Geometrical arrangement of the human body model and the radiating antenna to which it is coupled.

distribution inside the body of an operator and the power absorbed when he is in direct contact with the ground are compared to the case when he is isolated from the ground.

6.2 Antenna-Body System Operating At 80 MHz.

This system is shown in Fig. 6.1. The shape of the body has the basic look of a human adult. Permittivity and conductivity of this model are assumed uniform within the entire volume. This system realizes a situation of an isolated system with a radiating dipole antenna and a biological body in its near-zone. The system has a symmetry about the vertical plane passing through the axis of the body and this reduces the number of unknowns of this system. The number of cells chosen to model the adult frame is 56. Using the symmetry of the problem the effective number of cells is only 28 i.e. electric fields in only the right half of the body need to be determined (see Chapter VII). For economical reasons, a trade off has to be made between the shape of the body and the number of cells. Since in this case the program has to be utilized many times we have found it satisfactory to choose the model of Fig. 6.1, even though its weight is not realistic. The dielectric constant (real) at 80 MHz is taken as 80.00 and the conductivity at the same frequency, as 0.84 S/m. The current distribution on the antenna can not be assumed symmetric in general, however, as proven in the following paragraph, it is nearly so for antennas of height $h < \lambda_o/4$.

The first case is an antenna of height $0.125\,\lambda_o$. The current distribution on the antenna and the electric fields induced in the body are given in Fig. 6.2 (b) and 6.3 (a) respectively. These

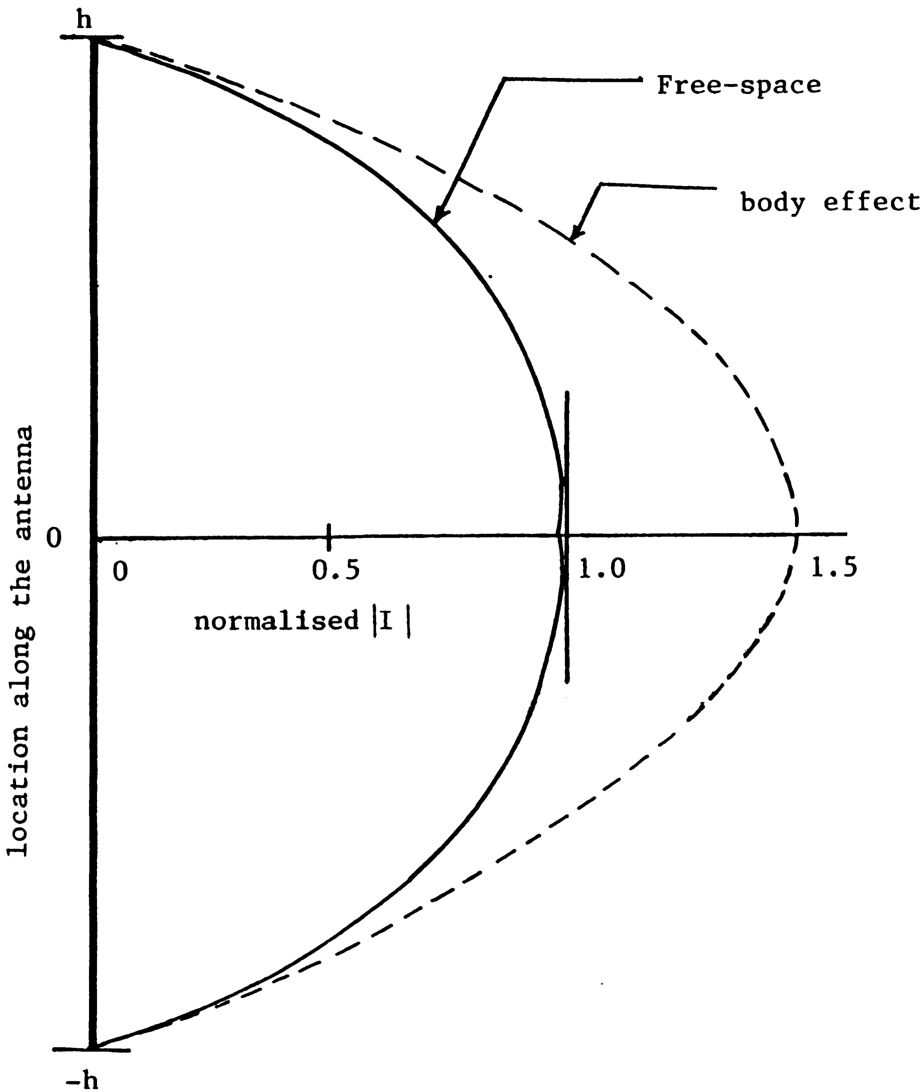

(a) $h = 0.25\ \lambda_o$ $x_o = 34$ cm
$y_o = 0.00$ cm $z_o = 20$ cm

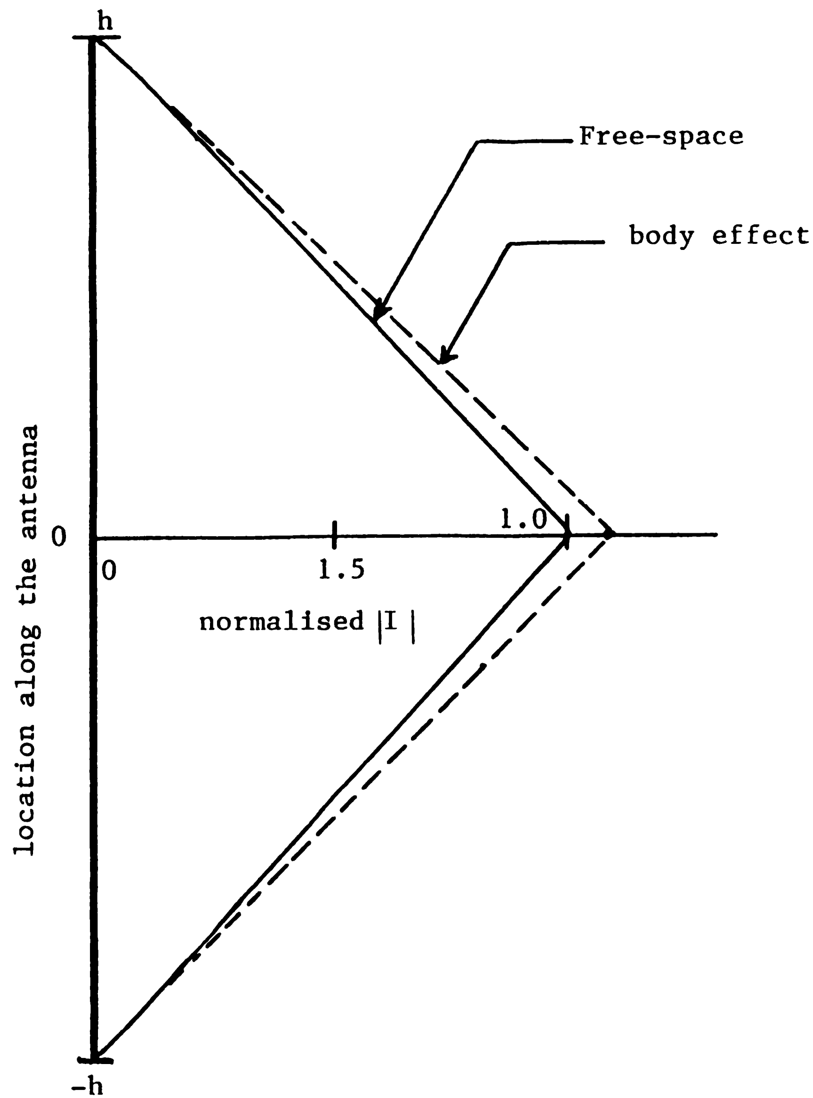

(b) $h = 0.125\ \lambda_o$ $x_o = 34$ cm
$y_o = 0.0$ cm $z_o = 20$ cm

Fig. 6.2. Current on antenna in presence of body compared to that in free-space where antenna is driven by identical input voltages. Geometry, dimensions and parameters are specified in Fig. 6.1.

(a)
$h = .125\ \lambda_o$
$f = 8o$ MHz

front layer		back layer	
3.28		1.81	
3.38		2.71	
3.17	1.64	2.80	1.02
2.83	2.36	2.25	1.11
1.98	2.13	1.39	.816
1.08	1.27	.597	.603
.628		.549	
.338		.753	
.167		.722	
.152		.475	

$x_o = 34$ cm
$y_o = 0.0$ cm
$z_o = 20$ cm

(b)
$h = 0.25\ \lambda_o$
$f = 80$ MHz

front layer		back layer	
3.61		1.76	
4.77		2.68	
4.84	3.46	3.30	1.81
4.56	5.32	3.66	2.14
4.56	5.31	3.38	2.01
4.73	3.50	2.63	1.73
4.32		2.01	
3.10		1.51	
2.00		1.19	
1.15		.804	

Fig. 6.3. $|\vec{E}|$ field (V/m) induced in human body model by an input current of 1.0 Amp when the antenna is placed very close to the body at neck level. Refer to Fig.6.1 for other constants of the system.

electric field values are based on 1 amp. current input and the center of the antenna is located at neck-level (x_o=34 cm) spaced at 20 cms from the body. Next the current distribution and the electric fields are specified for h = 0.25 λ_o in Figs. 6.2(a) and 6.3(b) respectively. Even though non-symmetric current on the antenna has been anticipated, these results have shown that to a first approximation, current may be assumed symmetric. This information supports the assumption made by Nyquist et. al.(5) who assumed a known current distribution for ellectrically short dipoles or monopoles for such a case.

An interesting observation was made by using h = 0.382 λ_o which is close to the anti-resonant length. The antenna was centered at top of the head (x_o = 0.cm) at a spacing of 20 cms in between the two. Other parameters were kept the same as in previous cases. The current distribution for this case was non-symmetric. This evidence is illustrated in Fig. 6.4. Other results of this study are given in Fig. 6.5 and the Tables 6.1, 6.2 and 6.3. The far-zone radiation fields in the H-plane are quite different from the free-space case. Moreover these curves are dependent on the level along the vertical axis. The radiation fields are greatly perturbed from their free-space distribution when the antenna is placed around the center of the body. Table 6.1 shows the effects of placing the body at various locations along the horizontal axis. The ratio of the power dissipated to the power input (P_d/P_{in}) goes on reducing as we move the body away from the antenna. Table 6.2 gives an interesting piece of information. The ratio P_d/P_{in} changes as the body is moved vertically. The maximum is attained when the antenna is positioned at the neck level. This effect does not seem to f = 80 MHz

h = 0.382 $\lambda_o \doteq$ anti-resonant height

x_o = 0.0 cm

y_o = 0.0 cm

z_o = 20 cm

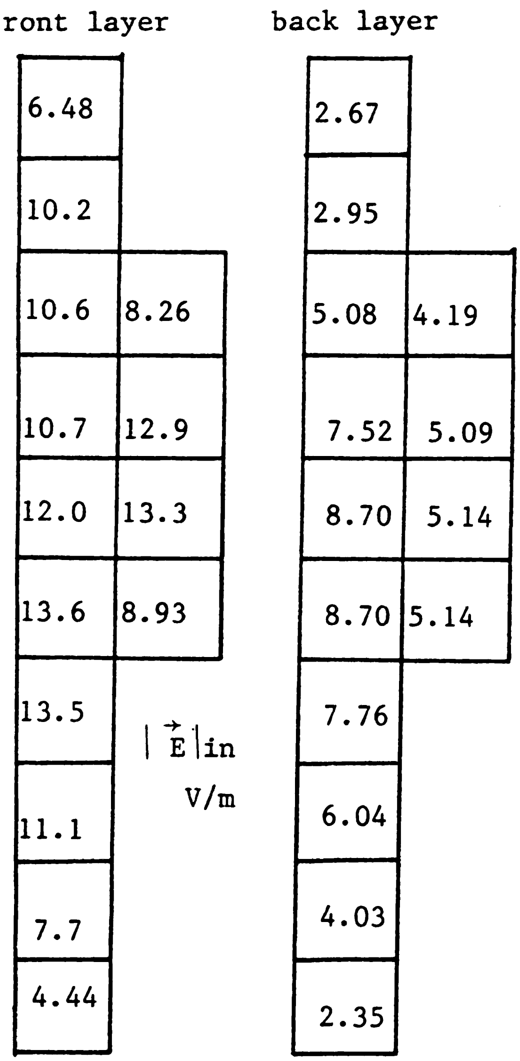

(a) $|\vec{E}|$ field induced in human body by an input current of 1.0 Amp when placed near an antenna.

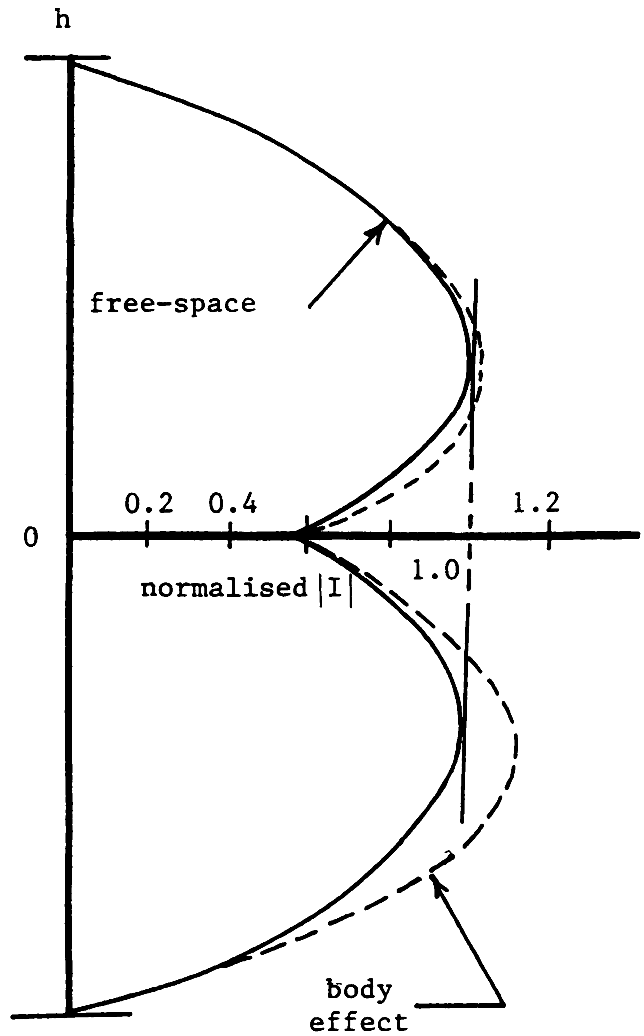

(b) Current distribution on antenna in presence of body and in free space when h is near anti-reso -nant length.

Fig. 6.4. Induced body field and antenna current for antenna of near anti-resonant length in proximity to human body (geometry, dimensions and parameters are specified in in Fig. 6.1).

$A : h = 0.125\ \lambda_o,\ x_o = -0.17$ m

$B : h = 0.25\ \lambda_o,\ x_o = -0.17$ m

$C : h = 0.125\ \lambda_o,\ x_o = 0.85$ m

These curves represent relative values of $|\vec{E}^r|$ in H-plane ($\phi = 90^o$)

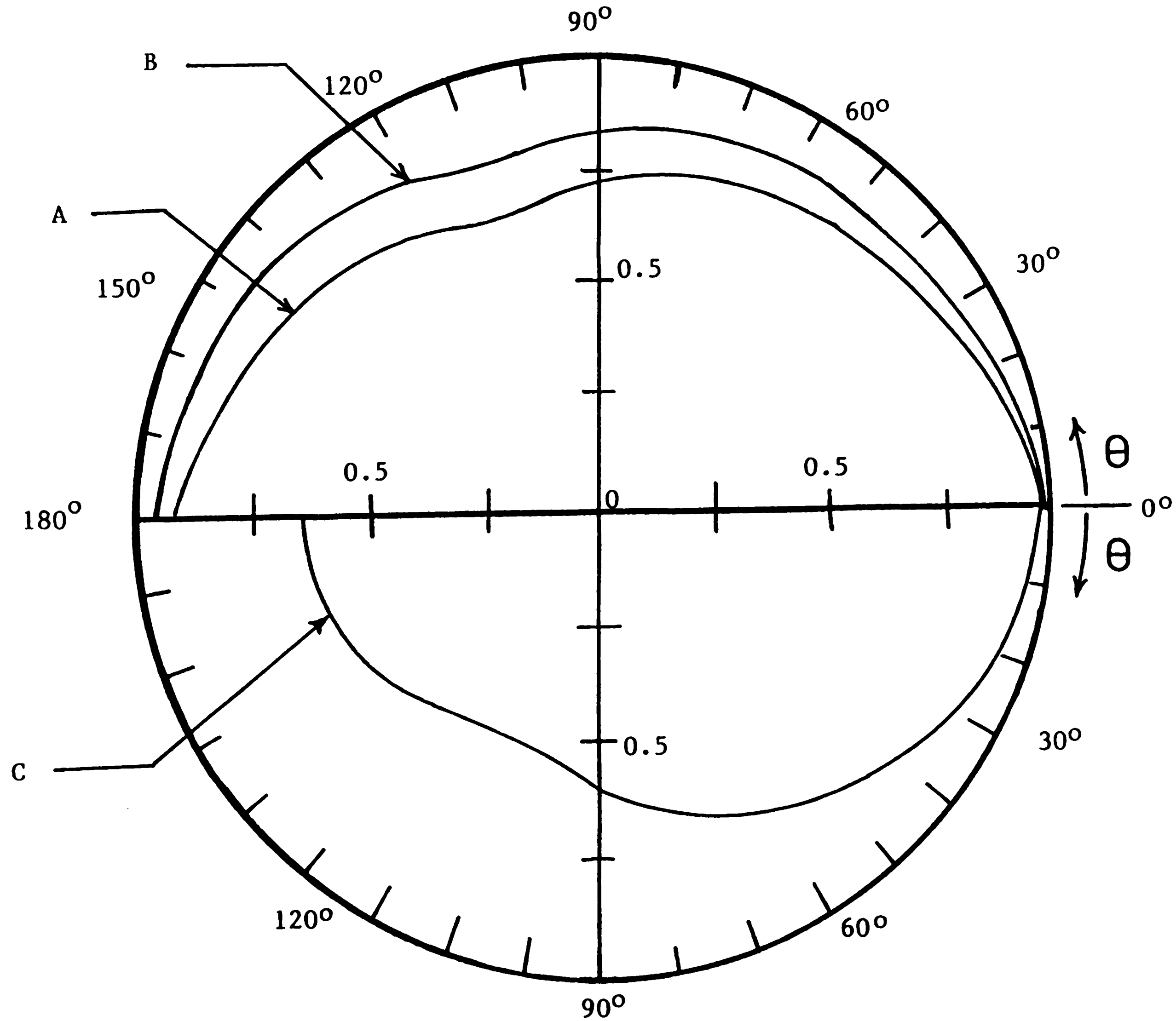

Fig. 6.5. Radiation field pattern maintained by dipole antenna coupled to the human body model in H-plane of the dipole (geometry, dimensions and parameters are same as in Fig. 6.1).

f = 80 MHz　　$Z_o = 85.96 + j32.18$　　x_o = 34.00 cm　　h/a = 100

$h = 0.25\ \lambda_o$　　I_{in} = 1.0 Amp　　y_o = 0.0 cm　　λ_o = 3.75 m

z_o/λ_o	z_o(cm)	Z_p(ohms)	Z_{in}(ohms)	P_{in}(W)	P_d(W)	P_r(W)	P_d/P_r	P_d/P_{in}
.027	10.0	-31.6 - j2.93	54.37 + j29.25	27.18	1.80	25.38	.071	.066
.053	20.0	-32.7 - j6.64	53.27 + j25.54	26.63	1.30	25.33	.051	.049
.080	30.0	-29.52 - j3.88	56.44 + j28.03	28.22	1.03	27.19	.038	.036
.133	50.0	-19.19 + j0.59	66.67 + j32.77	33.35	0.75	32.60	.023	.022
.267	100.0	0.38 + j6.61	86.34 + j25.57	43.17	0.18	42.99	.004	.004

TABLE 6.1.　Dependence of impedances and dissipated and radiated powers upon dipole location z_o (geometry dimensions and parameters specified in Fig. 6.1). Z_{in} = input impedance of antenna Z_p = perturbation to antenna impedance due to proximity effect, Z_o = free-space antenna impedance and $Z_{in} = Z_o + Z_p$.

$f = 80$ MHz | $Z_o = 16.19 - j441.02$ | $z_o = 20.0$ cm | $h/a = 100$

$h = 0.125\ \lambda_o$ | $I_{in} = 1.0$ Amp | $y_o = 0.0$ cm | $\lambda_o = 3.75$ m

Loc.	x_o(cm)	Z_p(ohms)	Z_{in}(ohms)	P_{in}(W)	P_d(W)	P_r(W)	P_d/P_r	P_d/P_{in}
above head	-17.0	1.45 + j3.32	17.64 - j437.7	8.82	0.234	8.586	.027	.026
head level	0.0	-0.81 + j4.22	15.38 - j436.8	7.69	0.209	7.481	.028	.027
neck level	34.0	-0.97 + j14.82	15.22 - j426.2	7.61	0.376	7.234	.052	.049
body center	85.0	-0.82 + j18.02	15.37 - j423.0	7.68	0.356	7.324	.049	.046

TABLE 6.2. Dependence of impedances and dissipated and radiated powers upon dipole location x_o (geometry, dimensions and parameters are specified in Fig. 6.1.) $Z_{in} = Z_o + Z_p$ (Z_o = free-space impedance, Z_p = perturbation due to body proximity effect and Z_{in} is input impedance of the antenna).

$h = 0.25\ \lambda_o$ $z_o = 20.0$ cm $Z_o = 85.96 + j32.2$ $h/a = 100$

$f = 80$ MHz $y_o = 0.0$ cm $I_{in} = 1.0$ Amp $\lambda_o = 3.75$ m

Loca.	x_o(cm)	Z_p(ohms)	Z_{in}(ohms)	P_{in}(W)	P_d(W)	P_r(W)	P_d/P_r	P_d/P_{in}
above head	-17.0	-17.63 - j15.98	68.33 + j16.22	34.16	0.936	33.22	.028	.027
head level	0.0	-24.37 - j15.46	61.59 + j16.74	30.80	1.04	29.76	.035	.034
neck level	34.0	-32.69 - j6.66	53.27 + j25.54	26.64	1.30	25.34	.051	.049
body center	85.0	-30.7 + j9.06	55.26 + j41.24	27.63	1.47	26.16	.056	.053

TABLE 6.3. Dependence of impedance and dissipated and radiated powers upon dipole location x_o (geometry, dimensions and parameters specified in Fig. 6.1). $Z_{in} = Z_o + Z_p$ (Z_o = free-space impedance, Z_p = perturbation due to body proximity effect and Z_{in} is input impedance of the antenna).

exist for the quarter-wave dipole whose results are tabulated in Table 6.3.

6.3 Antenna-Body System Operating at 27 MHz.

This system is fairly simple in its appearance and does not quite resemble a human frame. However its size and its weight (68 kg) are those of an average adult. This model was used to compare the power dissipated inside the body exposed to the radiation from a CB radio antenna or a similar device, to the power dissipated when exposed to $10 mW/cm^2$ plane wave radiation. The body model is shown in Fig. 6.6. It consists of 68 cells, however fields are to be determined in the cells forming the right half of the model. The antenna is of height $h = 0.25\ \lambda_o$. The height of the human body model is 170 cm, and uniform permittivity and conductivity has been assumed inside the body. Fig. 6.6 defines an isolated system with symmetry about the vertical plane, as in the model of section 6.2. Other relevant data are given in the figure. Fig. 6.7 depicts the case of this body being illuminated by radiation from a monopole antenna above infinite ground plane. In Fig. 6.8 the same body has been illuminated by $10\ mW/cm^2$ plane wave, the maximum value set by the Radiation Safety Standards. In the first case the total power dissipated inside the body, when the antenna is fed by 1 watt , is 6.44 mW. In the second case the power dissipated is 0.084 W, more than ten times increase over the previous case. In both cases spacing between the antenna and the body has been kept as 20 cms. In the third case with $10\ mW/cm^2$ incident wave intensity, the power dissipated is 11.14 watts. Comparing it with the grounded system, antenna input power of about 140 watts will dissipate the same amount of

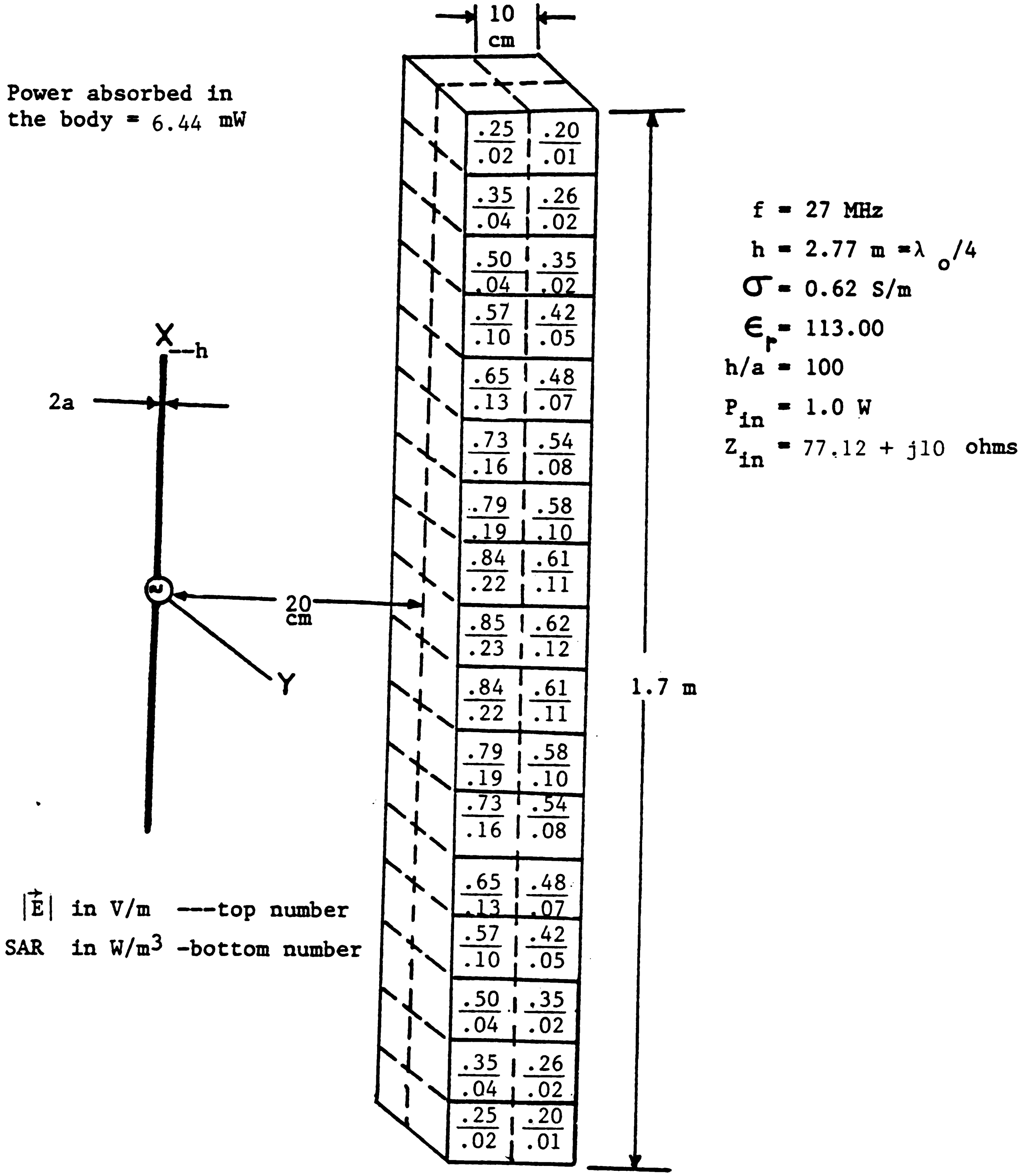

Fig 6.6. Distribution of induced elictric fields and the power density(SAR) at the central location of each cell of the body for an isolated antenna-body system. Antenna is driven by an input power of 1 W.

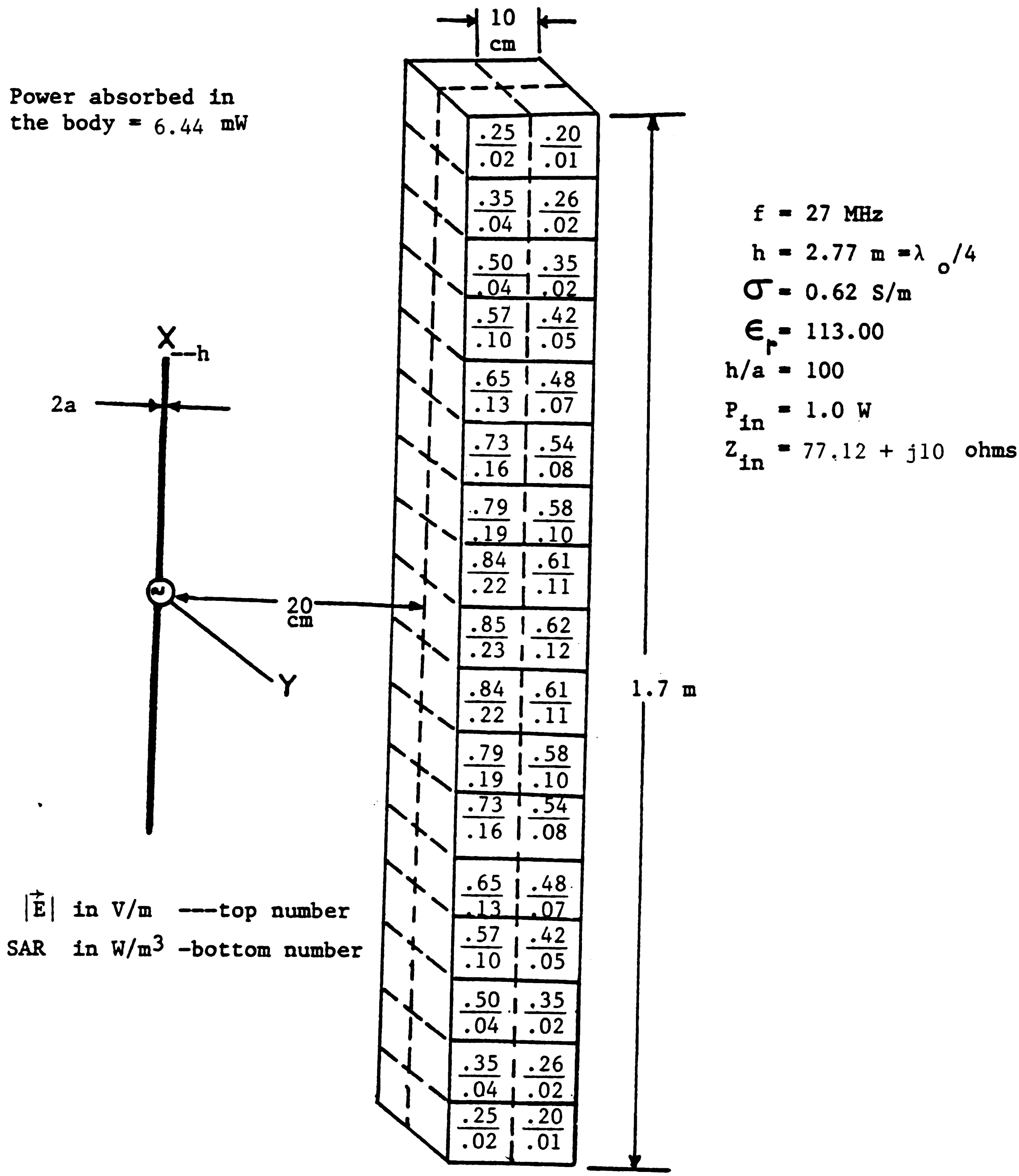

Fig 6.6. Distribution of induced elictric fields and the power density(SAR) at the central location of each cell of the body for an isolated antenna-body system. Antenna is driven by an input power of 1 W.

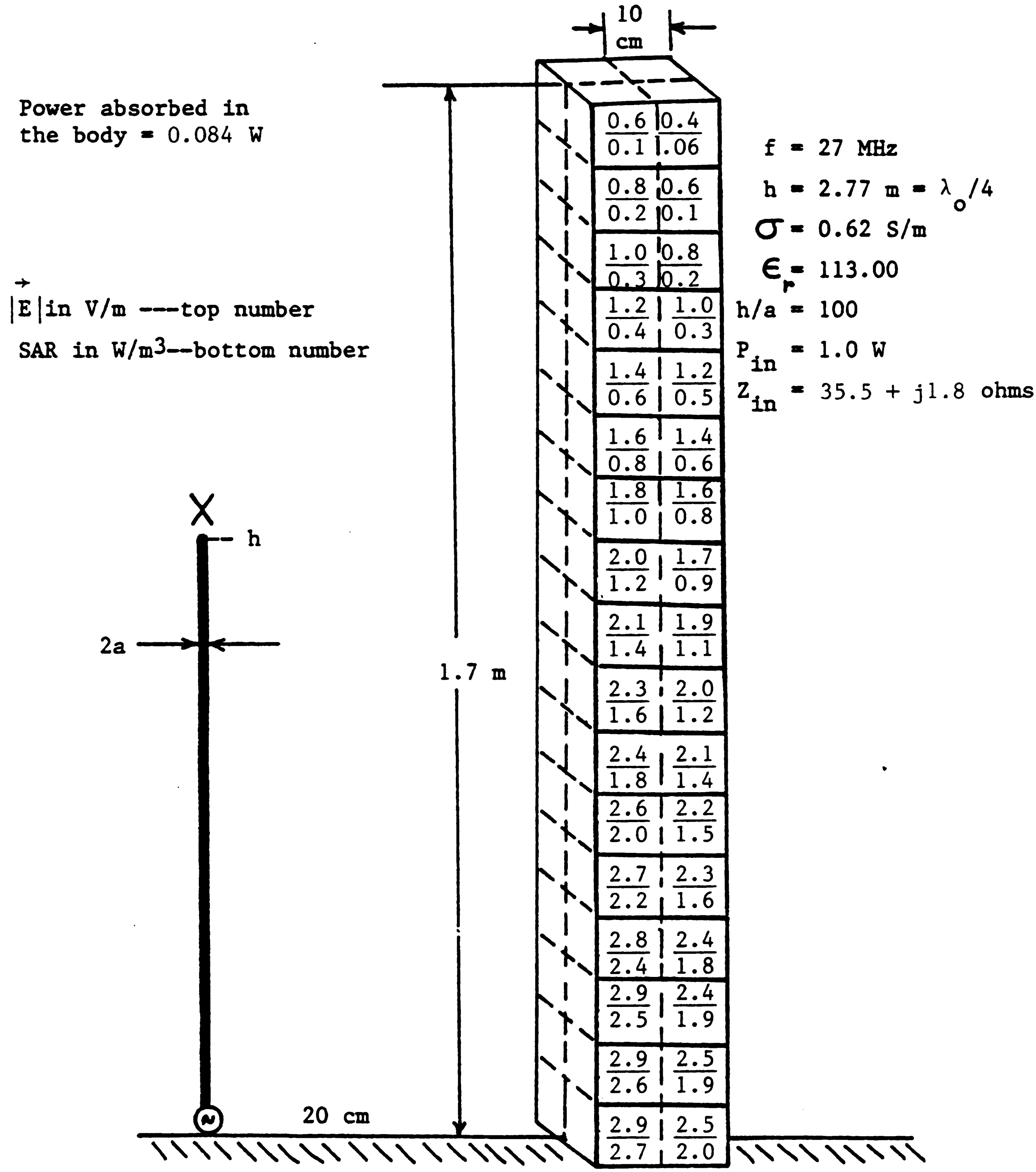

Fig. 6.7. Distribution of induced electric fields and the power density(SAR) at the central location of each cell of the body for an antenna-body system over infinite ground plane. Antenna is driven by an input power of 1 W.

power in the body as will a plane wave of 10 mW/cm^2. By this study we are able to conclude that unrestricted use of high power transmitter may prove hazardous. A similar result is derived in the next section where a more realistic situation is presented.

6.3.1 Test of Numerical Ability of Our Program.

A test was made at this stage to determine the computational ability of the program FIELDS given in Chapter VII. The body under study is placed at a distance of 100 meters from the antenna which is nearly ten times the wavelength. This case is the same as the isolated system of Fig. 6.6 except for the spacing between antenna and the body. We have thus created a situation in which antenna and the body, to a first approximation, can be considered uncoupled. The body can therefore be considered as being irradiated by a far-zone EM field of the antenna with known current distribtuion (free-space). Far-zone electric fields from an antenna of height h = 0.25 λ_o are given by

$$E_\theta^r = \frac{j\eta_o I_z(0)}{2\pi r} \exp(-jk_o r)\ F(\theta) \tag{6.1}$$

where $F(\theta) = \cos\ (\frac{\pi}{2} \cos\theta)/\sin\theta$ and θ is the inclination from the vertical. In the region of space formed by the body; and by the manner in which the antenna and body are located; electric field can be considered of constant amplitude, transverse and vertically polarized in $\theta = 90^o$ plane. Also 274.6 V/m are produced by a current of 457.67 amps. using equation (6.1) for $\theta = 90^o$. Therefore, the power dissipated in the body spaced 100 m from the antenna when the antenna is driven by 457.67 amps. of current, must be approximately equal to 11.14 watts

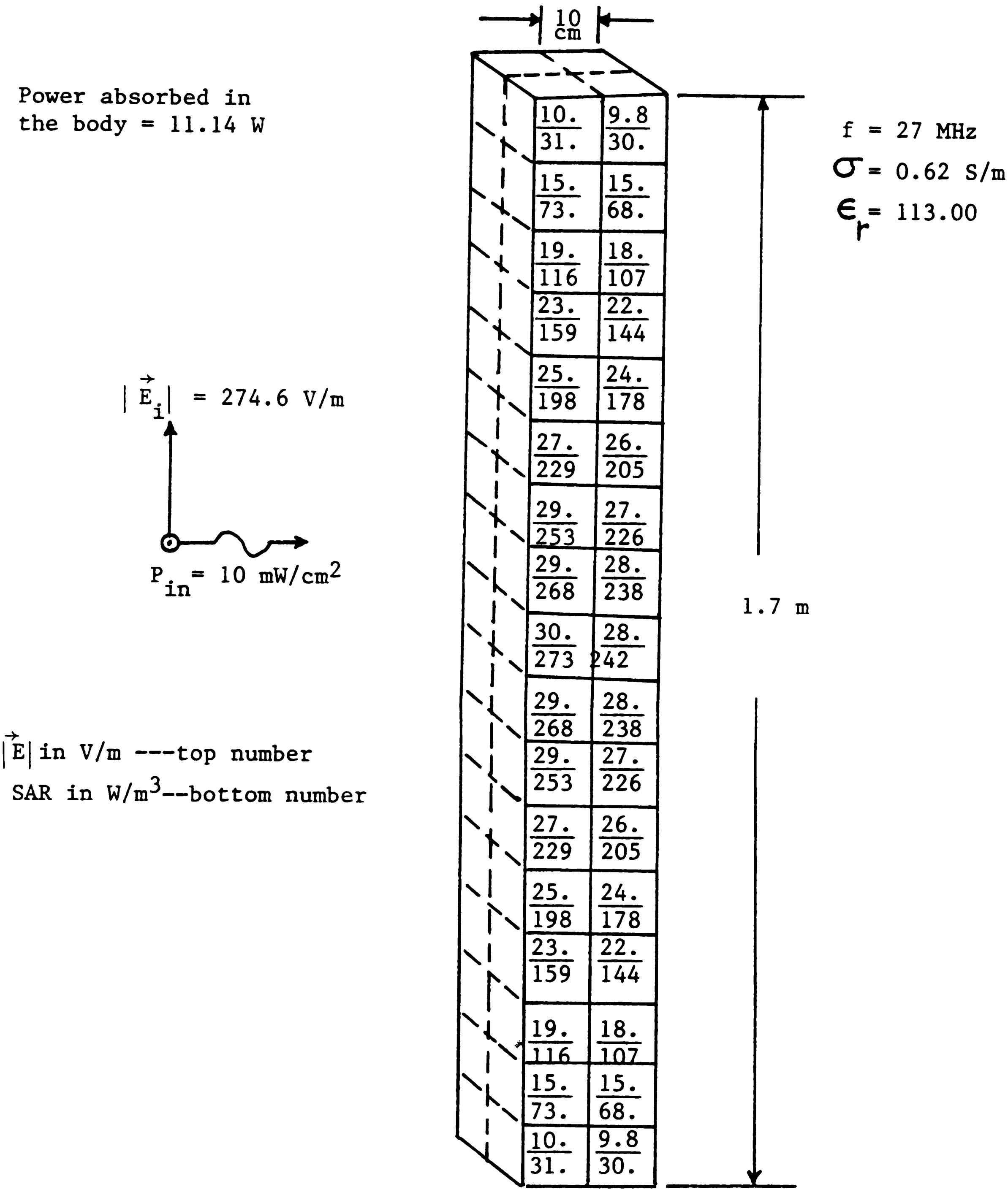

Fig. 6.8. Distribution of the induced electric fields and SAR at the central location of each cell of the body irradiated by a plane EM wave of 27 MHz frequency and intensity 10mW/cm^2.

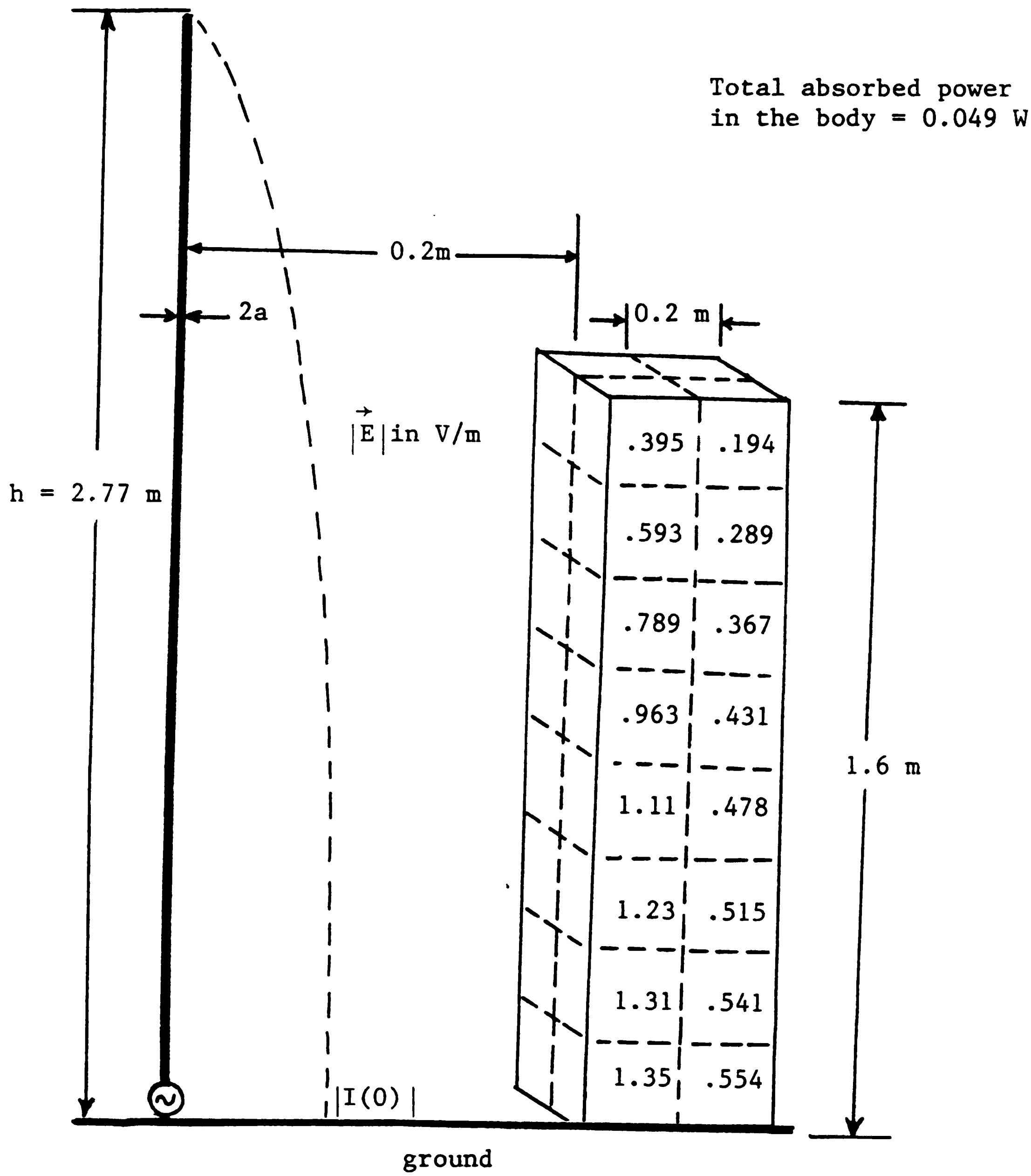

f = 27 MHz

Input power P_{in} = 1.0 W

Input impedance = 32.0 + j6.6 ohms

σ = 0.62 S/m

ϵ_r = 113.00

h/a = 100

Fig. 6.9. Distribution of the induced electric fields inside a cylindrical model of man in direct contact with the ground and located in the immediate vicinity of a grounded quarter-wave monopole antenna.

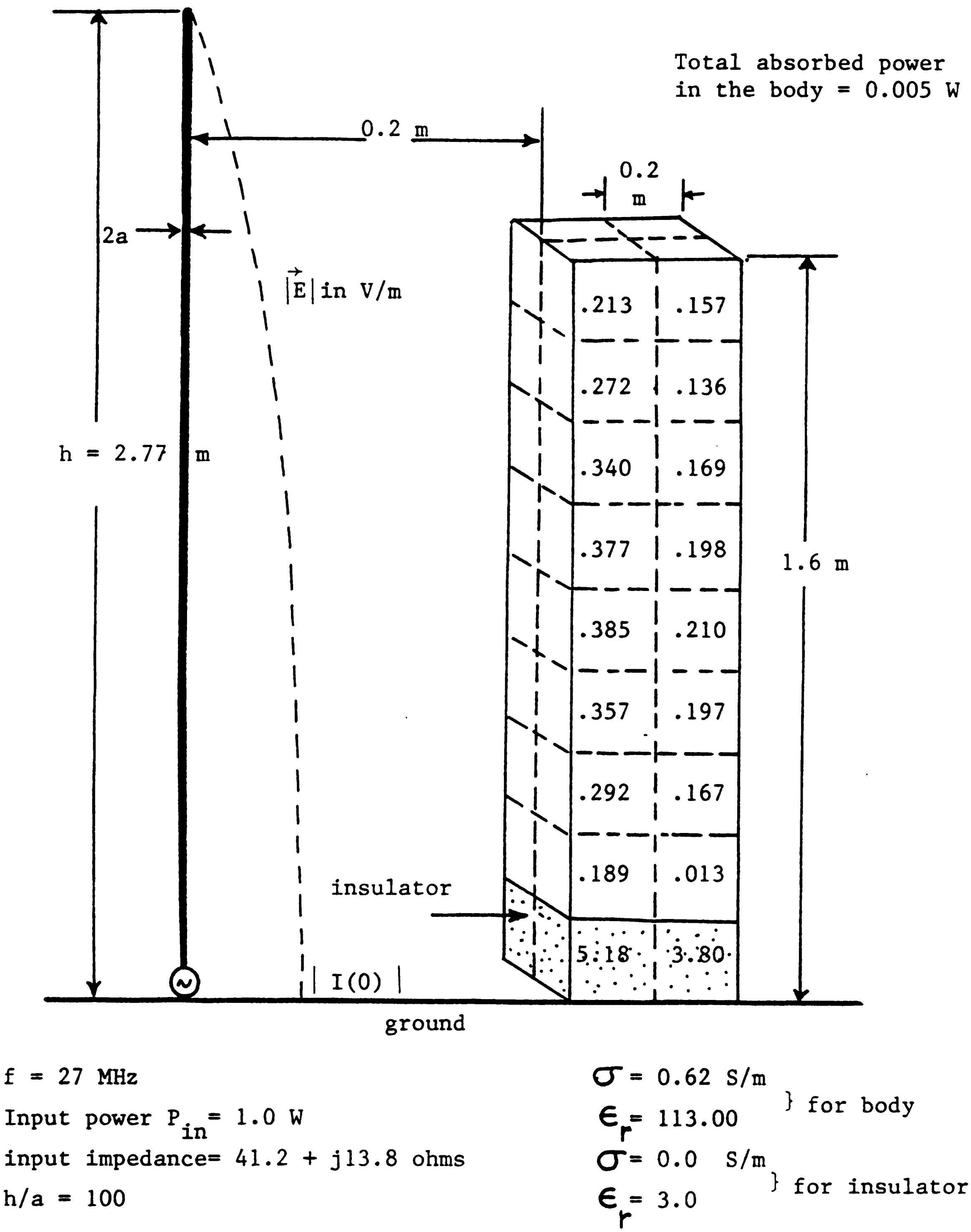

Fig. 6.10. Distribution of the induced electric fields inside a cylindrical model of man insulated from the ground and located in the immediate vicinity of a grounded quarter-wave monopole antenna.

dissipation caused by plane wave of 10 mW/cm^2 intensity. Program FIELDS is used to determine the former while the latter has been determined by using Guru's program (9). The program FIELDS gave 0.55632×10^{-4} W with 1 amp. input current. 457.67 amps. input current will therfore dissipate $(457.67)^2 \times 0.55632 \times 10^{-4} = 11.65$ W in the body. This value is also close to the 12 watts predicted by Massoudi et.al. (18) for a body of similar dimensions.

Effects of isolation from ground are shown by using a different model and working with the same frequency. This situation is shown in Fig. 6.9 and Fig. 6.10. The dissipated power in the body, when it is in direct contact with ground, is nearly ten times higher than the case when it is isolated from the ground by an insulator. By this evidence an operator of a transmitter should feel much safer when he is wearing shoes that are preventing him from a direct contact with the ground.

6.4 Antenna-Body System With Operating Frequency of 90 MHz.

The human body model chosen in this case is the best representation so far of the true situation. The height of the model is 1.7 m and the weight is 179 lbs. An antenna of height $h = 0.25\ \lambda_o$ has been used for this study. The effective number of cells are the cells in which induced electric fields have to be determined from the use of computer program. In this way there are 47 cells, and unlike the previous cases, all of them are not of the same size. The objective here is to study the induced electric fields inside the body, the power density and the total dissipated power at 90 MHz. The conductivity is 0.85 S/m and the dielectric constant is 75.00 at 90 MHz. The coupling problem based on quarter-wave monopole over infinite ground plane is formulated and the

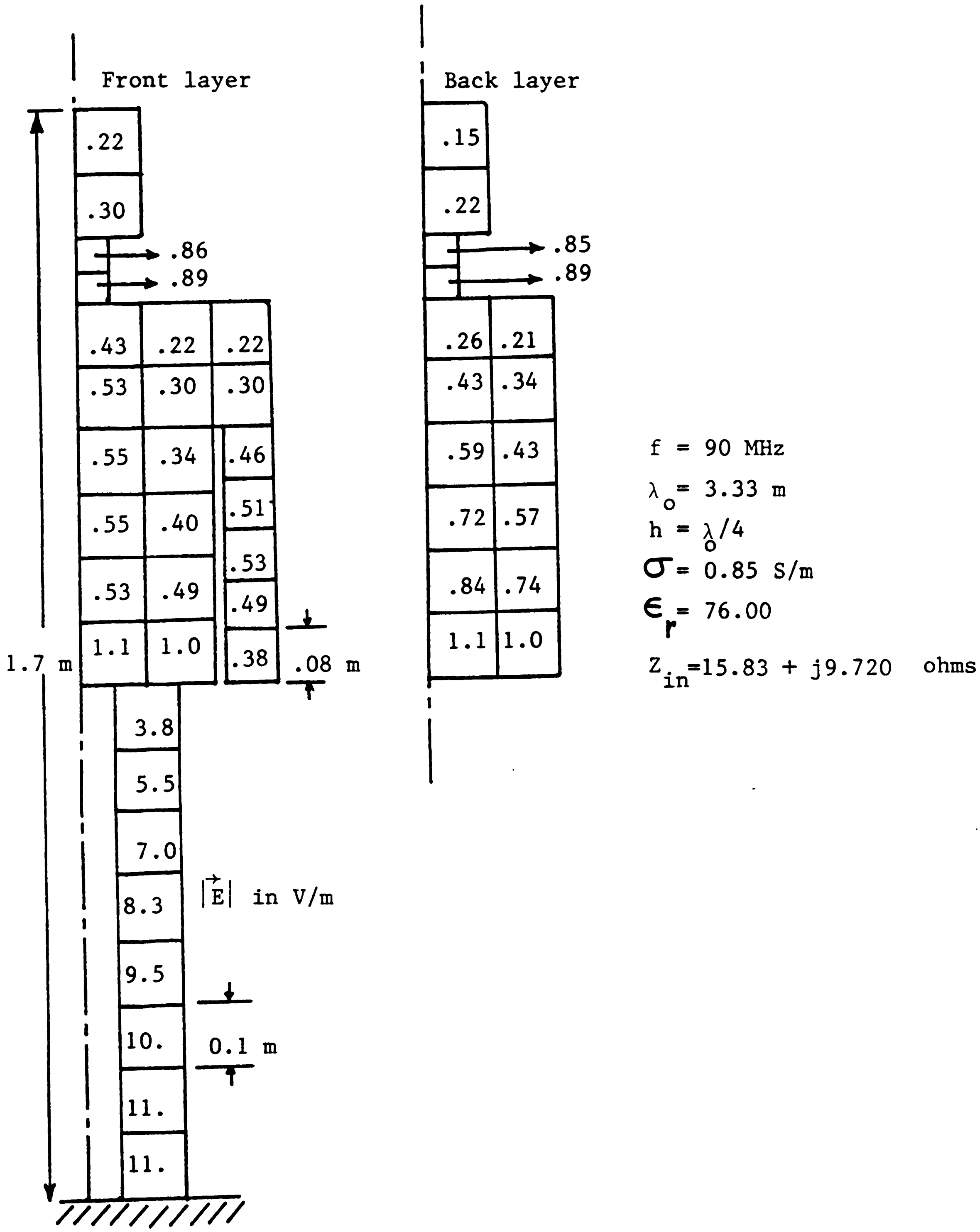

Fig. 6.11. Distribution of the induced electric fields inside the realistic model of a man located in the immediate vicinity of a grounded quarter-wave monopole antenna. Values are based on input power of 1.0 W and spacing of 20 cm between the dipole and the antenna.

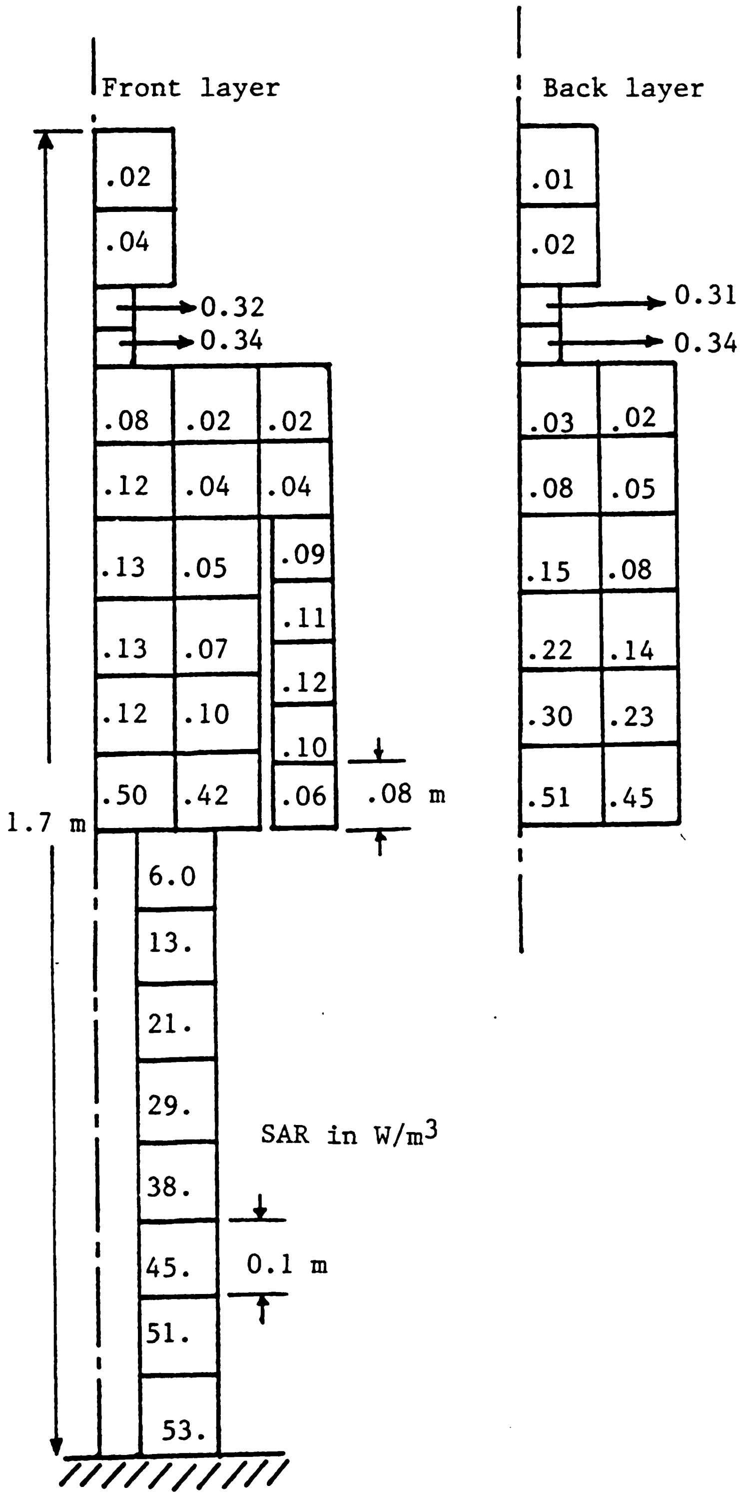

f = 90 MHz

$\lambda_o = 3.33$ m

$h = \lambda_o/4$

$\sigma = 0.85$ S/m

$\epsilon_r = 76.00$

$Z_{in} = 15.83 + j9.72$ ohms

Total power absorbed in the body = 0.5216 W

Fig. 6.12. Distribution of the dissipated power density(SAR) inside the realistic model of man located in the immediate vicinity of a grounded quarter-wave monopole antenna. Values are based on input power of 1.0 W and spacing of 20 cm between the dipole and antenna.

results are given in Fig. 6.11 and 6.12. The spacing between the antenna and the body has been kept at 20 cms. Absorbed power is now 0.5216 watts. Exposure to $10 mW/cm^2$ plane wave dissipate 14.2 watts in the body, thus, the input power to the antenna must be kept below 30 watts for safe operation.

6.5 Problem of Arbitrarily Shaped, Thin-wire Antennas.

A brief outline is given to explain the problem of antenna-body system of Fig. 2.1. In this case equation (2.18) remains the same. However equation (2.19) which is written exclusively for linear antenna directed along the X-axis, is now written in its generalized form

$$\hat{s} \cdot \vec{E}^a(s) + \hat{s} \cdot \vec{E}^b(s) = -V_o \delta(s)$$

Integrals for $\vec{E}^a$ and $\vec{E}^b$ are given in equations (2.16) and (2.17) respectively. In principle, a numerical solution to this problem using pulse function expansion and point matching is possible. However difficulties may arise in modeling an approximate delta function and coping with the size of the resultant matrix; since in this case the currents on the antenna are not uni-directional. Feasibility of this method is questionable. This problem does have considerable practical significance and a wider range of problems could be handled once this problem is solved.

CHAPTER VII

A USER'S GUIDE TO COMPUTER PROGRAM

7.1 Introduction.

This chapter explains the computer program "FIELDS" that provides a numerical solution to the coupled-integral-equations given in equations (2.24) and (2.25) of Chapter II. A major part of this chapter has been devoted to explain in detail, the formulation of a given problem. In this formulation, the antenna-body system as given by the existing situtation of the problem is reduced to a theoretical computer model; this can later be used on the computer to quantify the electric fields in the body and the current distribution on the antenna. In addition to the listing of the program, an example has been worked out to help the user understand the sequential order of data files and the results on printout. A listing of the program "ZFREE", which determines the free-space current distribution and the input impedance of an antenna has also been provided. The listing of FIELDS is valid for the problem given in the example and therefore a brief description of the alteration for implementation of other problems is also given.

7.2 Formulation Of The Problem.

This program finds its true application to problems dealing with linear antennas. More specifically, problems involving interaction of a center-fed, linear dipole antenna with some simple biological systems can be solved successfully. By using image method in EM theory the problems involving base-fed monopole antennas over a conducting plane of infinite extent can also be solved.

The very first step in the numerical formulation of the problem is to visualize a theoretical model of the system which accurately represents the actual physical problem that needs to be solved. This model is obtained as follows. The body is carefully divided into (imaginary) cubic cells not necessarily of the same size. The size of the cells should be sufficiently small. One approximation requires that the edge of the largest cube should not exceed $(1/10)\lambda$ where λ is the wavelength of the radiation inside the body. However, in many cases this requirement can be relaxed. The coordinate system is chosen such that the origin is the feed-point of the antenna and the x-axis lies along the antenna axis. Finally the antenna is assumed to be partitioned into an appropriate number of equal segments. Problems involving monopole antenna over ground plane are first transformed into equivalent dipole arrangement using method of images. See Fig. 7.1.

The maximum size of the coefficient matrix the program can handle is limited by the capacity of the computer system. This restriction imposes an upper limit on the number of cells in the body and the number of partitions on the antenna. This also means that the size of body will have to be smaller as frequency gets larger. "Symmetry of

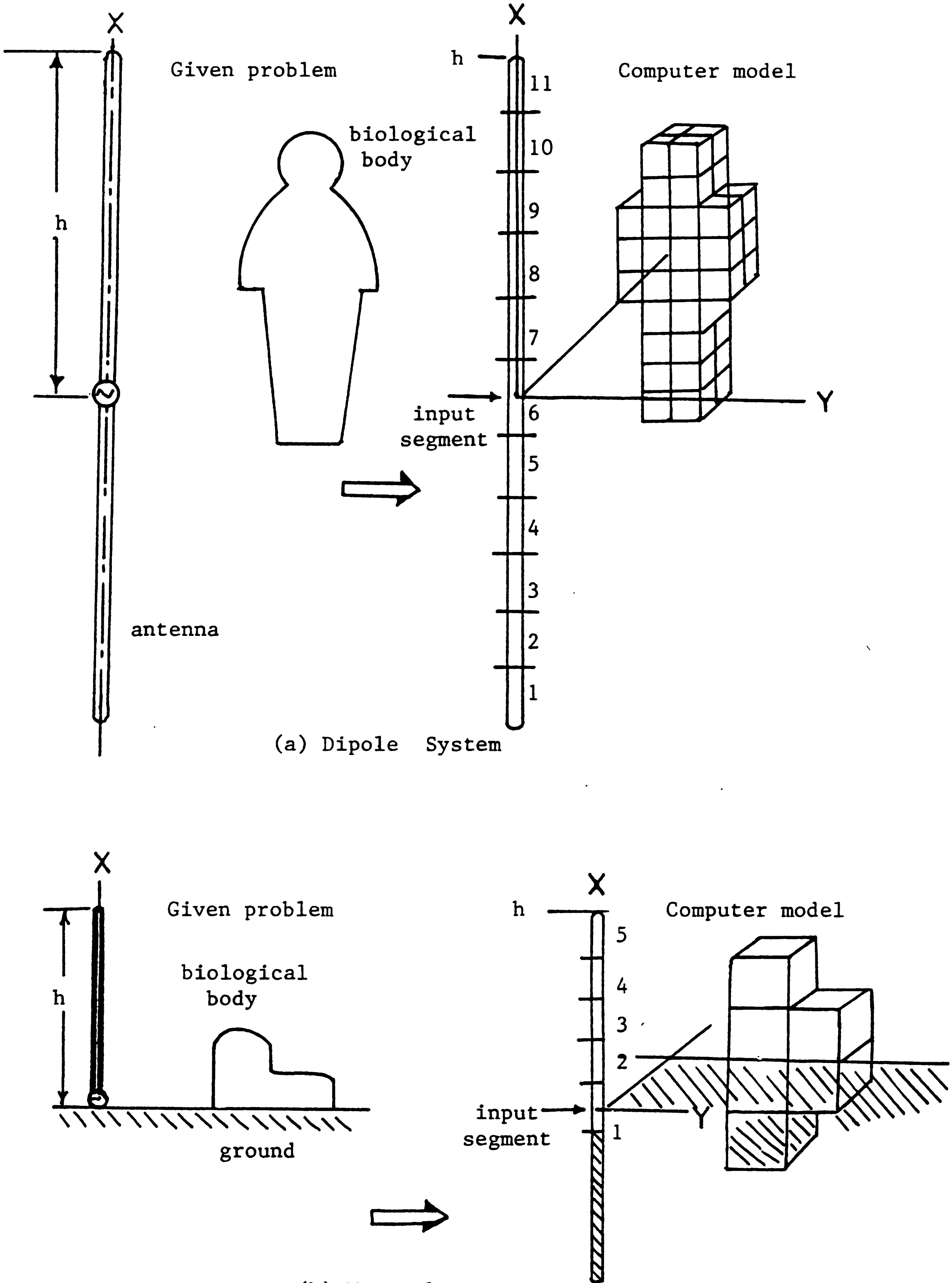

(a) Dipole System

(b) Monopole system

Fig. 7.1. Transformation of the physical system of an antenna and a biological body into a computer model for program FIELDS.

the system" will help us cope with this problem to a great degree. A system will have a "2-quadrant vertical plane symmetry" (2-QUAD VPS) if in the model, a plane passing through the x-axis divides the body in halves one being the mirror image of the other. Again a system will have a "2-quadrant horizontal plane symmetry" (2-QUAD HPS) if the y-z plane divides the body in similar way as above. A system with both types of symmetry existing is said to have a "4-quadrant symmetry" (4-QUAD SYM). Figs. 7.2 and 7.3 demonstrate these definitions more clearly. In case of 2-QUAD VPS the field in cells forming the right half of the body need to be determined; in case of 2-QUAD HPS the fields in cells forming the upper half of the body need only to be determined; and in case of 4-QUAD SYM fields in cells forming the upper right quadrant need to be determined. Furthermore in case of 4-QUAD SYM or 2-QUAD HPS the current distribution is symmetric and hence currents in the segments forming the upper half of the antenna and the input-segment of the antenna need only to be determined. Once the unknowns have been found, the fields in other cells (shaded in Fig. 7.2/3) can be obtained by the field relationships as given in those figures. The order in which the antenna segments are numbered is extremely important i.e. segments are numbered starting from bottom most segment in which current is to be determined, and ending at the top segment. $\lambda_o/40$ is a suitable upper limit on the length of a segment, λ_o being the free-space wavelength.

Referring to Fig. 7.2/3 the fields/(currents) in unshaded

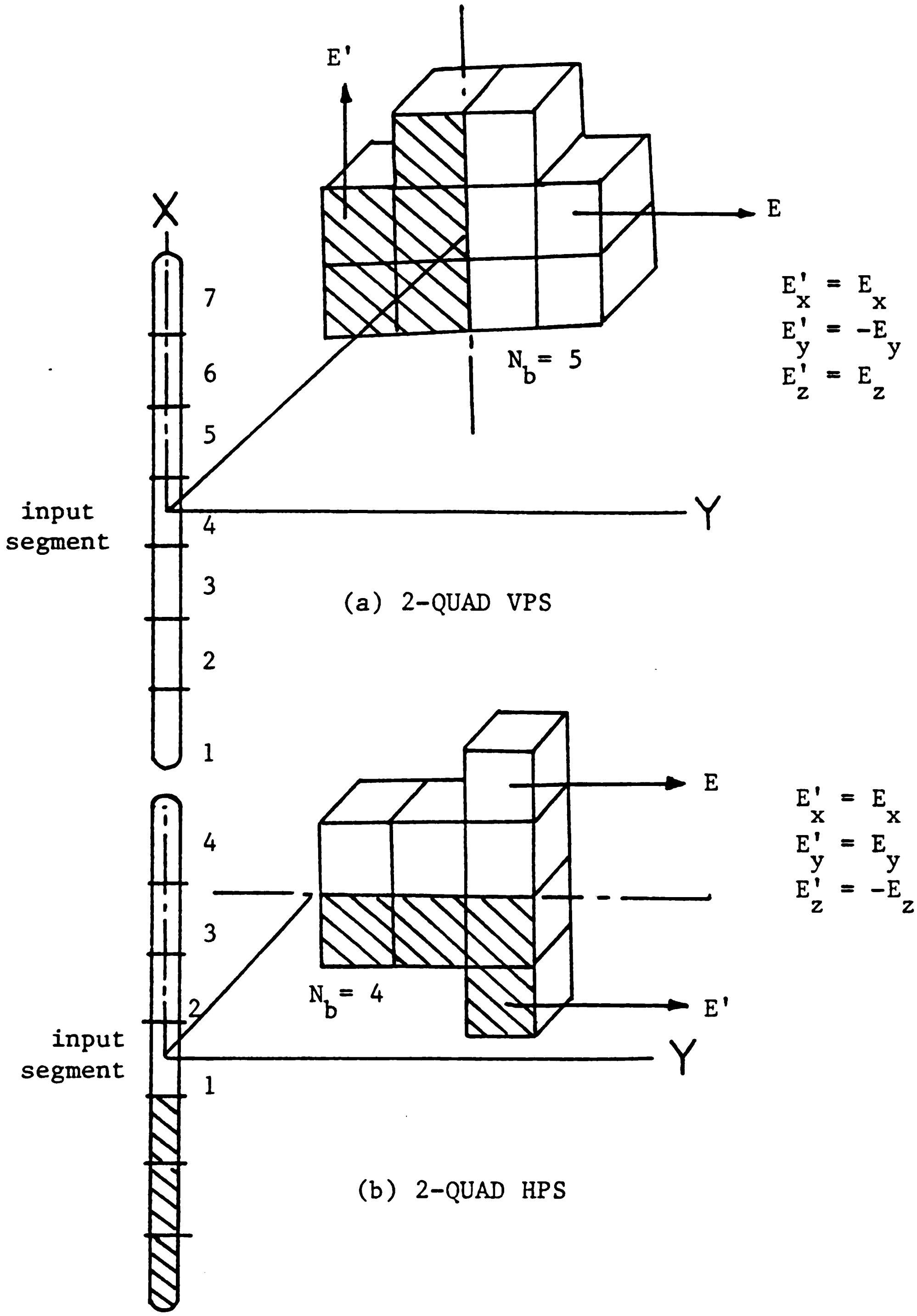

Fig 7.2. Illustration of (a) two quadrant vertical plane symmetry (2-QUAD VPS) and (b) two quadrant horizontal plane symmetry (2-QUAD HPS).

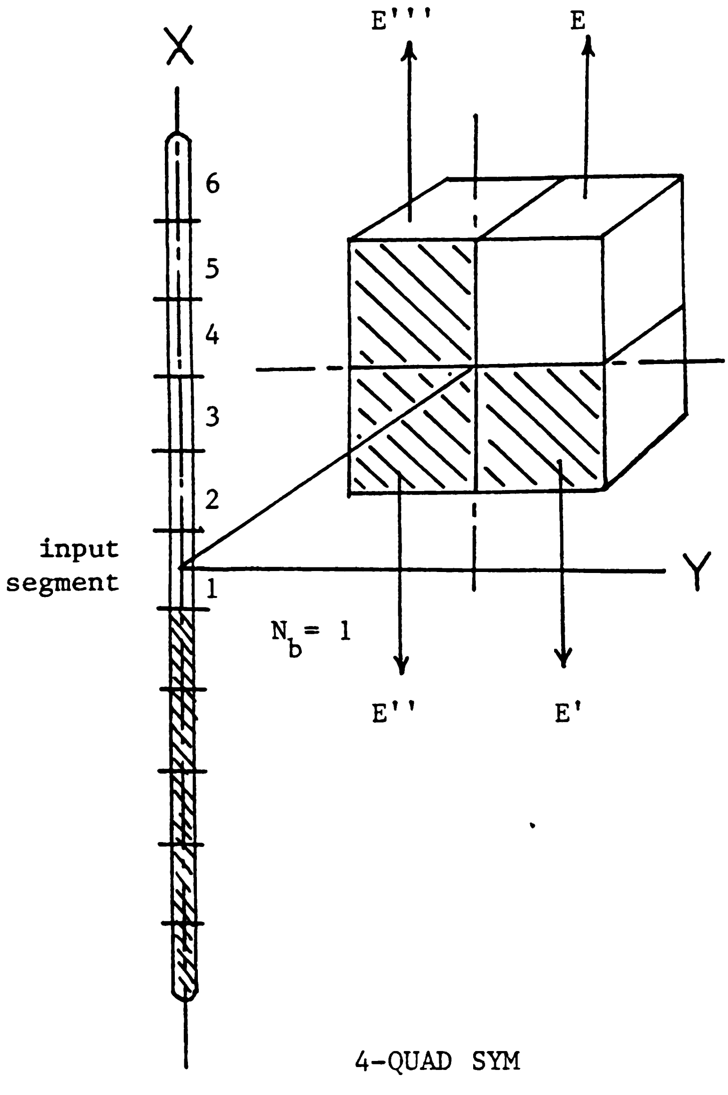

$E'_x = E_x$
$E''_x = E_x$
$E'''_x = E_x$

$E'_y = -E_y$
$E''_y = E_y$
$E'''_y = -E_y$

$E'_z = -E_z$
$E''_z = -E_z$
$E'''_z = E_z$

Fig. 7.3. Illustration of four quadrant symmetry (4-QUAD SYM).

cells/(segments) are to be solved only by the execution of computer program thereby reducing the size of matrix. The size of matrix is given by the expression $(3N_b + N_a) \times (3N_b + N_a)$ where N_b and N_a are the "effective number of cells" in body and "effective number of segments" on antenna. In case of symmetry, N_b will be the number of unshaded cells and N_a will be the number of unshaded segments on the antenna.

The next step in numerical formulation of the program is the specification of the location of each cell of the body. This location is specified by its central coordinates. The body may not be homogeneous and hence the electrical parameters of all cells may not be alike. These parameters are therefore specified for each cell too. The central coordinates of antenna segments are obtained by the program itself (once the height h and N_a are specified) and the right hand side of the system of equations is automatically computed. The program assumes input voltage to antenna as 1 volt (peak value) at the central segment or input segment.

7.2.1 Description of Program.

The computer program is coded in FORTRAN - IV and can be compiled on any FTN compiler. The main program is symbolically named FIELDS. It has a number of subroutines for the numerical evaluation of induced fields in the biological body, unknown antenna current and the radiation pattern in the far-zone. The coefficient matrix obtained by the system of equations generated by the coupled-integral-equations (2.24) and (2.25) is shown below.

$$M = \left|\begin{array}{c|c} A & B \\ \hline C & D \end{array}\right|$$

"MATAA" --- is a subroutine that computes the elements of matrix A.

"MATAB" --- is a subroutine that computes the elements of matrix B.

"MATBA" --- is a subroutine that computes the elements of matrix C.

"MATBB" --- is a subroutine that computes the elements of matrix D.

"CMATP" --- is a subroutine that solves the system of equations by Gauss's - elimination process to determine the unknown fields induced in the body and the currents on the antenna.

"RAD" --- is a subroutine that computes the far zone radiation fields produced by the antenna and body currents at $\phi = 90^{\circ}$ plane (see Fig. 2.3) at intervals of $\Delta\theta = 10^{\circ}$.

Input to the program contains numerical information about the frequency, antenna height, cell location, electrical parameters etc. as well as logical information to enable the program to make decisions with respect to symmetry conditions. These will be discussed in the following section in details. A listing of the entire program is provided in the end of the chapter. The listing for subroutines appears in the order they are called by the main program.

7.3 Data Structure and Input Variables.

The data deck is composed of three files. The first two files have one card. The third file has exactly N_b cards where N_b is the "effective number" of body cells. These files are read by the program, the data being thereby transferred to its corresponding variable names or array names. We will adopt a convention as follows: "for any variable name xxx, (xxx) will represent the data stored under that name, needless to mention that this data will be provided by the user". We will now discuss the data files in detail. The example given in the next section will clarify any ambiguity that may be encountered in this section.

Data File No. 1 This file has one card.

FIELD ALLOCATED	FORMAT CODE	VARIABLE NAME
Col. 1 & 2	I2	NDIV
Col. 3 & 4	I2	NA
Col. 5 & 6	I2	NB
Col. 7 & 8	I2	NQD
Col. 9 & 10	I2	NSYM
Col. 11	I1	CRNT

NDIV Specifies the number of subdivisions an edge of each cell will undergo in integration process in subprogram "MATBB". A suitable choice is (NDIV)=02.

NA (NA) will be equal to the total number of segments on antenna if unsymmetric current distribution is anticipated and it must be an "odd integer". (NA) will be one less than the effective number of segments N_a on antenna in case current distribution on the antenna is considered symmetric.

NB (NB) will be equal to the effective number of cells of the body model if symmetry exists otherwise equal to the total number of cells in the body model.

NQD Specifies the number of identical volumes generated by the symmetry conditions. (NQD)=01 for no symmetry.

(NQD)=02 for 2-QUAD VPS or 2-QUAD HPS.

(NQD)=04 for 4-QUAD SYM.

NSYM Specifies the type of symmetry.

(NSYM)=00 symmetry code for 4-QUAD SYM, 2-QUAD HPS or no symmetry.

(NSYM)=01 symmetry code for 2-QUAD VPS.

CRNT signifies the symmetry condition for the current distribution on the antenna.

(CRNT)=8 for symmetric current assumption.

(CRNT)=9 for non-symmetric current.

Data File No. 2 This file has one card.

FIELD ALLOCATED	FORMAT CODE	VARIABLE NAME
Col. 1 to 10	F 10.1	FMEG
Col. 11 to 20	F 10.1	H
Col. 21 to 30	F 10.1	ANTRD

FMEG (FMEG) is equal to the frequency of the system in MEGA HERTZ.

H (H) is equal to the height "h" of antenna in meters.

ANTRD (ANTRD) is equal to the radius of antenna "a" in meters. The h/a value ranges between 40-125 for best results.

Data File No. 3 This file has exactly N_b cards. To every cell there must be one card and the cells must be numbered in the same sequence as the cards are arranged in the file. In the following description, details are for the "n^{th}" array element of XB, SIGIA, EPRA and DBXA and will contain the data from the n^{th} card of file No. 3.

FIELD ALLOCATED	ARRAY ELEMENT	FORMAT CODE
Col. 1 to 10	XB(n,1)	F 10.1
Col. 11 to 20	XB(n,2)	F 10.1
Col. 21 to 30	XB(n,3)	F 10.1
Col. 31 to 40	DBXA(n)	F 10.1
Col. 41 to 50	EPRA(n)	F 10.1
Col. 51 to 60	SIGIA(n)	F 10.1

XB(n,1) Its contents are the x- coordinate of n^{th} cell in meters.

XB(n,2) Its contents are the y- coordinate of n^{th} cell in meters.

XB(n,3) Its contents are the z- coordinate of n^{th} cell in meters.

DBXA(n) Edge size of n^{th} (cubic) cell in meters.

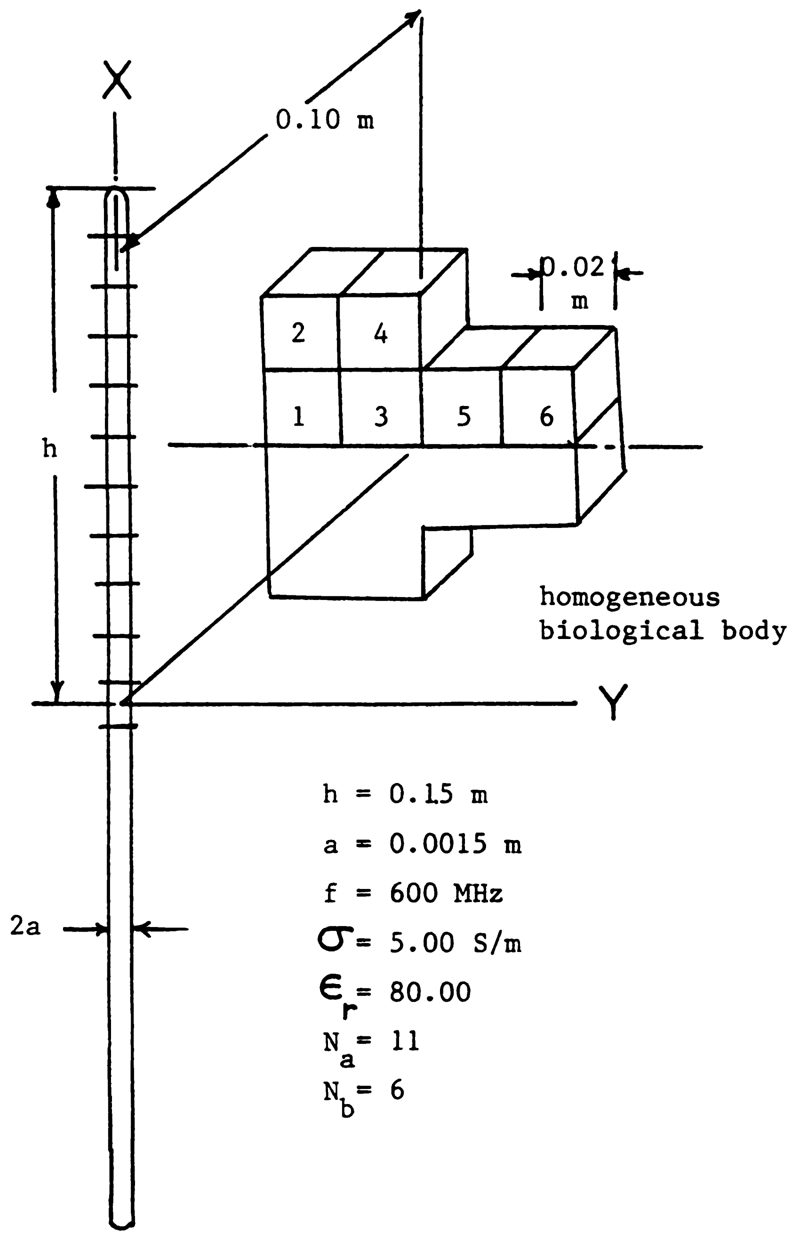

Fig. 7.4. Theoretical model of the system given in the example of section 7.4.

EPRA(n) Relative permittivity (real constant) at the n^{th} cell is stored here.

SIGIA(n) Effective conductivity (S/m) at the n^{th} cell is stored here.

7.4 Example.

Let us assume that a theoretical model of a physical problem has been obtained as discussed in section 7.1, where symmetric current distribtuion and a 2-QUAD HPS is anticipated. This situation is shown in the Fig. 7.4. The body is homogeneous and all cells are of the same size and reasonably small. All input information is listed in Fig. 7.4.

Preparation of Data Deck:

Data File No. 1

Following is the list of numbers and the corresponding variable names that the user should provide in File No. 1.

NUMBERS	VARIABLE NAME	FIELD	REMARKS
02	NDIV	Col. 1 & 2	Economical choice
10	NA	Col. 3 & 4	Since N_a=11
06	NB	Col. 5 & 6	Since N_b=6
02	NQD	Col. 7 & 8	Two identical parts
00 (blank)	NSYM	Col. 9 & 10	Symmetry code for 2-QUAD HPS.
8	CRNT	Col. 11	Code for symmetric current distribution.

Data File No. 2

Following is the list of numbers and corresponding variable names that the user must provide in File No. 2.

NUMBERS	VARIABLE NAME	FIELD	REMARKS
600.00	FMEG	Col. 1 to 10	Frequency in MHz.
0.1500	H	Col. 11 to 20	Height "h" in meters
0.0015	ANTRD	Col. 21 to 30	Radius of antenna in meters.

File No. 3

This file will contain exactly 6 data cards, with information entered as follows. Card numbers in Table 7.1 correspond to the cell numbers in Fig. 7.4.

7.5 Free-Space Program "ZFREE".

This program is used in cases where free-space input impedance of the antenna under consideration is needed. It also gives the current distribution on the antenna at an excitation voltage of 1 volt peak value. In this program an additional feature is incorporated by the use of subroutine "EIMP" and it is an optional. By virtue of this subroutine, electric fields at any location or various locations in space, can be computed. Even though this is an independent program, it is suggested that the same effective number of segments N_a be used in this program as were used in FIELDS. The following data file is prepared to determine the free-space current distribution and input impedance of the antenna. A listing of this program appears after the FIELDS.

card no	NUMERICAL DATA ON THE CARDS					
1	0.01	-0.03	0.11	0.02	80.00	5.00
2	0.03	-0.03	0.11	0.02	80.00	5.00
3	0.01	-0.01	0.11	0.02	80.00	5.00
4	0.03	-0.01	0.11	0.02	80.00	5.00
5	0.01	0.01	0.11	0.02	80.00	5.00
6	0.01	0.03	0.11	0.02	80.00	5.00
Symb	XB(n,1)	XB(n,2)	XB(n,3)	DBXA(n)	EPRA(n)	SIGIA(n)
fld.	col 1 to 10	col 11 to 20	col 21 to 30	col 31 to 40	col 41 to 50	col 51 to 60
Dim.	meters	meters	meters	meters	------	S/m

TABLE 7.1. Data in FILE no. 3. This data corresponds to the example problem of section 7.4.

Data File No. 1 It has one card only.

NUMBER	VARIABLE NAME	FIELD ALLOCATED	REMARKS
600.00	FMEG	Co. 1 to 10	Frequency (MHz)
0.1500	H	Col. 11 to 20	Antenna of height "h" (m)
0.00150	ANTRAD	Col. 21 to 30	Antenna of radius "a" (m)
10	NA	Col. 31 to 32	11 segments
0	EFIELD	Col. 40	Electric field is not desired.

When electric field is required, Col. 40 of Data File No. 1 must be filled by any integer other than 0; furthermore, following data files must be inserted after File No. 1.

Data File No. 2 Comprise of one card. It contains the number of locations (at which the electric fields are desired) in first two columns.

Data File No. 3 The number of cards in this file is equal to the number of locations specified in File No. 2.

FIELD ALLOCATED	LOCATIONS' COORDINATES
Col. 1 to 10	x-coordinate (m)
Col. 11 to 20	y-coordinate (m)
Col. 21 to 30	z-coordinate (m)

7.6 The Printout of Results.

The printed output shown in the following pages contains the results of the example problem. Major part of this is self explanatory.

Page 1 provides a check of the input data supplied by the user, page 2 gives the currents in the segments of antenna, page 3 gives the induced electric fields, power density and power absorbed in upper half of the body and page 4 gives the normalized absolute value of the radiation-zone fields. We will now discuss some points which need extra attention. On page 2 the current values are in amperes based on 1 volt peak driving voltage and are printed in exactly the same order as the segments are numbered in Fig. 7.4. In general the current values are printed in the same order as that shown in Fig. 7.2. Similarly on page 3 the serial number identifying the fields, power density etc. is also the cell number to which that field value belongs, recalling that the cells have been numbered in the same sequence as their representative data cards in File No. 3. Finally electric fields are given in volts/m, power density in watts/meter^3 and power in upper half in watts all based upon an assumed voltage of 1 volt peak at the driving point of antenna. For a dipole system, to get total absorbed power, the value referred to by "power in quadrant 1" is to be multiplied by 1 if no symmetry, by 2 if 2-QUAD VPS or 2-QUAD HPS and by 4 if 4-QUAD SYM exists. On page 4 the normalized absolute values of electric fields are the fields at 10° interval, first value corresponding to $\theta = 0^\circ$ and the last to $\theta = 180^\circ$, on a $\phi = 90^\circ$ plane according to the Fig. (2.3). Printout for ZFREE is similar and details need not be repeated. Current in amps. is based on 1 volt peak driving voltage at the input as before.

A Complete FORTRAN-IV listing of FIELDS and ZFREE for this sample problem has been provided following the printout of results. Discussion that follows is for FIELDS. To save on the storage space of computer, the dimensions of array G and A in the main program and the subroutine CMATP respectively, must be kept equal to the dimension of the augumented matrix of the problem. These adjustments can be easily made on card 009 and 423, (see the listing). On CDC6500 this minor difficulty can be completely eliminated by the use of SETFL, a system subroutine. In this case the following changes must be incorporated.

(1) Card 009 should be "COMMON G(120,1)"
(2) Card 423 should be "DIMENSION A(120,1)"
(3) Insert card "CALL SETFL (G(MA,MAP1))" between card 029 & 030.

The program will then automatically dimension these arrays to the required size. The matrix size must not exceed (117x118) since this is the maximum that can be handled by the above mentioned system. In cases where radiation fields are of no importance, cards 131-148 in the main program and subroutine "RAD" can be removed to improve efficiency of the program. As a final word, for large matrix size "MERIT" system has proven more efficient than CDC6500. The FIELDS listing given here is compatible with both systems and except for changes in control cards, no other changes are required in the program.

PAGE NO. 1

```
*******************************************
----------CONSTANTS  OF THE SYSYEM----------    SPACE DIMENSION IN METERS
*******************************************
 FREQ. =     600.00   HEIGHT H =     .1500
PARTITION NA=10   NUM OF SUBDIV= 2
 2 QUAD SYMMETRY USED WITH CODE  0


 NUM OF ROWS    29      NUM OF COLMS   30
```

	X1	X2	X3	EPR	SIG	EDGE
1	.1000E-01	-.3000E-01	.1100E+00	.8000E+02	.5000E+01	.2000E-01
2	.3000E-01	-.3000E-01	.1100E+00	.8000E+02	.5000E+01	.2000E-01
3	.1000E-01	-.1000E-01	.1100E+00	.8000E+02	.5000E+01	.2000E-01
4	.3000E-01	-.1000E-01	.1100E+00	.8000E+02	.5000E+01	.2000E-01
5	.1000E-01	.1000E-01	.1100E+00	.8000E+02	.5000E+01	.2000E-01
6	.1000E-01	.3000E-01	.1100E+00	.8000E+02	.5000E+01	.2000E-01

PAGE NO. 2

CURRENT DISTRIBUTION ON THE ANTENNA .

1	.3389E-02	-.3528E-02
2	.3313E-02	-.4201E-02
3	.3185E-02	-.4438E-02
4	.2984E-02	-.4469E-02
5	.2716E-02	-.4315E-02
6	.2386E-02	-.3990E-02
7	.2004E-02	-.3506E-02
8	.1576E-02	-.2878E-02
9	.1111E-02	-.2114E-02
10	.6107E-03	-.1219E-02
11	0.00	

INPUT IMPEDANCE= .14161E+03 .14742E+03

PAGE NO.3

INDUCED ELECTRIC FIELDS IN QUADRANT 1 .

N	EX(V/M)		EY(V/M)		EZ(V/M)	
1	-.12262E+00	.76436E-01	.35545E-02	.14764E-02	-.58094E-04	-.15710E-02
2	-.91674E-01	.54487E-01	.22159E-01	-.46737E-02	-.57614E-03	-.77291E-02
3	-.13459E+00	.61335E-01	-.33427E-02	.56060E-02	.30128E-04	-.13028E-02
4	-.10171E+00	.46607E-01	-.34609E-02	.87035E-02	-.36353E-03	-.84480E-02
5	-.35588E-01	.10874E-01	-.12783E-01	.94553E-02	-.80488E-04	-.29054E-02
6	-.44749E-01	.22557E-01	-.16251E-01	.82205E-02	-.22356E-03	-.34846E-02

N	EX(V/M)	EY(V/M)	EZ(V/M)	POWER DENSITY
1	.14449651E+00	.38488999E-02	.15720811E-02	.52241320E-01
2	.10664403E+00	.22646907E-01	.77505823E-02	.29864760E-01
3	.14790472E+00	.74035434E-02	.13031780E-02	.54830795E-01
4	.11187584E+00	.93663232E-02	.84558170E-02	.31688580E-01
5	.37211893E-01	.15899690E-01	.29065246E-02	.41149325E-02
6	.50112408E-01	.18211739E-01	.34917836E-02	.71377837E-02

POWER IN QUADRANT 1 .14390F-05

PAGE NO. 4

RADIATION FIELDS

1	.92262E+00
2	.92170E+00
3	.92046E+00
4	.91944E+00
5	.91934E+00
6	.92086E+00
7	.92457E+00
8	.93069E+00
9	.93900E+00
10	.94888E+00
11	.95943E+00
12	.96970E+00
13	.97891E+00
14	.98654E+00
15	.99239E+00
16	.99648E+00
17	.99896E+00
18	.10000E+01
19	.99968E+00

PAGE NO. 1

CURRENT DISTRIBUTION ON ANTENNA IN FREE-SPACE

1	.33848E-02	-.34134E-02
2	.33099E-02	-.40876E-02
3	.31826E-02	-.43282E-02
4	.29830E-02	-.43656E-02
5	.27161E-02	-.42202E-02
6	.23881E-02	-.39062E-02
7	.20065E-02	-.34362E-02
8	.15796E-02	-.28225E-02
9	.11142E-02	-.20752E-02
10	.61301E-03	-.11974E-02
11	0.	0.

ADMITTANCE = .33848E-02 -.34134E-02 IMPEDANCE = .14648E+03 .14771E+03

```
      PROGRAM FIELDS(INPUT,OUTPUT)                                              001
C*******************************************************************************
C  THIS PROGRAM DETERMINES THE CURRENT DISTRIBUTION ON ANTENNA AND              001
C  INDUCED FIELD INSIDE THE BODY, BY SOLVING THE COUPLED INTEGRAL EQUATION      001
C*******************************************************************************
      REAL MU                                                                   002
      INTEGER CRNT                                                              002
      COMPLEX AJ,G,CIL,DIN(3),FML(3),SMGBR,ZO,DET                               003
      COMPLEX A(30)                                                             004
      DIMENSION E(20)                                                           004
      DIMENSION XA(21),XB(34,3),DBXA(34),EPRA(34),SIGIA(34)                     005
      COMMON/MATO/XA,XB,NA,NB,DBXA                                              006
      COMMON/MAT1/DAX,ANTRD,CRNT                                                007
      COMMON/MAT24/EPS,EPRA,SIGIA,NQD,NSYM/MAT3/MU,OMEG,PI,BO                   008
      DIMENSION G(29,30)                                                        009

C*********************************************************** ********* **********

C   READ DATA AND OFFSET DATA IF NECESSARY                                      010

      READ 1,NDIV,NA,NB,NQD,NSYM,CRNT                                           011
      READ 3,FMEG,H,ANTRD                                                       012
      DO 5 M=1,NB,1                                                             013
      READ 2,(XB(M,J),J=1,3),DBXA(M),EPRA(M),SIGIA(M)                           014
    5 CONTINUE                                                                  015

C*******************************************************************************

      PRINT 153                                                                 016
      PRINT 154,FMEG,H,NA,NDIV,NQD,NSYM                                         017


      IF(CRNT.EQ.8) GO  TO  21                                                  018
      DAX=2.0*H/NA                                                              019
      XAO=-H+DAX/2.0                                                            020
      KK=(NA/2)+1                                                               021
      GO TO 22                                                                  022
   21 DAX=2*H/(NA*2+1)                                                          023
      NA=NA+1                                                                   024
      XAO=0.0                                                                   025
      KK=1                                                                      026
   22 MA=3*NB+NA                                                                027
      MAP1=MA+1                                                                 028
      PRINT 30,MA,MAP1                                                          029
      DO 4 J=1,MA,1                                                             030
      DO 4 I=1,MAP1,1                                                           031
      G(J,I)=CMPLX(0.0,0.0)                                                     032
    4 CONTINUE                                                                  033
```

```
      PI=3.14159264                                                     034
      SO=120*PI                                                         035
      EPS=8.854E-12                                                     036
      OMEG=2*PI*FMEG*1.0E+06                                            037
      MU=4*PI*1.0E-07                                                   038
      AJ=CMPLX(0.0,1.0)                                                 039
      BO=OMEG*SQRT(MU*EPS)                                              040
      DO 8 M=1,NA,1                                                     041
      XA(M)=XAO+(M-1)*DAX                                               041
      G(M,MAP1)=-AJ*2*PI*SIN(BO*ABS(XA(M)))/SO                          042
    8 CONTINUE                                                          043
      PRINT 9                                                           044
C***********************************************************************
C     PRINT CO-ORDINATES OF CELLS AND ITS PARAMETERS
C***********************************************************************
      DO 10 M=1,NB,1                                                    045
      PRINT 11,M,(XB(M,J),J=1,3),EPRA(M),SIGIA(M),DBXA(M)               046
   10 CONTINUE                                                          047
      DO 12 L=1,NA,1                                                    048
      DO 12 I=1,NA,1                                                    049
      XF=XA(I)                                                          050
      XS=XA(L)                                                          051
C***********************************************************************
C    SUBROUTINE MATAA DETERMINES THE UPPER L.H.S SUBMATRIX NA BY NA     052
C    NA=NUMBER OF PARTITIONS ON ANTENNA                                 052
      CALL MATAA(NA,BO,XF,XS,I,L,CIL)                                   053
C***********************************************************************
      G(I,L)=CIL                                                        054
   12 CONTINUE                                                          055
      DO 13 N=1,NB,1                                                    056
      DO 13 I=1 ,NA,1                                                   057
      N1=NA+N                                                           058
      N2=NA+NB+N                                                        059
      N3=2*NB+NA+N                                                      060
C***********************************************************************
C    SUBROUTINE MATAB  DETERMINES THE UPPER R.H. SUBMATRIX NA BY 3NB    061
C    NA=NUMBER OF PARTITIONS ON ANTENNA   NB= NUMBER OF CELLS IN BODY   061
      CALL MATAB(I,N,DIN)                                               062
C***********************************************************************
      G(I,N1)=DIN(1)                                                    063
      G(I,N2)=DIN(2)                                                    064
      G(I,N3)=DIN(3)                                                    065
   13 CONTINUE                                                          066
```

```
      DO 14 L=1,NA,1                                                    067
      DO 14 M=1,NB ,1                                                   068
      M1=NA+M                                                           069
      M2=M+NA+NB                                                        070
      M3=M+NA+2*NB                                                      071
      IF(L.EQ.NA)GO TO 15                                               072
      IF((L.EQ.1).AND.(CRNT.EQ.9))   GO   TO  15                        073
C*********************************************************************

C   SUBROUTINE MATBA  DETERMINES THE LOWER L.H.S SUBMATRIX 3NB BY NA    074
C   NA=NUMBER OF PARTITIONS ON ANTENNA    NB= NUMBER OF CELLS IN BODY   074
      CALL MATBA(M,L,FML)                                               075

C*********************************************************************
      G(M1,L)=FML(1)                                                    076
      G(M2,L)=FML(2)                                                    077
      G(M3,L)=FML(3)                                                    078
      GO TO 14                                                          079
   15 G(M1,L)=CMPLX(0.0,0.0)                                            080
      G(M2,L) =CMPLX(0.0,0.0)                                           081
      G(M3,L)=CMPLX(0.0,0.0)                                            082
   14 CONTINUE                                                          083
      DO 16 NQ=1,3,1                                                    084
      DO 16 N=1 ,NB,1                                                   085
      DO 16 MP=1 ,3,1                                                   086
      DO 16 M=1,NB,1                                                    087
      I=NA+M+(MP-1)*NB                                                  088
      J=NA+N+(NQ-1)*NB                                                  089
C*********************************************************************

C   SUBROUTINE MATBB  DETERMINES THE LOWER R.H.S SUBMATRIX 3NB BY 3NB   090
C   NB=NUMBER OF CELLS IN BODY                                          090
      CALL MATBB(NDIV,M,N,MP,NQ,SMGBR)                                  091

C*********************************************************************
      G(I,J)=SMGBR                                                      092
   16 CONTINUE                                                          093
C*********************************************************************

C   SUBROUTINE  CMATP   SOLVES THE SYSTEM OF (3NB+NA) EQUATIONS BY      094
C        GAUSS- ELIMINATION PROCESS                                     095
      CALL CMATP(G,MA,1,DET,1.0E-100)                                   096

C*********************************************************************
      PRINT 101                                                         097
      DO 17 I=1,NA,1                                                    098
      IF(I.EQ.NA) GO TO 20                                              099
      IF((I.EQ.1).AND.(CRNT.EQ.9))   GO   TO  20                        100
```

```
      PRINT 102, I, G(I, MAP1)                                          101
      GO TO 17                                                          102
   20 PRINT 106, I                                                      103
   17 CONTINUE                                                          104
      ZO=1/G(KK, MAP1)                                                  105
      PRINT 105, ZO                                                     106
      PRINT 155                                                         107
      PRINT 103                                                         108
      DO 18 K=1, NB, 1                                                  109
      K1=NA+K                                                           110
      K2=NA+NB+K                                                        111
      K3=NA+2*NB+K                                                      112
      PRINT 104, K, G(K1, MAP1), G(K2, MAP1), G(K3, MAP1)               113
   18 CONTINUE                                                          114
      PRINT 156                                                         115
      PTOT=0. 0                                                         116
      DO 19 K=1, NB, 1                                                  117
      K1=NA+K                                                           118
      K2=NA+NB+K                                                        119
      K3=NA+2*NB+K                                                      120
      EF1=CABS(G(K1, MAP1))                                             121
      EF2=CABS(G(K2, MAP1))                                             122
      EF3=CABS(G(K3, MAP1))                                             123
      SIGI=SIGIA(K)                                                     124
      DBX=DBXA(K)                                                       125
      PWR=(EF1**2+EF2**2+EF3**2)*SIGI*0. 5                              126
      PTOT=PTOT+PWR*DBX**3                                              127
      PRINT 157, K, EF1, EF2, EF3, PWR                                  128
   19 CONTINUE                                                          129
      PRINT 158, PTOT                                                   130
C***********************************************************************

C  WHEN USING RAD DIMENSION OF ARRAY A =3NB+NA+1
C REMOVE CARDS NO. 131--148 AND SUBRT. RAD  IF RADIATION FIELDS NOT REQD.

C***********************************************************************
      DO 24 J=1, MA, 1                                                  131
      A(J)=G(J, MAP1)                                                   132
   24 CONTINUE                                                          133
      PHI=90. 0                                                         134
      NTHET=19                                                         135A
      PRINT 159                                                        135B
  159 FORMAT(1H1, 15X, 16HRADIATION FIELDS)                             136
      EMAX=0. 0                                                         137
      DO 25 J=1, NTHET, 1                                               138
      THETA=(J-1)*10. 00                                                139
```

```
C*************************************************************************** RAD*****
C    SUBROUTINE RAD COMPUTES AND PRINTS THE RADIATION FIELDS
        CALL RAD(A,THETA,PHI,ERAD,EMAX)

C*************************************************************************** RAD*****
        E(J)=ERAD
     25 CONTINUE
        DO 23 I=1,NTHET,1
        ENOR=E(I)/EMAX
        PRINT 107,I,ENOR
    107 FORMAT(1H0,15X,I3,E13.5)
     23 CONTINUE
C***********************************************************************************

C     PROGRAM FORMATS.

C***********************************************************************************

      1 FORMAT(5I2,I1)
      2 FORMAT(6F10.1)
      3 FORMAT(3F10.1)
      9 FORMAT(1H0,16X,2HX1,12X,2HX2,12X,2HX3,11X,3HEPR,11X,3HSIG,11X,4HED
       1GE)
     11 FORMAT(1H0,I3,5X,6E14.4)
     30 FORMAT(1H0,2X,12HNUM OF ROWS ,I5,6X,12HNUM OF COLMS,I5,///)
    101 FORMAT(1H1,20X,37HCURRENT DISTRIBUTION ON THE ANTENNA .)
    102 FORMAT(1H0,I3,2E14.4)
    103 FORMAT(1H0,2X,1HN,19X,7HEX(V/M),28X,7HEY(V/M),28X,7HEZ(V/M))
    104 FORMAT(1H0,I3,9X,2(E12.5,3X),4X,2(E12.5,3X),4X,2(E12.5,3X))
    105 FORMAT(1H0,16HINPUT IMPEDANCE=,3X,2E14.5)
    106 FORMAT(1H0,I3,5X,4H0.00)
    153 FORMAT(1H1,44H********************************************,//,
       11X,44H----------CONSTANTS  OF THE SYSYEM----------,4X,25HSPACE DIM
       3ENSION IN METERS,//,
       21X,44H********************************************)
    154 FORMAT(1H0,1X,7HFREQ.  =,F10.2,3X,10HHEIGHT H =,F10.4,//,
       11X,13HPARTITION NA=,I2,3X,14HNUM OF SUBDIV=,I2,//,
       21X,I2,29H QUAD SYMMETRY USED WITH CODE,I3,/////)
    155 FORMAT(1H1,//,25X,39HINDUCED ELECTRIC FIELDS IN QUADRANT 1 .)
    156 FORMAT(1H0,//,16X,1HN,8X,7HEX(V/M),11X,7HEY(V/M),11X,7HEZ(V/M),13X
       C,13HPOWER DENSITY)
    157     FORMAT(1H0,13X,I3,3X,4(E16.8,2X))
    158 FORMAT(1H0,//,1X,22H  POWER IN QUADRANT 1 ,E12.5)
        END
```

```
      SUBROUTINE MATAA(NA,BO,XI,XL,I,L,CIL)
      INTEGER CRNT
      COMPLEX CIL,Y1Y5,YEVEN,YODD,AJ,TOTAL
      COMMON/MAT1/DAX,ANTRD,CRNT
      IF(L.EQ.NA) GO TO 2
      IF((L.EQ.1).AND.(CRNT.EQ.9)) GO  TO  3
      K=1
      TOTAL=CMPLX(0.0,0.0)
    1 A=XL-DAX/2
      IF((I.EQ.L).AND.(K.EQ.1))  GO TO 4
      Y1Y5=CMPLX(0.0,0.0)
      YEVEN=CMPLX(0.0,0.0)
      YODD=CMPLX(0.0,0.0)
      DELTX=DAX/10
      DO 5 M=1,11,1
      AA=A+(M-1)*DELTX
      R=SQRT((XI-AA)**2+ANTRD**2.0)
      AJ=CEXP(CMPLX(0.0,-BO*R))
      GO TO (10,20,30,20,30,20,30,20,30,20,10)M
   10 Y1Y5=Y1Y5+AJ/R
      GO TO 5
   20 YEVEN=YEVEN+AJ/R
      GO TO 5
   30 YODD=YODD+AJ/R
    5 CONTINUE
      TOTAL=TOTAL+(Y1Y5+YEVEN*4.0+YODD*2.0)*DELTX/3.0
      GO TO 6
    4 B=A+DAX
      AAA=ALOG((XI-A+SQRT((XI-A)**2+ANTRD**2.0))/
     *(XI-B+SQRT((XI-B)**2+ANTRD**2.0)))
      TOTAL=CMPLX(AAA,0.0)
    6 IF(L.EQ.1)  GO  TO  7
      IF(CRNT.EQ.9)  GO  TO  7
      IF(K-2)8,7,7
    8 K=K+1
      XL=-XL
      GO TO 1
    7 CIL=TOTAL
      GO  TO  99
    2 CIL=CMPLX(COS(BO*XI),0.0)
      GO  TO  99
    3 CIL=CMPLX(SIN(BO*XI),0.0)

   99 RETURN
      END
```

```
      SUBROUTINE MATAB(I,N,DIN)
      REAL MU
      COMPLEX AJ,DIN(3),FALFA,Y1Y9,YEVEN,YODD,EXPO,CONST,D(4)
      DIMENSION XA(21),XB(34,3),DBXA(34),EPRA(34),SIGIA(34)
      COMMON/MATO/XA,XB,NA,NB,DBXA
      COMMON/MAT24/EPS,EPRA,SIGIA,NQD,NSYM/MAT3/MU,OMEG,PI,BO
      EPR=EPRA(N)
      SIGI=SIGIA(N)
      DBX=DBXA(N)
      IF(XA(I).EQ.0.0)  GO TO 7
      DO 100 K=1,4,1
      D(K)=CMPLX(0.0,0.0)
  100 CONTINUE
      KK=32
      NK=KK+1
      AJ=CMPLX(0.0,1.0)
      SO=120*PI
      DELTX=XA(I)/KK
      CONST=(OMEG*MU*BO/SO)*(SIGI + AJ*OMEG*EPS*(EPR-1.0))*DBX**3.0
      X3=XB(N,3)
      DO 6 NQ=1,3,1
      DO 9 JK=1,NQD,1
      IF(JK.EQ.1)  GO  TO  22
      IF(NSYM.EQ.0)  GO  TO  22
      KQ=4
      GO  TO  21
   22 KQ=JK
   21 Y1Y9=CMPLX(0.0,0.0)
      YEVEN=CMPLX(0.0,0.0)
      YODD=CMPLX(0.0,0.0)
      GO TO (11,12,13,14)KQ
   11 X1=XB(N,1)
      X2=XB(N,2)
      GO TO 15
   12 X1=-XB(N,1)
      X2=XB(N,2)
      GO TO 15
   13 X1=-XB(N,1)
      X2=-XB(N,2)
      GO TO 15
   14 X1=XB(N,1)
      X2=-XB(N,2)
   15 DO 5 M=1,NK,1
      U=(M-1)*DELTX
      R=SQRT((U-X1)**2+X3**2+X2**2)
      ALPHA=BO*R
      EXPO=CEXP(CMPLX(0.0,-ALPHA))/(ALPHA**3)
      IF(NQ-2)1,2,3
    1 FALFA =EXPO*SIN(BO*(XA(I)-U))*((ALPHA**2-1-AJ*ALPHA)+
     C((U-X1)**2)*(3-ALPHA**2+3*AJ*ALPHA)/R**2)
```

```
      GO TO 4
    2 FALFA =EXPO*SIN(BO*(XA(I)-U))*(-X2)*(U-X1)*
     C(3-ALPHA**2+3*AJ*ALPHA)/R**2
      GO TO 4
    3 FALFA =EXPO*SIN(BO*(XA(I)-U))*(-X3)*(U-X1)*
     C(3-ALPHA**2+3*AJ*ALPHA)/R**2
    4 IF((M.EQ.1).OR.(M.EQ.NK)) GO TO 10
      K=M/2
      IF(2*K-M)30,20,30
   30 YODD=YODD+FALFA*CONST
      GO TO 5
   20 YEVEN=YEVEN+FALFA*CONST
      GO TO 5
   10 Y1Y9=Y1Y9+FALFA*CONST
    5 CONTINUE
      D(KQ)=(Y1Y9+4.0*YEVEN+2.0*YODD)*DELTX/3.0

    9 CONTINUE
      IF(NQ-2)16,17,18
   16 DIN(NQ) =D(1)+D(2)+D(3)+D(4)
      GO TO 6
   17  DIN(NQ)=D(1)+D(3) -D(2)-D(4)
      GO TO 6
   18 DIN(NQ)=D(1)+D(4)-D(2)-D(3)
    6 CONTINUE
      GO TO 8
    7 DIN(1)=CMPLX(0.0,0.0)
      DIN(2)=CMPLX(0.0,0.0)
      DIN(3)=CMPLX(0.0,0.0)
    8 RETURN
      END
```

```
      SUBROUTINE MATBA(M,L,FML)
      REAL MU
      INTEGER CRNT
      COMPLEX AJ,FML(3),FALFA,Y1Y5,YEVEN,YODD,EXPO,CONST
      DIMENSION XA(21),XB(34,3),DBXA(34)
      COMMON/MAT0/XA,XB,NA,NB,DBXA
      COMMON/MAT1/DAX,ANTRD,CRNT/MAT3/MU,OMEG,PI,BO
      AJ=CMPLX(0.0,1.0)
      KK=8
      NK=KK+1
      DELTX=DAX/KK
      CONST=-AJ*OMEG*MU*BO/(4.0*PI)
      DO 6 NP=1,3,1
      XL=XA(L)
      K=1
      FML(NP)=CMPLX(0.0,0.0)
    7 A=XL-DAX/2.0
      Y1Y5=CMPLX(0.0,0.0)
      YEVEN=CMPLX(0.0,0.0)
      YODD=CMPLX(0.0,0.0)
      DO 5 N=1,NK,1
      AA=A+(N-1)*DELTX
      R=SQRT((XB(M,1)-AA)**2+XB(M,2)**2+XB(M,3)**2)
      ALPHA=BO*R
      EXPO=CEXP(CMPLX(0.0,-ALPHA))/(ALPHA**3)
      IF(NP-2)1,2,3
    1 FALFA =EXPO*((ALPHA**2-1-AJ*ALPHA)+((XB(M,1)-AA)**2)*
     C(3.0-ALPHA**2+3.0*AJ*ALPHA)/R**2)
      GO TO 4
    2 FALFA =EXPO*(XB(M,2))*(XB(M,1)-AA)*(3.0-ALPHA**2+3.0*AJ*ALPHA)/
     CR**2
      GO TO 4
    3 FALFA =EXPO*(XB(M,3))*(XB(M,1)-AA)*(3.0-ALPHA**2+3.0*AJ*ALPHA
     C)/R**2
    4 IF((N.EQ.1).OR.(N.EQ.NK))GO TO 10
      KP=N/2
      IF(2*KP-N)30,20,30
   30 YODD=YODD+FALFA*CONST
      GO TO 5
   20 YEVEN = YEVEN+FALFA*CONST
      GO TO 5
```

```
10 Y1Y5=Y1Y5+FALFA*CONST
 5 CONTINUE
   FML(NP)=FML(NP)+(Y1Y5+4.0*YEVEN+2.0*YODD)*DELTX/3.0
   IF(L.EQ.1)      GO TO 6
   IF(CRNT.EQ.9)   GO  TO  6
   IF(K-2)8,6,6
 8 K=K+1
   XL=-XL
   GO TO 7
 6 CONTINUE
   RETURN
   END


   SUBROUTINE MATBB(NS,M,N,MP,NQ,SMGBR)
   REAL MU
   COMPLEX GBAR(4),AJ,EXPO,CONST,SMGBR
   COMPLEX TAU,FACT1,FACT2
   DIMENSION A(3)
   DIMENSION XA(21),XB(34,3),DBXA(34),EPRA(34),SIGIA(34)
   COMMON/MATO/XA,XB,NA,NB,DBXA
   COMMON/MAT24/EPS,EPRA,SIGIA,NQD,NSYM/MAT3/MU,OMEG,PI,BO
   SIGI=SIGIA(N)
   EPR=EPRA(N)
   DBX=DBXA(N)
   DO 8J=1,4,1
   GBAR(J)=CMPLX(0.0,0.0)
 8 CONTINUE
   AJ=CMPLX(0.0,1.0)
   TAU=SIGI+AJ*OMEG*EPS*(EPR-1.0)
   CONST=-AJ*OMEG*MU*BO*TAU/(4.0*PI)
   DELTA=DBX/NS
   X30=XB(N,3)-(DBX-DELTA)/2.0
   DO 5 JK=1,NQD,1
   IF(JK.EQ.1)  GO  TO  22
   IF(NSYM.EQ.0)  GO  TO  22
   KQ=4
   GO  TO  21
22 KQ=JK
21 IF((M.EQ.N).AND.(KQ.EQ.1))    GO TO 1
   GO TO (10,20,30,40)KQ
10 X10=XB(N,1)-(DBX-DELTA)/2.0
```

```
      X20=XB(N,2)-(DBX-DELTA)/2.0
      GO TO 7
   20 X10=-XB(N,1)-(DBX-DELTA)/2.0
      X20=XB(N,2)-(DBX-DELTA)/2.0
      GO TO 7
   30 X10=-XB(N,1)-(DBX-DELTA)/2.0
      X20=-XB(N,2)-(DBX-DELTA)/2.0
      GO TO 7
   40 X10=XB(N,1)-(DBX-DELTA)/2.0
      X20=-XB(N,2)-(DBX-DELTA)/2.0
    7 DO 3 J3=1,NS,1
      A(3)=X30+(J3-1)*DELTA
      DO 3 J2=1,NS,1
      A(2)=X20+(J2-1)*DELTA
      DO 3 J1=1,NS,1
      A(1)=X10+(J1-1)*DELTA
      R=SQRT((XB(M,1)-A(1))**2+(XB(M,2)-A(2))**2+(XB(M,3)-A(3))**2)
      ALPHA=BO*R
      EXPO=CEXP(CMPLX(0.0,-ALPHA))/ALPHA**3
      FACT1=(XB(M,NQ)-A(NQ))*(XB(M,MP)-A(MP))*(3-ALPHA**2+3*AJ*ALPHA)
     C /R**2
      IF(NQ.EQ.MP)   GO   TO   4
      GBAR(KQ)=GBAR(KQ)+EXPO*CONST*FACT1*DELTA**3
      GO TO 3
    4 FACT2=ALPHA**2-1.0-AJ*ALPHA
      GBAR(KQ)=GBAR(KQ)+EXPO*CONST*(FACT1+FACT2)*DELTA**3
    3 CONTINUE
      GO        TO       5
    1 IF(NQ.EQ.MP)      GO   TO   2
      GBAR(KQ)=CMPLX(0.0,0.0)
      GO TO 5
    2 AN=(3.0*DBX*DBX*DBX/(4.0*PI))**(1.0/3.0)
      GBAR(KQ)=(-AJ*2*MU*OMEG)/(3*BO**2)*(CEXP(CMPLX(0.0,-BO*AN))*(1+
     CAJ*BO*AN)-1.0)*TAU-(1.0+TAU/(3.0*AJ*OMEG*EPS))
    5 CONTINUE
      IF(NQ-2)11,12,13
   11  SMGBR =GBAR(1)+GBAR(2)+GBAR(3)+GBAR(4)
      GO TO 6
   12         SMGBR =GBAR(1)+GBAR(3)-GBAR(2)-GBAR(4)
      GO TO 6
   13     SMGBR =GBAR(1)+GBAR(4)-GBAR(3)-GBAR(2)
    6 RETURN
      END
```

```
      SUBROUTINE CMATP(A,N,M,DET,EP)
         COMPLEX A,B,DET,CONST,S
      DIMENSION A(29,30)
      DET=CMPLX(1.0,0.0)
      NP1=N+1
      NPM=N+M
      NM1=N-1
       DO 4 J=1,NM1
      C=CABS(A(J,J))
      JP1=J+1
      DO 5 I=JP1,N
      D=CABS(A(I,J))
      IF(C-D)6,5,5
6      DET=-DET
      DO 7 K=J,NPM
      B=A(I,K)
      A(I,K)=A(J,K)
7      A(J,K)=B
      C=D
5     CONTINUE
      IF(CABS(A(J,J))-EP)14,15,15
15    DO 4 I=JP1,N
      CONST=A(I,J)/A(J,J)
         DO 4 K = JP1,NPM
4     A(I ,K)=A(I,K)-CONST*A(J,K)
      IF(CABS(A(N,N))-EP)14,18,18
14    DET=CMPLX(0.0,0.0)
      PRINT 30
      RETURN
18    CONTINUE
      DO 12 I=1,N
      K=N-I+1
      KP1=K+1
      DO 12 L=NP1,NPM
      S=CMPLX(0.0,0.0)
         IF( N - KP1 ) 12,19,19
19       DO 13 J = KP1,N
13       S = S + A(K,J) * A(J,L)
12       A(K,L) = (A(K,L) - S)/A(K,K)
30       FORMAT(1X,42HTHE DETERMINANT OF THE SYSTEM EQUALS ZERO./
     1           1X,36HTHE PROGRAM CANNOT HANDLE THIS CASE.//)
      RETURN
      END
```

```
      SUBROUTINE RAD(A,THETA,PHI,ERAD,EMAX)
      COMPLEX A,EAQ,EXPOA,EAFI,TAU,EBQ,EBFI,JX(3),EXPOB
      DIMENSION XA(21),XB(50,3),DBXA(50),EPRA(50),SIGIA(50)
      DIMENSION A(30)
      COMMON/MAT0/XA,XB,NA,NB,DBXA
      COMMON/MAT1/DAX,DM1,CRNT
      COMMON/MAT24/EPS,EPRA,SIGIA,NQD,NSYM/MAT3/MU,OMEG,PI,BO
      FI=PI*PHI/180.0
      Q=PI*THETA/180.0
      NAM1=NA-1
      EAQ=CMPLX(0.0,0.0)
      EAFI=CMPLX(0.0,0.0)
      DO 1 N=1,NAM1,1
      K=0
      IF((N.EQ.1).AND.(CRNT.EQ.9))  GO  TO  1
    7 K=K+1
      IF(K-2)5,6,6
    6 XA(N)=-XA(N)
    5 EXPOA=CEXP(CMPLX(0.0,-BO*SIN(Q)*COS(FI)*XA(N)))
      EAQ=EAQ+A(N)*COS(Q)*COS(FI)*EXPOA*DAX
      EAFI=EAFI+(-A(N))*SIN(FI) *EXPOA*DAX
      IF(N-1)1,1,4
    4 IF(CRNT.EQ.9)  GO  TO  1
      IF(K-2)7,1,1
    1 CONTINUE
      EBQ=CMPLX(0.0,0.0)
      EBFI=CMPLX(0.0,0.0)
      DO 2 N=1,NQD,1
      DO 2 M=1,NB,1
      TAU=SIGIA(M)+CMPLX(0.0,OMEG*(EPRA(M)-1)*EPS)
      DBX=DBXA(M)
      M1=NA+M
      M2=NA+NB+M
      M3=NA+2*NB+M
      JX(1)=A(M1)*TAU
      X3=XB(M,3)
      IF(NSYM.EQ.1)GO TO 8
      GO TO (10,20,30,40)N
    8 GO TO (10,40,30,20)N
   10 X1=XB(M,1)
      X2=XB(M,2)
      JX(2)=A(M2)*TAU
      JX(3)=A(M3)*TAU
      GO TO 3
```

```
20  X1=XB(M,1)
    X2=XB(M,2)
    JX(2)=-A(M2)*TAU
    JX(3)=-A(M3)*TAU
    GO TO 3
30. X1=-XB(M,1)
    X2=-XB(M,I)
    JX(2)=A(M2)*TAU
    JX(3)=-A(M3)*TAU
    GO TO 3
40  X1=XB(M,1)
    X2=XB(M,2)*(-1)
    JX(2)=-A(M2)*TAU
    JX(3)=A(M3)*TAU
 3  EXPOB=CEXP(CMPLX(0.0,-BO*(X1*SIN(Q)*COS(FI)+X2*SIN(Q)*SIN(FI) +
   * X3*COS(Q))))
    EBQ=(JX(1)*COS(Q)*COS(FI)+JX(2)*COS(Q)*SIN(FI)-JX(3)*SIN(Q))*
   *   EXPOB*DBX**3+EBQ
    EBFI=(-JX(1)*SIN(FI)+JX(2)*COS(FI))*EXPOB*DBX**3+EBFI
 2  CONTINUE
    EQ=CABS((EAQ+EBQ))
    EFI=CABS((EAFI+EBFI))
    ERAD=SQRT((EQ**2+EFI**2))
    IF(ERAD-EMAX)11,12,12
12  EMAX=ERAD
11  RETURN
    END
```

```
      PROGRAM ZFREE(INPUT,OUTPUT,TAPE1,TAPE2)
      INTEGER EFIELD
      COMPLEX AJ,CIL,G(69,70),YO,ZO,ANT(69),DET
      COMMON/MAT1/DAX,ANTRAD,NA,BO,XA(69)
      COMMON XB(40,3),FMEG,NB
      READ 1,FMEG,H,ANTRAD,NA,EFIELD
    1 FORDAT(3F10.1,I2,7X,IA)
      DAX=2*H/(2*NA+1)
      NA=NA+1
      XAO=0.0
      NAP1=NA+1
      MAP1=NAP1
      DO 2 J=1,NA,1
      DO 2 I=1,NAP1,1
      G(J,I)=CMPLX(0.0,0.0)
    2 CONTINUE
      PI=3.14159264
      SO=120*PI
      ALAMDA=(3.0*1.0E+08)/(FMEG*1.0E+06)
      BO=2*PI/ALAMDA
      AJ=CMPLX(0.0,1.0)
      DO 3 M=1,NA,1
      AXAO=XAO+(M-1)*DAX
      XA(M)=AXAO
      G(M,NAP1)=-AJ*2*PI*SIN(BO*ABS(XA(M)))/SO
    3 CONTINUE
      DO 5 L=1,NA,1
      DO 5 I=1,NA,1
      CALL MATAA(I,L,CIL)
      G(I,L)=CIL
    5 CONTINUE
      CALL CMATPAC(G,NA,1,DET,1.0E-100)
      PRINT 7
      DO 8 J=1,NA,1
      IF(NA-J)10,10,9
   10 G(J,MAP1)=CMPLX(0.0,0.0)
    9 PRINT 11,J,G(J ,MAP1)
    8 CONTINUE
    7 FORMAT(1H1,//,31HCURRENT DISTRIBUTION ON ANTENNA)
   11 FORMAT(1HO,//,3X,I3,4X,2E12.5)
      K=1
      YO=G(K,NAP1)
      ZO=1.0/YO
      PRINT 6,YO,ZO
    6 FORMAT(1HO,//,3X,12HADMITTANCE =,2X,2E14.5,3X,11HIMPEDANCE =,
     C2X,2E12.5)
      IF(EFIELD.EQ.0)  GO  TO  99
```

```
      DO 12 M=1,NA,1
      ANT(M)=G(M,MAP1)
   12 CONTINUE
      READ 13,NB
   13 FORMAT(I2)
      DO 14 J=1,NB,1
      READ 15,(XB(J,K),K=1,3)
   15 FORMAT(3F10.1)
   14 CONTINUE
      CALL EIMP(NA,DAX,XA,ANT)
   99 STOP
      END
      SUBROUTINE MATAA(I,L,CIL)
      COMPLEX CIL,Y1Y5,YEVEN,YODD,AJ,TOTAL
      COMMON/MAT1/DAX,ANTRAD,NA,BO,XA(69)
      XI=XA(I)
      XL=XA(L)
      IF(L.EQ.NA)GO TO 1
      TOTAL=CMPLX(0.0,0.0)
      K=1
    8 A=XL-DAX/2
      IF((I.EQ.L).AND.(K.EQ.1))    GO    TO    2
      Y1Y5=CMPLX(0.0,0.0)
      YEVEN=CMPLX(0.0,0.0)
      YODD=CMPLX(0.0,0.0)
      DELTAX=DAX/10
      DO 5 M=1,11,1
      AA=A+(M-1)*DELTAX
      R=SQRT((XI-AA)**2+ANTRAD**2)
      AJ=CEXP(CMPLX(0.0,-BO*R))
      GO TO (10,20,30,20,30,20,30,20,30,20,10)M
   10 Y1Y5=Y1Y5+AJ/R
      GO TO 5
   20 YEVEN=YEVEN+AJ/R
      GO TO 5
   30 YODD=YODD+AJ/R
    5 CONTINUE
      TOTAL=TOTAL+(Y1Y5+4*YEVEN+2*YODD)*DELTAX/3.0
      GO TO 6
    2 B=A+DAX
      AAA=ALOG((XI-A+SQRT((XI-A)**2+ANTRAD**2))/
     *(XI-B+SQRT((XI-B)**2+ANTRAD**2)))
      TOTAL=CMPLX(AAA,0.0)
    6 IF(L.EQ.1)GO TO 7
      IF(K-2)9,7,7
    9 K=K+1
      XL=-XL
```

```
      GO TO 8
    7 CIL=TOTAL
      GO TO 99
    1 CIL=CMPLX(COS(BO*XI),0.0)
   99 RETURN
      END


        SUBROUTINE CMATPAC(A,N,M,DET,EP)
        COMPLEX A,B,DET,CONST,S
      DIMENSION A(69,70)
      DET=CMPLX(1.0,0.0)
      NP1=N+1
      NPM=N+M
      NM1=N-1
       DO 4 J=1,NM1
      C=CABS(A(J,J))
      JP1=J+1
      DO 5 I=JP1,N
      D=CABS(A(I,J))
      IF(C-D)6,5,5
6      DET=-DET
      DO 7 K=J,NPM
      B=A(I,K)
      A(I,K)=A(J,K)
7      A(J,K)=B
      C=D
5     CONTINUE
      IF(CABS(A(J,J))-EP)14,15,15
15    DO 4 I=JP1,N
      CONST=A(I,J)/A(J,J)
        DO 4 K = JP1,NPM
4     A(I ,K)=A(I,K)-CONST*A(J,K)
      IF(CABS(A(N,N))-EP)14,18,18
14    DET=CMPLX(0.0,0.0)
      PRINT 30
      RETURN
18    CONTINUE
      DO 12 I=1,N
      K=N-I+1
      KP1=K+1
      DO 12 L=NP1,NPM
      S=CMPLX(0.0,0.0)
        IF( N - KP1 ) 12,19,19
19      DO 13 J = KP1,N
13      S = S + A(K,J) * A(J,L)
12      A(K,L) = (A(K,L) - S)/A(K,K)
30      FORMAT(1X,42HTHE DETERMINANT OF THE SYSTEM EQUALS ZERO./
     1             1X,36HTHE PROGRAM CANNOT HANDLE THIS CASE.//)
      RETURN
      END
```

```
      SUBROUTINE EIMP(NN,DX,XP,ANT)
      TYPE COMPLEX EXI,EYI,EZI,CONST,ANT(69),IN
      TYPE REAL LO,KO
      DIMENSION XP(69)
      COMMON XB(40,3),FMEG,NB
      PI=3.1415926536   $   ZO=120.0*PI
      FREQ=FMEG*1.0E+6
      LO=3.0E+8/FREQ   $   KO=2.0*PI/LO
      CONST=CMPLX(0.0,-ZO/(4.0*PI*KO))
      DO 6 NE=1,NB,1
      X=XB(NE,1)
      Y=XB(NE,2)
      Z=XB(NE,3)
      EXI=CMPLX(0.0,0.0)   $   EYI=CMPLX(0.0,0.0)   $   EZI=CMPLX(0.0,0.0)
      NM1=NN-1
      DO 2 N=1,NM1,1          $          IF(N-1)10,10,20
   20 IN=ANT(N)               $           GO TO 11
   10 IN=ANT(N)/2.0
   11 R1=SQRT((X-XP(N))**2+Y**2+Z**2)
      R2=SQRT((X+XP(N))**2+Y**2+Z**2)
      R3=SQRT((X-(XP(N)+DX/2.0))**2+Y**2+Z**2)
      R4=SQRT((X-(XP(N)-DX/2.0))**2+Y**2+Z**2)
      R5=SQRT((X-(-XP(N)+DX/2.0))**2+Y**2+Z**2)
      R6=SQRT((X-(-XP(N)-DX/2.0))**2+Y**2+Z**2)
      EXI=EXI+IN*((KO**2)*(CEXP(CMPLX(0.0,-KO*R1))/R1+CEXP(CMPLX(0.0,-KO
     1*R2))/R2)*DX+(X-(XP(N)+DX/2.0))*CMPLX(1.0,KO*R3)*CEXP(CMPLX(0.0,-K
     2O*R3))/R3**3-(X-(XP(N)-DX/2.0))*CMPLX(1.0,KO*R4)*CEXP(CMPLX(0.0,-K
     3O*R4))/R4**3+(X-(-XP(N)+DX/2.0))*CMPLX(1.0,KO*R5)*CEXP(CMPLX(0.0,-
     4KO*R5))/R5**3-(X-(-XP(N)-DX/2.0))*CMPLX(1.0,KO*R6)*CEXP(CMPLX(0.0,
     5-KO*R6))/R6**3)
      EYI=EYI+IN*Y*(CMPLX(1.0,KO*R3)*CEXP(CMPLX(0.0,-KO*R3))/R3**3-CMPLX
     1(1.0,KO*R4)*CEXP(CMPLX(0.0,-KO*R4))/R4**3+CMPLX(1.0,KO*R5)*CEXP(CM
     2PLX(0.0,-KO*R5))/R5**3-CMPLX(1.0,KO*R6)*CEXP(CMPLX(0.0,-KO*R6))/R6
     3**3)
      EZI=EZI+IN*Z*(CMPLX(1.0,KO*R3)*CEXP(CMPLX(0.0,-KO*R3))/R3**3-CMPLX
     1(1.0,KO*R4)*CEXP(CMPLX(0.0,-KO*R4))/R4**3+CMPLX(1.0,KO*R5)*CEXP(CM
     2PLX(0.0,-KO*R5))/R5**3-CMPLX(1.0,KO*R6)*CEXP(CMPLX(0.0,-KO*R6))/R6
     3**3)
    2 CONTINUE
      EXI=EXI*CONST   $   EYI=EYI*CONST   $   EZI=EZI*CONST
      E1=CABS(EXI)
      E2=CABS(EYI)
      E3=CABS(EZI)
      PRINT7,NE,E1,E2,E3
    7 FORMAT(1HO,2X,I2,3E16.5)
    6 CONTINUE
      RETURN
      END
```

CHAPTER VIII

SUMMARY

The objective of this thesis was to solve the problem of electromagnetic coupling between an antenna and a biological body. This thesis has verified experimentally the theoretical results that were obtained by computer aided numerical analysis. The study was necessary to understand the nature of the coupling problem and to make an assessment of the potential radiation hazard to operators exposed to high power radiation from thin-wire antennas.

As an introduction a rigorous mathematical analysis was carried out for linear dipole antenna having a biological body in its vicinity. Integral equations which have been named as coupled-integral-equations were obtained and later transformed by the method of moments into a system of consistent equations for the unknown electric fields in the body and the currents on the antenna. These were solved by standard numerical techniques on a computer.

Experiments were conducted to verify the theoretical results obtained for an antenna-body coupled system. These results were verified for (a) the input impedance of the antenna; (b) the induced electric field distribution inside the body; (c) the current distribution on the antenna.

The experimental verification of the theory developed earlier gave us enough confidence to get additional information about various practical situations. This information was gathered by the computer program "FIELDS". The prominent features resulting from this were the effect on the radiation pattern due to coupling, the effect on the current distribution on antenna, and the effect on induced fields in the body due to direct contact with ground and isolation from the ground. Ratios of the power dissipated to the power radiated and power input to antennas, were also determined. It was concluded that quarter wave monopole antennas with input powers of about 140 watts at 27 MHz or 30 watts at 90 MHz would dissipate the same amount of power in the body of an operator in the near-zone of antenna, as would a plane electromagnetic wave of intensity 10 mW/cm^2.

In addition the computer program FIELDS which furnishes all the required quantitative information regarding a coupling problem has been explained by working out an example. This program is compatible for all FORTRAN IV systems.

The problem of a linear dipole antenna or a monopole antenna over infinite ground plane has been dealt with success in this thesis. As a next step it would be interesting to attempt solving a problem involving thin-wire antenna of arbitrary shape.

BIBLIOGRAPHY

BIBLIOGRAPHY

1. H.P. Schwan, "Radiation biology, medical applications and radiation hazards", Microwave Power Engineering, Vol. 2, E.C. Okress, Ed., New York: Academic Press, 1968, pp. 215-232.

2. C.C. Johnson and A.W. Guy, "Nonionizing electromagnetic wave effects in biological materials and systems", Proceedings of the IEEE, Vol. 60, No. 6, pp. 692-719, June 1972.

3. K.M. Chen and B.S. Guru, "Induced electromagnetic field and absorbed power density inside human torso", Engineering Research Report, Michigan State University, East Lansing, Michigan, 1976.

4. K.M. Chen, D.E. Livsay and B.S. Guru, "Induced field in and scattered field from a finite cylinder with arbitrary conductivity and permittivity", IEEE Transactions on Antennas and Propagation, Vol. AP-24, No. 3, pp. 330-336, May 1976.

5. D.P. Nyquist, K.M. Chen and B.S. Guru, "Coupling between small thin-wire antennas and a biological body", IEEE Transactions on Antennas and Propagation, Vol. AP-25, No. 6, pp. 863-866, Nov. 1977.

6. Chen-To Tai, "Dyadic Green's function in electromagnetic theory", Intext Educational Publishers, Ed., Pennsylvania: Haddon Craftsmen Inc., Scranton, pp. 46-65, 1971.

7. K.M. Chen, "A simple physical picture of Tensor Green's function in source region", Proceedings of the IEEE, Vol. 65, No. 8, pp. 1202-1204, Aug. 1977.

8. D.E. Livesay and K.M. Chen, "Electromagnetic fields induced inside arbitrarily shaped biological bodies", IEEE Transactions on Microwave Theory and Techniques, Vol. MT-22, No. 12, pp. 1173-1280, Dec. 1974.

9. B.S. Guru, "An experimental study on the interaction of electromagnetic fields with arbitrarily shaped biological bodies", Ph.D. dissertation, Michigan State University, East Lansing, Michigan, 1976.

10. R. Cooper, "The electrical properties of salt water solutions over the frequency range 1-4000 MHz", The Journal of the Institute of Electrical Engineers, Radio and Communication Engineering, Vol. 93, part III, No. 22, pp. 69-75, March 1946.

11. L.K. Lepley and W.M. Adams, "Electromagnetic dispersion curves for natural waters", Water Resources Research, Vol. 7, No. 6, pp. 1538-1547, Dec. 1971.

12. J.A. Saxton and J.A. Lane, "Electrical properties of sea water", Wireless Engineering, pp. 269-275, Oct. 1952.

13. S.H. Mousavinezhad, "Implantable electromagnetic field probes in finite biological bodies", Ph.D. dissertation, Michigan State University, East Lansing, Michigan, 1977.

14. R.W.P. King, "Theory of Linear Antennas", Harvard University Press, Cambridge, Massachusetts, pp. 251-252, 1956.

15. G.S. Smith, "The electric-field probe near a material interface with applications to the probing of fields in biological bodies", IEEE Transactions on Microwave Theory and Techniques, Vol. MTT-27, No. 3, pp. 270-278, March 1979.

16. J. Van Bladel, "Some remarks on Green's dyadic for infinite space", IRE Transaction Antennas Propg., Vol. AP-9, pp. 563-566, Nov. 1961.

17. K.M. Chen, S. Rukspollmuang and D.P. Nyquist, "Measurement of induced electric fields in a phantom model of man", presented at International Symposium on Biological Effects of Electromagnetic Waves held on July 31 to Aug. 8, 1978, in Helsinki, Finland.

18. H. Massoudi, C.H. Durney and C.C. Johnson, "Long-wavelength EM power absorption in ellipsoidal model of man and animals". IEEE Transactions on Microwave Theory and Techniques, MTT-25, No. 1, pp. 47-52, Jan. 1977.